Techno-Economic Analysis of Different Price Signals in Local Energy Markets Using Open Data

Tom Schelo

Vollständiger Abdruck der von der TUM School of Engineering and Design
der Technischen Universität München zur Erlangung des akademischen Grades eines

Doktors der Ingenieurwissenschaften

genehmigten Dissertation.

Vorsitzende(r):

Prof. Dr.-Ing. Harald Klein

Prüfer(innen) der Dissertation:

1. Prof. Dr. rer. nat. Thomas Hamacher
2. Prof. Dr.-Ing. Wolfgang Kellerer

Die Dissertation wurde am 24.09.2021 bei der Technischen Universität München eingereicht
und durch die TUM School of Engineering and Design am 02.11.2022 angenommen.

Abstract

The electric power distribution grid will play a significant role in the ongoing energy transition worldwide, as its traditionally relatively passive role within the power system will shift to a more active one. In light of the ongoing integration of distributed energy resources, represented by volatile and controllable distributed generators and new intermittent loads, such as electric vehicles and heat pumps, new methodologies and tools for the planning and operation of the distribution grid become necessary. To counteract the strains that these new technologies put on the system, Distribution Locational Marginal Prices (DLMPs) have been proposed in the research community and proven to provide a highly granular price signal that allows the optimal operation of the distribution grid. However, current research fails to provide a proper analysis of the effects of this nodal pricing signal on a distribution grid level in a realistic context.

To this end, this thesis presents a systematic approach for assessing the impact of DLMPs in comparison with different price signals of lower spatial and temporal granularity both from a technical and an economic perspective, with a particular focus on social welfare effects. As the results are highly dependent on the underlying data and models, a large set of power system-related data is collected and aggregated from publicly available sources for the development of realistic scenarios. Using this dataset as a basis, representative synthetic distribution grid models are developed and an existing thermal building model is parameterized. The thermal building models serve as flexible heat pumps in our scenarios, as they represent large, intermittent loads and an equally large source of flexibility within the power system.

In a first attempt, the thesis shows the effect of time-varying price signals on the load coincidence of flexible heat pumps. The case study concludes that price signals must be carefully designed, as flexible distributed energy resources are expected to be controlled by price-sensitive aggregators that aim at profit maximization/cost minimization. The systematic analysis subsequently introduces the nodal pricing signal in addition to a constant and a time-varying price signal. The results show that from a technical perspective, DLMPs inherently lead to efficient grid usage, which comes at the cost of smaller security margins, as any dynamic pricing signal increases load coincidence of price-following distributed energy resources. Consequently, the grid is operated closer to its limits. The economic analysis shows that the overall impact on social welfare is small, which means that the DLMP-based local energy market presents a cost-efficient solution to minimize losses and alleviate voltage violations and congestion in the distribution grid. However, the implementation efforts and the unfair distribution of prices might not justify the efficiency increase that could be managed with other, more fair corrective measures. Inevitably, these alternative measures will always be economically less efficient than DLMPs.

Zusammenfassung

Im Zuge der weltweiten Energiewende wird sich die traditionell eher passive Rolle des elektrischen Verteilnetzes innerhalb des Energiesystems zu einer aktiveren wandeln. Angesichts der fortschreitenden Integration verteilter Energieressourcen, die sowohl aus volatilen und steuerbaren dezentralen Erzeugern als auch aus neuartigen intermittierenden Lasten wie Elektrofahrzeugen und Wärmepumpen bestehen, werden neue Methoden und Werkzeuge für die Planung und den Betrieb von Verteilnetzen erforderlich. Um den Belastungen dieser neuen Technologien auf das System entgegenzuwirken, werden derzeit in der Forschung sogenannte Distribution Locational Marginal Prices (DLMPs) diskutiert, die ein hochgranulares Preissignal darstellen, das nachweislich einen optimalen Betrieb des Verteilnetzes ermöglicht. Die derzeitige Forschung bietet jedoch keine angemessene Analyse der Auswirkungen dieses Preissignals auf Verteilnetzebene in einem realistischen Kontext.

Zu diesem Zweck wird in dieser Arbeit ein systematischer Ansatz zur Bewertung der Auswirkungen von DLMPs im Vergleich zu verschiedenen Preissignalen mit geringerer zeitlicher wie räumlicher Granularität sowohl aus technischer als auch aus wirtschaftlicher Sicht vorgestellt, wobei der Schwerpunkt auf den Auswirkungen auf die soziale Wohlfahrt liegt. Da die Ergebnisse in hohem Maße von den zugrundeliegenden Daten und Modellen abhängen, wird für die Entwicklung realistischer Szenarien ein großer Datensatz von Energiesystem-Daten aus öffentlich zugänglichen Quellen gesammelt und aggregiert. Auf Basis dieses Datensatzes werden repräsentative, synthetische Verteilnetzmodelle entwickelt und ein bestehendes thermisches Gebäudemodell parametrisiert. Die thermischen Gebäudemodelle dienen in unseren Szenarien als flexible Wärmepumpen, da sie große, intermittierende Lasten und eine ebenso große Flexibilitätsquelle innerhalb des Energiesystems darstellen.

In einem ersten Versuch zeigt die Arbeit die Auswirkung von zeitvariablen Preissignalen auf die Lastkoinzidenz von flexiblen Wärmepumpen. Die Fallstudie kommt zu dem Schluss, dass die Preissignale sorgfältig gestaltet werden müssen, da davon auszugehen ist, dass flexible verteilte Energieressourcen von preissensiblen Aggregatoren gesteuert werden, die eine Gewinnmaximierung/Kostenminimierung anstreben. In der systematischen Analyse wird dann zusätzlich zu einem konstanten und einem zeitvariablen Preissignal das nodale Preissignal (DLMPs) eingeführt. Die Ergebnisse zeigen, dass aus technischer Sicht DLMPs inhärent zu einer effizienten Netznutzung führen, die auf Kosten kleinerer Sicherheitstoleranz geht, da jedes dynamische Preissignal die Lastkoinzidenz der preissensiblen, verteilten Energieressourcen erhöht und das Netz daher näher an seinen Grenzen betrieben wird. Die wirtschaftliche Analyse zeigt, dass die Auswirkungen auf die soziale Wohlfahrt insgesamt gering sind, was bedeutet, dass der DLMP-basierte, lokale Energiemarkt eine kosteneffiziente Lösung zur Minimierung von Verlusten, Spannungsverletzungen und Engpässen im Verteilnetz darstellt. Allerdings rechtfertigen der Implementierungsaufwand und die ungerechte Preisverteilung möglicherweise nicht die Effizienzsteigerung, die mit anderen, aber faireren Korrekturmaßnahmen erreicht werden könnte. Diese alternativen Maßnahmen werden jedoch immer wirtschaftlich weniger effizient sein als DLMPs.

Contents

List of acronyms

AB Apartment Block
AC Alternating Current

BAG Basisregistratie Adressen en Gebouwen
BDEW German Association of the Energy and Water Industry

CF Coincidence Factor
CNA Complex Network Analysis
CoBMo Control-oriented Building Model
COP Coefficient of Performance

DER Distributed Energy Resource
DLMP Distribution Locational Marginal Price
DSO Distribution System Operator

ENTSO-E European Network of Transmission System Operators for Electricity
EPL Energy Performance Level
EV Electric Vehicle

GIS Geographic Information System

HP Heat Pump
HVAC Heating Ventilation and Air Conditioning

KNMI Royal Dutch Meteorological Institute

LMP Locational Marginal Price
LV Low Voltage

MESMO Multi-Energy System Modeling and Optimization
MFH Multi Family House
MV Medium Voltage

NWCPL normalized weighted characteristic path length

P2P Peer-to-Peer
PV Solar Photovoltaics

RES Renewable Energy Source

RTP Real Time Pricing

SFH Single Family House

TABULA Typology Approach for Building Stock Energy Assessment
TH Terraced House
TSO Transmission System Operator

VBP Volumetric Block Pricing

WCPL weighted characteristic path length

List of figures

List of tables

List of algorithms

Chapter 1

Introduction

1.1 The role of the distribution grid: a paradigm shift

The European power system is subject to significant changes over the next decades to reach the goal of net-zero greenhouse gas emissions by the year 2050 as agreed in the *European Green Deal* and manifested in the proposed *European Climate Law* [1]. The electric power system will play a major role in this transition. New technology, both on the supply and the demand side, is emerging, and much of the thermal energy demand, such as space heating or industrial processes, will likely shift to being supplied with electric power. One highly affected element of the electric power system is the distribution grid, whose original role within the system was to distribute electricity to the end consumers for different consumption purposes on medium- and low-voltage levels. To fulfill this elementary purpose, distribution grids were traditionally designed and operated based on a "fit and forget" strategy [2], planned to withstand the highest estimated coincident load [3] and with limited visibility of, control over, and feedback from consumers [4]. This passive role in the power system originated from the fact that barely any active intervention in the distribution grid operation was needed.

However, the role of the distribution system is expected to change significantly as the transition of the power system continues, which is depicted in Figure 1.1. The ongoing integration of Distributed Energy Resources (DERs) in the distribution grid, which includes the advent of uncontrollable, distributed generators and new rapidly changing consumers like electric vehicles (EVs) and heat pumps (HPs), is driving the transition of the distribution grid towards a more active role within the power system [4]. According to [5], the rapid growth of DERs has been stimulated by a combination of forces, including national decarbonization policy goals, infrastructure investment deferral opportunities, reliability and power quality concerns, a trend towards electricity autonomy, the falling costs of DER technologies, and a stronger focus on consumer needs. Altogether, these trends call for the development of novel market mechanisms and new network operation and planning strategies to allow consumers and flexible DERs to be actively engaged with the future energy system [6].

While DERs offer a wide range of opportunities for the power system when efficiently exploiting their flexibility potential, if not controlled properly, they can cause congestion, higher losses and voltage issues in the distribution grid as reported in [7]–[11]. To this end, Distribution System
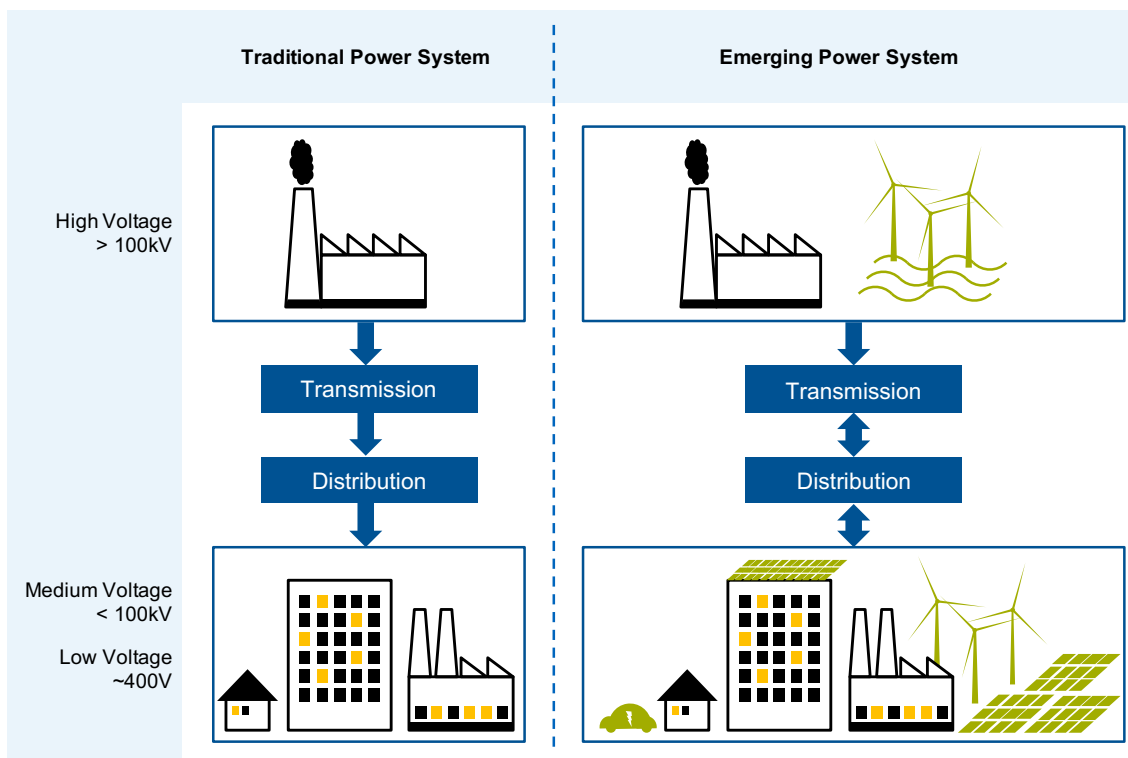
Figure 1.1: The power system is undergoing a fundamental transition, turning the distribution grid's role into a more active one

Operators (DSOs) need more comprehensive methodologies and tools for the planning and operation of the distribution grid in the presence of DERs [12]. This includes an advanced monitoring and communication infrastructure, which promises real-time availability of information on the current state of the grid and the ability to send the right control signals. With the right signal, the full potential of flexible DERs can be exploited, and the need for massive grid expansion minimized, given that the distribution grid makes up a large proportion of all assets in the electric power system. As a basis for the right control signal, the true costs and values of DERs within the distribution grid must be better understood, and efficient signals must be derived to cope with the increasing strain on the grid. Economic signals can serve to coordinate planning and operational decisions related to all resources and make it possible to achieve efficient outcomes. Ideally, these signals will evoke efficient responses from all resources, at all times, no matter where they are located in the grid [13].

1.2 Motivation of this thesis

Most power systems today employ simplified prices and charges to allocate fixed and variable power system costs to most electricity consumers, which have been deemed inadequate in the face of increasing DER penetration and emerging opportunities for flexible demand by authors [13], [14]. This need for more sophisticated economic signals becomes apparent when envisioning a power system in which all participants can provide different system-related services to any other agent on all voltage levels. It becomes obvious that in the light of the

physical laws, which electricity flows obey, the value of electricity is highly locational, which will be covered in more detail in the following chapter. One way of dealing with the locational nature of the electricity system is by applying economic signals of higher spatial granularity, such as seen in nodal pricing-based markets. Such economic signals are currently under discussion for an application in the European electricity system [15], [16]. However, even in power systems with high granularity price signals in the transmission level wholesale market in place, such as parts of the United States, according to authors in [13] spatial granularity is lost when the economic signal is passed through to the consumers and producers connected at diverse voltage levels in the distribution grids. Presenting temporal variance only for entire zones (i.a. individual distribution grids) may dull the impact of binding constraints on price-responsive DERs that could contribute to an efficient response [13]. For this reason, distribution level economic price signals are at the core of the analysis in this thesis to evaluate how they can unlock flexibility of DERs where appropriate and when needed.

It is well understood that the value of DERs is locational in terms of time and space [17], which means that an economically reflexive understanding of the true costs of feeding-in and delivering energy into a given node in the distribution grid at a given time is imperative. That is why cost causation-based pricing schemes have been promoted in recent research [3], [12], [18], [19]. It is argued that this type of pricing scheme on the distribution grid level could introduce economic incentives to network users for efficient use of resources and investments in grid-friendly hardware. The authors in [12] consider a correct allocation of costs as the key to promoting DERs "in the right places in the network, in the right time with the right profile of energy injections".

For a truly cost causation-based pricing scheme, [18] and [20] identify two main features that must be satisfied: Firstly, coming from an average cost tariff and removing many of the cross-subsidies, it is vital to understand all the potential drivers for changes in the system state and to decompose and isolate the individual effects [18]. Secondly, it is necessary to focus on the incremental or marginal costs of an action in contrast to the average cost of a collection of decisions. According to [20], the marginal cost, other than the average cost, is relevant to decisions and support of economic efficiency.

On a transmission grid level, the nodal pricing scheme of Locational Marginal Prices (LMPs), as originally developed in [21], [22], provides exactly these two features. LMPs have been used to design several transmission level wholesale markets worldwide, like the one in California, Texas, Singapore, or New Zealand [23]–[25]. The demonstrated value of LMPs has been to provide near-term scheduling and operating incentives consistent with grid conditions [26]. In the presence of DERs, this is what pricing on the distribution grid level should achieve. The distribution level counterpart to LMPs, Distribution Locational Marginal Prices (DLMPs) have only recently gotten attention in the research community and have been proposed to form local distribution grid markets, e.g. in [7], [27], [28]. Both LMPs and DLMPs are considered spatial and temporal spot prices which reflect the "truest cost of the overall system" [21], since the electricity price reflects the producer and consumer preferences, i.e. individual utility and cost functions. To promote the motivation towards a cost causation-based pricing scheme for distribution grids outlined above, DLMPs qualify as the economically most efficient price signal. However, as the subsequent section will show, current research strongly focuses on

the calculation of DLMPs and the organization of such a market while it fails to provide a profound analysis of their techno-economic impact in the context of flexible DERs in European distribution grids.

1.3 State of research on DLMPs

On a distribution level, one of the main challenges is the calculation of DLMPs in a decomposable and intuitive manner, which gives the market operator the possibility of fair financial settlement and identification of affected areas within the grid. The reason for this challenge lies in the highly non-linear power flow and inter-temporal energy requirements of flexible DERs such as battery storage systems, which require a profound understanding of the grid quantities [29]. To this end, a large amount of current work focuses on the formulation and derivation of DLMPs. This section, therefore, intends to provide an overview of the current state of research on DLMPs, which we separate into three subsections for categorization purposes.

1.3.1 DLMP formulation

The state-of-the-art literature considers maximizing the overall social welfare of the distribution grid, subject to a simplified [14], [30]–[33], relaxed [28], [34] and full [27]–[29], [35]–[39] grid model.

While [31], [32] assume a simplistic power flow model and the focus is given to reflect inter-temporal uncertain flexible demands. It is shown that DLMPs can serve as an optimal price signal which alleviates grid congestion. Building on these works of flexible demand model representation in combination with DLMPs, [29], [36], [40] investigate the suitability of the grid model in the calculation of DLMPs. To this end, a piecewise linear alternating current (AC) [40], non-linear AC [29], and multi-phase AC [36] power flow formulation is applied, respectively. The authors show that using a framework that combines convex optimization and power flow approximations, accurate non-linear AC power flows can be adopted in the DLMP formulation. Moreover, by utilizing the fixed-point form of AC power flow formulation, mathematically rigorous statements can be obtained regarding the feasibility of the framework, and a trust-region method can be deployed, which can be implemented using any open source or off-the-shelf optimization software. Authors in [37], [41] furthermore emphasize the importance of both active as well as reactive power DLMPs in distribution grids to account for the opportunity costs of providing reactive power. A multi-phase representation to account for unbalanced loading is furthermore considered in [37], [38].

Other research focuses on the derivation of DLMPs based on game-theoretical approaches, such as [42] and [43]. They aim at fairly allocating individual contributions to system losses to market participants to reduce overall losses. Furthermore, authors in [44] apply artificial intelligence based on a recurrent neural network to generate DLMP forecasts for a day-ahead market. The approach includes cold-start capacities to allow forecasts for new nodes in the grid with no history by using neighboring nodes.

1.3.2 DLMP application

Most theoretical work covering the concept of DLMPs appoint the DSO as the central entity for managing the local distribution grid market as an independent system operator [7], [27]–[33], [39], [45], [46], which is in the spirit of the role of the Transmission System Operator (TSO) in transmission level nodal pricing markets. However, a variety of approaches have been suggested to further facilitate the applicability of DLMPs.

In the light of data privacy concerns, the authors in [31], [32] show that, using convex optimization, an efficient iterative coordinating mechanism can be established to derive DLMPs. This allows the users and the grid operator to preserve their sensitive information, i.e., cost functions for the users and network information for the grid operator. Based on the ability to formulate DLMPs in the context of non-linear AC power flows and inter-temporally constrained DERs, a local distribution grid market organization is proposed in [29], [47]. The authors demonstrate that a local distribution grid market can be efficiently operated on a day-ahead basis, allowing to incorporate inter-temporal energy constraints, such as flexible load models [31], [32]. Moreover, this local distribution grid market achieves efficient flexibility resource allocation, i.e. maximizing the welfare of the local flexibility resources also maximizes the overall social welfare of the system. The price volatility of DLMPs, which occurs around weak spots in the network, has also been analyzed in [47] by proposing an ex-ante mechanism for so-called hedging rights, which minimizes this price volatility while at the same time obeying the conditions of the network and the energy demand from local, flexible demand. To facilitate the application of nodal pricing for larger regions with individual distribution grids, in [48] a framework in which DLMPs are defined across multiple regions is proposed. Each region maximizes its individual social welfare, with the individual problem comprising the coupled physical information from the neighboring regions without providing exact information. The consensus between all regions is reached in a distributed fashion based on a CAST algorithm, and DLMPs are derived from it.

With regard to the application of DLMPs in the context of different types of DERs, the latest research focuses on optimal EV charging [33], [49], [50], flexible Heating Ventilation and Air Conditioning (HVAC) units in buildings [31], [32], [51], and the optimal operation of biogas plants under DLMPs [39].

1.3.3 DLMP extension

Along with the DLMP formulations above, which are limited to power flow components, other research aims at extending the general framework. In [9] the DLMP principle is applied in a peer-to-peer (P2P) market design to address the problem of violations of network conditions in free P2P trade at the distribution network level, where, based on a distributed calculation, grid-violating transactions are compensated for by network usage fees for each P2P trade according to the location-dependent components of the DLMPs. Furthermore, the authors in [52], [53] incorporate congestion as well as asset (e.g. transformer) degradation to account for the true marginal system cost.

Another essential aspect that is currently gaining traction in the research community is the concept of sector coupling. In the context of DLMPs, authors in [54] propose the combined

operation of a district thermal and electrical grid based on DLMPs by applying adapted methods from [29] to thermal networks (i.e. district heating or district cooling systems). For this purpose, thermal and electrical network models are approximated in a linear form. The derivation and decomposition of DLMPs is then formulated based on the combined optimal load flow problem, whereby the known state-space formulations from [32] and [31] serve as flexible thermal and electric loads. To counteract the issue of varying price signals at all nodes, the authors in [6] propose a practical framework for the coexistence of both fixed tariffs and dynamic nodal prices in the distribution grid. While flexible users pay nodal prices, non-flexible consumers are charged a fixed price derived from the underlying nodal prices.

While the focus of current research lies mainly on the calculation and decomposition of DLMPs, the methodological extension with additional DERs, or the integration of such a local market with higher market layers, they fail to conduct a sound analysis of the applicability and potential of such a pricing scheme in realistic scenarios. While most do consider a high fidelity grid model in their case study, their analysis focuses on the decomposition scheme and its performance. Case studies in the context of DLMPs are usually designed to prove the mathematical derivation and the promised effects of the mechanisms. They are therefore often unrealistic and applicable only on a very small scale. While authors in [15] state that nodal pricing only applied on the transmission grid level is expected to support the regional balancing of supply and demand and therefore provides sufficient incentives to steer clear of congestion in the distribution grid, they do not provide any proof. In the light of increasing DER penetration, this implies a need for further analysis. Therefore, a detailed analysis of economic price signals in combination with emerging DER technology and their effect on the distribution grid is needed. The economic nature of DLMPs qualifies them as a reference point for the efficiency evaluation of different price signals and is therefore at the core of this thesis.

1.4 Objectives and contribution of this thesis

Using the flexibility of DERs, such as HPs or flexible renewable generation capacity, to their full potential can have a significant impact on reducing the costs of power systems. To exploit this potential, efficient economic signals are needed as indicators for both the value of electricity provided (consumed) and for economic flexible DER operation. However, high-level market structures as implemented today fail to provide such economic signals. DLMPs offer the highest degree of spatial and temporal granularity and represent the most efficient type of economic signal. Furthermore, given the expected more active role of consumers, in the distribution system and the market, we can expect them to follow price signals and minimize their power procurement costs using their flexibility potential.

To this end, this thesis aims to provide a systematic analysis of the impact of price signals of different granularity on the distribution system and social welfare. In the light of the electrification of thermal demand, the thesis will focus on residential HPs as a major source of flexibility and a significant additional load within the power system. To this end, a framework consisting of realistic scenario design, calculation routines, and proper result analysis is needed. To do so, this thesis provides the following contributions to the existing literature:

- Collection and aggregation of a large distribution system dataset that allows simulations as close to reality as currently possible based on publicly available data
- Development of a synthetization method for distribution grid models based on high-resolution spatial data
- Evaluation of a fully electrified residential heat demand under different price signals
- Development of a general framework for assessing the impact of DLMPs in comparison with different pricing signals both from a technical and economic perspective
- Ultimately, a first assessment of the policy implications of DLMPs in the context of current discussions

1.5 Publications

In preparation for this thesis, additional scholarly works by its author have been produced and are partially presented in this dissertation. Find below a list of publications and software releases with contributions by the author.

Conference papers

1. A. Bidel, **T. Schelo**, and T. Hamacher, "Synthetic Distribution Grid Generation Based on High Resolution Spatial Data". Presented at the 2021 IEEE International Conference on Environment and Electrical Engineering (EEEIC) in Bari, September 2021. doi: `10.1109/EEEIC/ICPSEurope51590.2021.9584691`.
2. **T. Schelo**, A. Bidel, and T. Hamacher, "Biogas Plant Operation under Distribution Locational Marginal Prices". Presented at the 2021 IEEE PowerTech in Madrid, June 2021. doi: `10.1109/PowerTech46648.2021.9494774`.

Software releases

1. S. Troitzsch, **T. Schelo**, V. Kleinschmidt, K. Zhang, and A. Ahmed, MESMO - Multi-Energy System Modeling and Optimization, Zenodo, 2021. doi: `10.5281/zenodo.4896047`. Available open-source: `https://purl.org/mesmo/repository`
2. **T. Schelo**, A. Bidel, BiPMo – Biogas plant model, version v0.1.0, 2020. doi: `10.5281/zenodo.4234721`. Available open-source: `https://github.com/tum-ens/bipmo/`

1.6 Organization of this thesis

The remainder of this thesis is organized as depicted in Figure 1.2. The subsequent Chapter 2 provides an overview of the inner workings of electricity markets and embeds the remaining chapters in its context. Chapter 3 introduces the data used for the parameterization and synthetization of thermal load and distribution grid models. Chapter 4 then introduces the ongoing electrification of the residential heat sector and the impact of cost-minimizing aggregators in combination with time-varying price signals. Chapter 5 then introduces our distribution grid synthetization methodology that allows generating realistic grid models. Chapters 6 and 7 present the analysis framework and the results of the simulation in detail. The discussions

Chapter 2

Electricity markets and their locational nature

Preliminaries on energy markets, price discovery, and the concept of social welfare as well as current developments in the European energy system.

Chapter 3

Data basis and context

Introduction of the underlying data that is used to generate realistic scenarios, in particular thermal building and grid models.

Chapter 4

Electrification of the residential heat sector: A case study

Evaluation of the impact of high HP penetration in the power system in the context of dynamic price signals.

Chapter 5

Electric grid synthetization

Synthetic distribution grid model generation based on high resolution spatial data.

Chapter 6

Analysis framework

Development of a framework for the analysis of DLMPs and detailed problem and model formulations.

Chapter 7

Simulation and results

Simulation scenario design and presentation and discussion of the results.

Chapter 8

Policy implications and discussion

First assessment of policy implications for the implementation of DLMPs based on the discussions from Chapter 2 and 7.

Figure 1.2: Organization of this thesis

on policy implications in Chapter 8 finally close the frame around the thesis. We conclude in Chapter 9 with a summary and an outlook on future studies.

Chapter 2

Electricity markets and their locational nature

The emergence of DERs has led to fundamental changes in power systems worldwide and will continue to challenge and change them dramatically over the following decades. These changes are also affecting existing power markets and driving them to adapt accordingly. Electricity markets are particular types of markets, as supply and demand must be balanced at all times, and the delivery of the commodity is bound to strict physical laws. This leads to a highly locational nature of power generation, consumption, and trade. Consequently, electricity has a locational value, which is handled differently in current electricity market setups, as we will discover throughout this chapter. To this end, this chapter aims to build an intuition about the basic principles of electricity spot markets and price discovery, which is at the core of the analysis in this thesis. The subsequent section will provide an overview of electricity market fundamentals. However, the section will not cover exhaustive treatment of regulatory and organizational issues but will focus instead on the fundamental mechanisms of price discovery in competitive electricity markets and how they deal with the underlying grid and its physical laws. After that, the following section will discuss in more detail the principle of nodal pricing and its role as a benchmark for market efficiency. The final section of this chapter will then briefly look into the future developments of power markets that are currently under discussion, focusing on a European setting, which will embed the analysis and the discussions in this thesis into a broader context.

2.1 Fundamentals of electricity markets

As opposed to traditional, unorganized markets, electricity markets can be referred to as designed markets, i.e., they were set up according to specific regulatory processes because of the importance of electricity as an essential service for societies and industry, and because of its particular properties [24]. According to [15], [24], [55], [56], every electricity market must deal with the following challenges:

1. Supply and demand must be balanced at all times, and electricity cannot be stored economically yet, which is why the value of electricity varies over time.
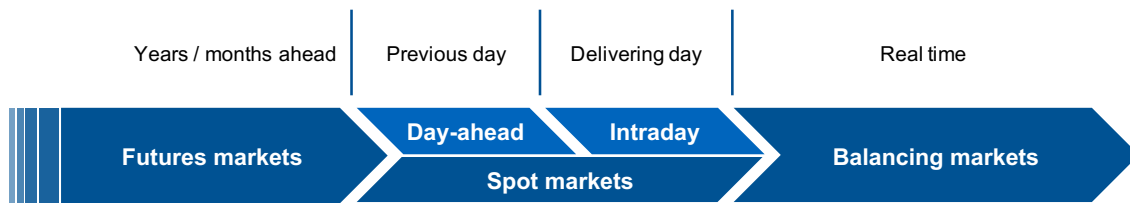
Figure 2.1: Illustration of different types of electricity markets that are commonly in place in relationship to the time of delivery on the far right

2. Physical limits of the transmission grid and generating sources must be obeyed at all times to prevent malfunction or the physical destruction of the system. Furthermore, electricity flows cannot be controlled easily as they must obey the physical laws of power flow. Hence, electricity has a different value over space.

3. Uncertainty in both supply and demand is increasing, as generators and network elements fail at times, demand varies, as well as the supply from uncontrollable Renewable Energy Sources (RESs). The ability to change the consumption/output of electricity at short notice, namely flexibility, consequently has a value.

Worldwide, there are different ways of dealing with these challenges. However, competitive electricity markets are all set up according to two basic principles: (i) To deal with balancing supply and demand with uncertainty on both sides, several subsequent markets are in place that complement each other and adjust the initial schedules to minimize deviations between schedules and final energy injections and withdrawals. The value of flexibility is mainly reflected in reserve capacity markets where the ability to generate or consume electricity is traded rather than energy volumes. (ii) Concerning the physical limitations, they can either be reflected or neglected in the market, which in the latter case means to deal with them according to ex-post compensation rules. This leads to different levels of granularity in the price discovery, which is at the core of this thesis.

Regarding (i), electricity markets in most countries worldwide have evolved to be separated into a set of different types of markets that are distinguished by their time to delivery of electricity in real-time and by the traded commodity: Energy or capacity. A summary of the markets that are typically in place can be seen in Figure 2.1. The adaption of several sequential markets has technical and financial reasons [24]. From a technical perspective, especially large thermal units need to schedule well in advance due to certain ramp-up and ramp-down constraints and related costs. Long-term trading of electricity in the futures markets decreases price volatility in the markets closer to the time of delivery and lowers the risk of participants exerting market power. In the context of this thesis, we will focus on the so-called spot markets, which refer to the day-ahead and/or intraday market and, in some regions, also the real-time market. In this case, the real-time market applies the identical principles of the day-ahead market again five minutes before delivery [24]. Following, we will use the term spot market and day-ahead market equivalently. The day-ahead market plays an essential role as it creates a forecast economic dispatch while, depending on the setup, performing congestion management by allocating scarce transmission resources between zones or nodes [16]. This way, the day-ahead market directly or indirectly reflects the physical limitations of the grid, as we will now discuss further.

To elaborate on the physical restrictions in (ii), just as with any physical good, the transportation of electricity can be subject to congestion constraints, which, in the case of common physical goods, can be alleviated by taking a different delivery path. However, in contrast to common physical goods, electricity cannot be sent along a specific contracted path but must follow the physical laws of the electricity grid. They divide this good among different lines according to Kirchhoff's law [57].

There are different philosophies behind the design of competitive electricity markets and how to deal with the physical laws of the underlying system. These differences in market design are rooted in individual technical, historical, and political and regulatory circumstances and have led to a variety of market concepts in place today. To understand the general mechanisms of competitive electricity markets, we will now develop an intuition of how markets are cleared based on economic theory and how the underlying electricity grid is reflected.

2.1.1 Price discovery in electricity markets: a simple example

The goal of every electricity market should be to maximize social welfare and to increase the system efficiency [24]. A common way of explaining the mechanism of price discovery and the locational value of electricity in competitive electricity markets is by looking at a simplified two-node network, as inspired from [57]: In a perfectly competitive market setting, where the transmission grid is neglected, all market participants can be represented as being located at a single transmission node, which is often referred to as one large "copper plate". With given generation capacities and no consideration of fixed or investment costs, the marginal cost of the marginal generator needed to serve all demand sets the uniform market-clearing price for all participants. We assume that the TSO clears the market as the independent market operator. Such a market situation is depicted in the simplified example in Figure 2.2 in the left graph for a single time period of the day-ahead market. We assume a single generator with a marginal cost function for generation $C(q) = q$, where q denotes the electricity production quantity. Consumption is described as an inverse demand function $p(d) = 10 - d$, with d being the electricity consumption quantity. As can be seen in the left graph in Figure 2.2, for the case of no transmission constraints, the intersection point A of the supply and demand curves characterizes both the equilibrium price of 5 €/MWh and the equilibrium of consumption and production of 5 MWh. Social welfare for the time period under investigation, which is the sum of consumer and producer surplus as represented by the areas between the demand and the supply curve, amounts to 25 €.

Now, let us assume that demand and generation are located at two different nodes in the network that are connected by a lossless transmission line with a capacity of 2 MWh. Generation is located at the southern node, and demand is located at the northern node. The described optimal solution with a generation and consumption quantity of 5 MWh evidently violates the transmission capacity, leading to the potential destruction of the transmission line if no corrective measures are taken. The reason for this physical infeasibility lies in the missing "congestion signal" of the uniform price, i.e., the uniform price does not incentivize an optimal use of the transmission line that interconnects the two nodes. Therefore, in an optimal solution that directly accounts for the limited transmission capacity between the two nodes, more than one (uniform) market price is needed to clear the market at both nodes,
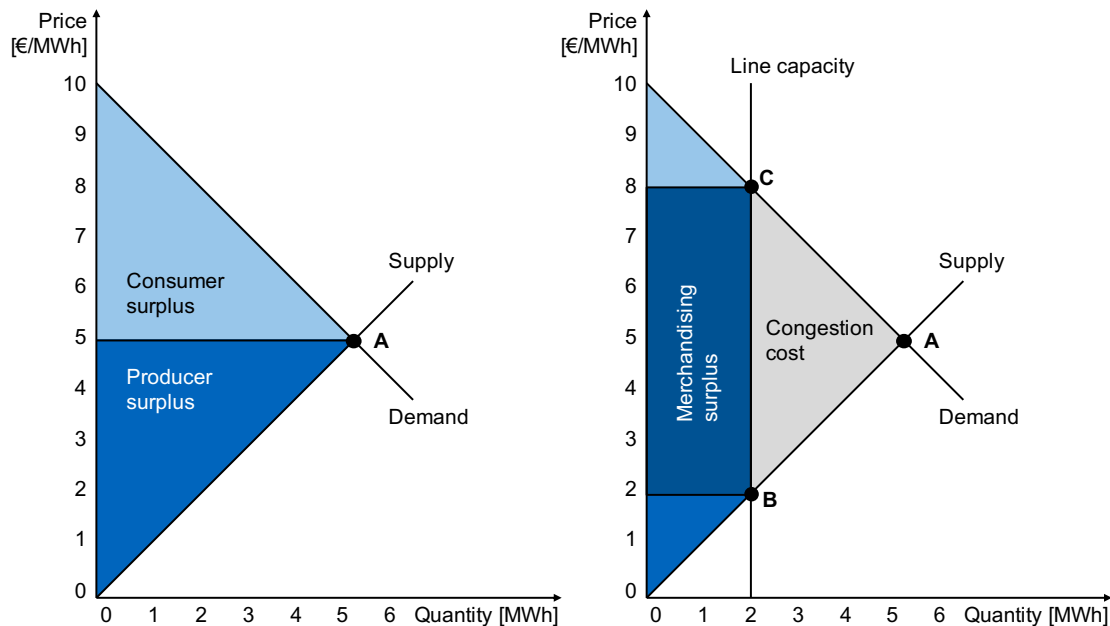
Figure 2.2: Price discovery in a two-node network for an unconstrained (left) and constrained (right) case, inspired by [57]

referred to as market splitting. Now looking at the right graph in the same Figure 2.2, for this case, in the south, the price will fall to 2 €/MWh with a corresponding optimal production of 2 MWh (point B). Analogously, in the north, the price will rise to 8 €/MWh reducing northern consumption to 2 MWh (point C), to make use of the transmission capacity optimally. The dark blue area in Figure 2.2 describes the so-called congestion rent or merchandising surplus that the TSO earns due to the price difference between the north and the south, which results from the fact that consumers pay more than producers receive. Hence, the TSO facilitates the market splitting as a spatial arbitrager. This merchandising surplus may be used by the TSO for network maintenance or expansion measures to ultimately free the grid of any congestion constraints in the long run, if financially viable. That is why the TSO must be an independent and regulated entity, as it would otherwise profit from a weak transmission grid. When turning to the welfare effects of the optimal network-constrained solution, as expected, welfare decreases compared to the unrestricted (single-node) case. The light grey area in the right graph of Figure 2.2 indicates this congestion cost, which is the welfare loss of an optimal network-constrained solution as compared to the unrestricted case with a uniform market price. Considering a uniform price, the resulting schedules must be adapted ex-post through counter trading or other corrective measures, which cause additional costs. The total effect on the overall costs of the counter trading (or corrective measures) is uncertain and will also depend on how the market is regulated. An upper bound on what can be achieved is the congestion cost (see the light grey area in Figure 2.2) of the optimal network-constrained solution, taking into account all grid constraints [58]. This optimal network-constrained solution is called nodal pricing, and the prices are termed LMPs. It represents the theoretical optimum and, therefore, the most efficient solution for managing congestion.

2.1.2 Practical implications

Finding our way back to real power systems, several simplifications from this small example must be pointed out. Although representing the most efficient solution, nevertheless, nodal pricing-based markets are only implemented in a few electricity markets worldwide.

One central point is that real power systems are much more complex than our simple two-node example, and the resulting social welfare optimization is computationally expensive and non-intuitive, as authors in [24] explain: In the simplest case, each supply resource has an increasing marginal cost curve, each demander has a decreasing marginal value curve, and all constraints on resources are linear. The optimization then is a standard convex optimization. Each supplier sells its profit-maximizing quantity at each time and location, given the prices and the physical constraints. Each demander buys its profit-maximizing quantity at each time and location, given the prices and constraints. The LMPs thus represent the cost of generating one additional unit (MWh) at the location in the given time period. These linear prices are used for settlement. However, the actual day-ahead optimization is not that simple, as there exist several non-convexities. They stem, for example, from ramp-up and ramp-down constraints of generators, which cause the supply curves to be non-linear. Furthermore, transmission losses are often neglected. In addition to the challenges of limited line capacities, losses cause further complexity for efficient congestion management [57]. This high complexity makes the resulting prices less intuitive as the non-convexities are dealt with by first calculating quantities and then approximating prices [24]. Nonetheless, the authors also suggest that the non-convexities, while important to address, are not too disruptive.

Another implication of nodal pricing-based markets in real power systems is the fact that the limited number of traders may yield relatively low liquidity and possibly low competition at individual nodes [57]. This can, in turn, lead to the exertion of market power at very weak nodes that are connected through often highly congested transmission lines. Congestion in the grid causes market splitting, which reduces the number of participants in every single market. One famous example for the abuse of market power in a competitive nodal pricing-based market setting was the infamous California energy crisis in the early 2000s, which was also discussed in the scientific community, see for example [59]. Apart from the low number of traders, another factor that increases the risk of abuse of market power is the small price elasticity of the demand side, which facilitates the exertion of market power by the producers. According to [60], on a price versus quantity diagram, the slope of the demand curve is very steep in reality, as opposed to our simplified example from above, which means that consumers are willing to accept even very high prices in exchange for the supply of electricity. Two economic and social factors explain this weak elasticity. First, the cost of electrical energy makes up only a small portion of the total cost of producing most industrial goods and represents only a small fraction of the cost of living for most households. At the same time, electricity is indispensable in manufacturing and most individuals in the industrialized world regard it as essential to their quality of life, while there is generally no substitute product to use instead. Therefore, most industrial consumers will not reduce their production drastically to avoid a slight increase in their electricity costs. Rather than simply reducing their demand in response to a sudden increase in the price of electrical energy, consumers instead may decide to delay this demand until a time when prices are lower. For example, residential consumers in some countries

take advantage of lower nighttime tariffs by waiting until later in the evening to wash and dry clothes or heat water. Shifting demand is possible only if the consumer can store intermediate products, like heat or electrical energy. Furthermore, managing demand requires more flexibility or more willingness to accept a loss of convenience than may be available. Therefore, most small residential and commercial consumers will not be very interested in reacting to hourly or half-hourly price changes. However, the ability to shift or delay demand instead of reducing it entirely is the basic principle of the flexibility potential exploited in this thesis.

2.2 Nodal pricing as the ultimate price signal

The simple example from above provides intuition about the locational value of electricity in different grid locations. This section presents the principle of price signal granularity from a more practical standpoint and discusses how the economic theory behind the price signals can serve as an efficiency proxy.

2.2.1 Uniform – zonal – nodal pricing

As discussed above, representing all market participants at a single node, we derive a uniform price signal equal for all. However, representing market participants at their individual nodes and with the entire transmission grid included, we derive different price signals for all nodes given congestion (or other binding constraints) in the grid. Thus, we are inherently increasing the spatial granularity of the price signals in the system. This spatial granularity is a major differentiating factor of electricity markets. Typically, one can distinguish between three types of electricity spot markets (day-ahead) with ascending spatial granularity: (i) uniform pricing, (ii) zonal pricing, and (iii) nodal pricing, as depicted in Figure 2.3. As explained above, uniform pricing models neglect all transmission constraints and completely separate energy trading from transmission [57]. This type of market-clearing method commonly leads to violations in grid constraints, which is why an ex-post adjustment of market quantities must follow it in the form of a redispatch. Here, schedules of generators are adjusted, resulting in a feasible power flow at the expense of redispatch costs, as the respective market participants must be compensated for this adjustment through, e.g. counter trading. The problem is that these measures are expensive, but the market does not reflect these costs. That is why social welfare (as defined in the context of this thesis) of markets with a uniform price is highest, while consequently, the costs for redisptach are greater compared to markets with higher price granularity. Finally, the consumer is held accountable for the costs that occur due to the inefficient uniform pricing-based market. In combination with more uncontrollable generation from RES in the market, this leads to increasing electricity costs for the end consumer [15].

As a compromise between uniform and nodal pricing markets, zonal pricing can be viewed as an approximation of the nodal pricing scheme [58]. The market is divided into fixed price zones, where a uniform price is found on market-clearing within each zone. The zones are defined, so that grid constraints ideally do not occur within a zone but only between zones. This way, prices can vary only between zones, and the need for ex-post adjustment is minimized, as potential occurrences of congestion in the grid have been taken into account already during market-clearing. The grid is then represented in an aggregated form, with one zone being
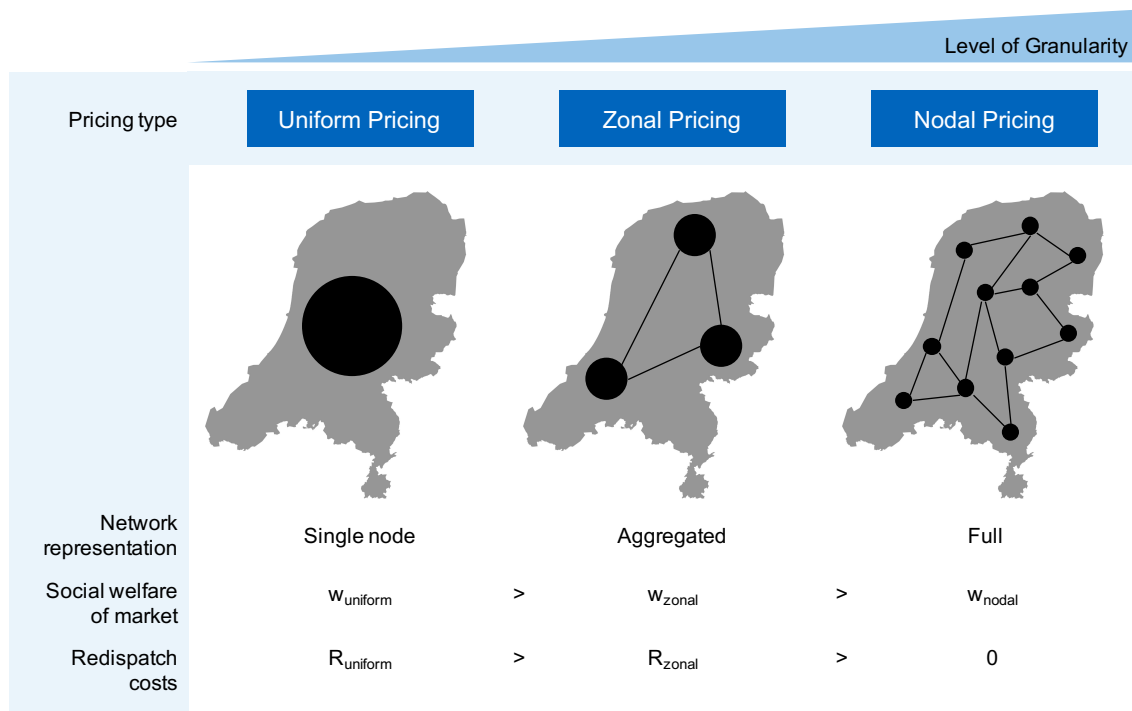
Figure 2.3: Social welfare and redispatch cost in uniform, zonal, and nodal pricing

equivalent to one larger node. One example of a zonal pricing market is the European electricity system: Single markets with uniform prices are coupled to form a large zonal pricing-based market. However, the authors in [58] claim that by using the national borders as zone limits to a great extent, it is questionable whether the price signals are based on real transmission constraints. If the market is cleared only with respect to the capacity limits between the zones, the internal bottlenecks will have to be resolved by counter trading or counter purchases, just like with uniform pricing. This implies a subsequent welfare loss following from the redistribution of quantities produced and consumed due to the counter trading, which is reflected in the redispatch cost, as seen in Figure 2.3.

When decreasing the size of the zones to its bare minimum, consequently increasing the spatial granularity of the price signal, one will end up at the nodal level of the underlying transmission grid. The resulting prices of maximum spatial granularity are termed nodal prices. These nodal prices are unique in the sense that they give the optimal value of energy in each node and that other mechanisms for dealing with transmission constraints must be consistent with these optimal nodal dispatch quantities to provide the same optimal solution. The optimal nodal prices can therefore be used as a benchmark when evaluating other methods for congestion management [58], as with a combination of a day-ahead and real-time market, no additional costs for redispatch will occur (see the right column in Figure 2.3). However, nodal pricing should not be mistaken with the final evolution step of electricity markets but rather a reference that any regulatory instrument, such as redispatch, feed-in management or regionally differentiated support schemes, should aim to match. Therefore, the following subsection elaborates more on this relationship and how it can serve as a measure of efficiency.

2.2.2   Evaluating price signal efficiency

The primary objective of congestion management methods is to alleviate network congestion and achieve an efficient dispatch of all resources. For the case of DLMPs, there exist numerous studies that simulate the operation of electric distribution grids under different scenarios and present their functionality, which have been presented in section 1.3. The studies conclude that DLMPs are indeed an effective method for alleviating congestion as well as voltage violations, and for minimizing losses. However, the studies fail to assess and quantify the efficiency and thus their actual benefit.

Market-based congestion management is purely based on price signals to steer the behavior of market participants, i.e., the consumers and producers. These nodal prices affect and alter the economic outcomes of the market compared to other pricing methods, as was shown above. To assess the overall benefits of congestion management methods, it is essential to understand the impact on individual surplus and overall welfare, as authors in [58] point out. This yields insights into the economic performance of nodal prices or markets in general, as all markets aim to maximize social welfare, and the welfare loss can serve as an indicator for the minimum costs of any countermeasure to achieve the optimal dispatch quantities of the nodal pricing-based market. The construct of social welfare is widely employed in welfare economic analysis and when determining the benefit of implementing policies [61]. Previous research has investigated the effects of price signal granularity on social welfare of transmission level wholesale markets [57], [62], [63]. To this end, the impact of price signal granularity on social welfare forms a cornerstone of the subsequent study of this thesis.

Finally, it is a question of regulatory, social and technical concerns, which of the pricing schemes a market applies. However, in light of the increase in uncontrollable RES and new intermittent loads such as EVs or HPs, the necessity and value of a market-based principle such as nodal pricing become more apparent, as support schemes and regulatory instruments become more complex and must be designed for regions individually, due to the locational nature of the energy system [15]. New formats for the European electricity system and its markets are being assessed and should therefore be mentioned for a proper discussion of the analysis results. The following section will therefore shed light on current issues.

2.3   European electricity markets in transition

Electricity markets have evolved from centralized monopolies to carefully designed markets that continuously change and adapt to technological, societal and political trends [15]. Existing market rules are based on the predominant generation technologies of the last decades, which means centralized, large-scale fossil fuel-based power plants with limited participation by consumers. The current transition is primarily driven by a strong trend away from traditional thermal generation technologies to wind and solar photovoltaics (PV) to address climate change. This is expected to continue over the following decades until fossil fuels are largely eliminated from the energy system. Technological progress can be identified as the second driver, which can be observed in falling costs for renewable technology and advances in storage and communication technology that can unlock the considerable potential of demand response. The main challenges for the market arise from PV and wind which share three

characteristics: (i) intermittent supply, (ii) zero marginal cost, and (iii) no (or limited) inertia. With today's share of traditional thermal power plants, there is sufficient inertia in the system, however this will become an increasing problem in the future, and markets will have to provide the right incentives and compensations to cope with these challenges. Still, today's best-practice market designs are likely to be able to support high levels of RES. European markets have run reliably with more than 50% of energy coming from wind. What is required as renewable penetration increases is the routine adjustment of market parameters such as the requirements of ancillary services, as well as the steady improvement in the market design to make the system more responsive and flexible [24].

To this end, European regulators and system operators are actively discussing potential changes to the current market design, as found in [1], [16]. Due to the lack of more granular cost-reflexive signals, European markets are not well suited to deal with increasing levels of renewable energy in the long run, and they do not embrace demand-side flexibility as prices are distorted by neglecting the physical system within price zones [15]. The strong regional focus of utility-scale RES in the form of, e.g. large off-shore wind parks, makes these market inefficiencies more apparent: When its physical limitations restrain the system from delivering high amounts of wind energy from a large supplier to a large demand center and eventually to the consumer down the voltage levels, markets must reflect this scarcity to prevent inefficiencies. From a theoretical standpoint, under the presence of transmission constraints, a uniform or zonal pricing scheme cannot guarantee efficient market outcomes, as scarcity is not reflected on a local level [15]. In addition, the demand side is becoming more active, emphasizing the empowerment and engagement of consumers [64]. Efficient market signals will stimulate the necessary investments and provide opportunities for consumers to reduce their electricity costs by actively participating in electricity markets through flexible DER technologies, such as demand response, distributed generation technology, or storage systems.

Therefore, a proposal for a directive on common rules for the internal market in electricity by the European Commission [65] calls for an adaption of the traditionally more rigid market and grid operation rules to a more flexible market-based fashion with little to no distortion of prices by public intervention, to maintain the stimulating short-term and long-term effects of the economic signals. The European proposal puts a strong focus on the consumer with the argument that a flexible demand side can significantly reduce the need for grid expansion or new backup capacities. That is why a critical goal of current European energy policies is to further open electricity markets to consumers [16]. Consequently, they see activating consumer participation at the core of managing the energy transition successfully and in a cost-effective way. While the current market design barely provides any incentive for active participation of the demand side, the proposal envisions transparent real-time price signals that stimulate consumer participation, either individually or through aggregation.

Market-based mechanisms to properly control all resources are promoted by policy-makers, regulators, and researchers alike. To increase market efficiency, authors in [15], [24], [66] strongly advertise the adoption of LMP-based wholesale markets in Europe. However, with the emergence of DERs, another problem with the current market setup is that small DERs participate in the market through aggregation without considering their location within the distribution grid. If not controlled properly, this can lead to voltage violations and congested

lines on a distribution grid level [7]–[10], [64], as uncoordinated trade on a distribution level reproduces the problems of the transmission grid in the lower voltage levels.

While authors in [15] claim that the effect of transmission LMPs carries over down the voltage levels, this needs further evaluation. After having now built an intuition of the price discovery in electricity markets and how they connect to the physical laws of power flow resulting in optimal temporal and locational signals, these concepts can now easily be transferred to the distribution grid level. Consequently, DLMPs naturally extend the principles of LMPs and are thus in the spirit of the envisioned European electricity market design guidelines. To this end, they deserve a profound analysis concerning their efficiency and their need in the future power system.

We have learned in this chapter that the choice of market design is based on many factors that range from regulatory over social to technological circumstances. To this end, it becomes apparent that realistic data is needed for the analysis, as the underlying grid and its characteristics are particularly important to draw conclusions from the results and discuss them in a European context. That is why the following chapter will cover the context and data basis used for modeling and simulating a realistic European distribution grid setting in this thesis.

Chapter 3

Context and data basis

For an adequate analysis of DLMPs, a sound knowledge of the DERs and the underlying electric grid is needed, as they have a significant impact on the resulting power flow and consequently the price signals. In this chapter, the data used for the subsequent analysis of different economic price signals is presented. The data were collected from different public sources, aggregated, and connected in a relational PostgreSQL database with a PostGIS extension to exploit the potential of spatial data efficiently. The following sections discuss the data requirements and summarize the available data sources and their characteristics.

3.1 Data requirements

The analysis of economic price signals significantly depends on the context in which they are embedded. This section intends to summarize the requirements of the data needed for the analysis. One major hurdle is the availability of data, as security and privacy issues are a major concern when it comes to making power system data available to the general public or the scientific community.

To be able to define the data requirements, we must first understand how the "context" in which our analysis is embedded is characterized. To this end, we define two main differentiating factors that render the context in an adequate manner, namely region and locality. In this thesis, region specifies the broader regional focus of our analysis, which we define to be set in continental Europe. Note that regulatory and organizational issues are not in the focus of this thesis. Instead, we are interested in the region's strong influence on how the grid is designed and operated and typical energy consumption behavior. The locality factor is defined by the population density and, in this thesis, can either be rural (low population density), suburban, or urban (high population density). This again influences the grid architecture and the types of loads that can be encountered in the distribution system, as authors in [67] point out.

As DLMPs are the result of an optimal power flow calculation and thus implicitly represent grid conditions, the underlying grid model is of utmost importance. However, the availability of grid models that accurately represent a particular region, such as Europe, is limited to small and often incomplete sets of public test systems. Distribution networks are often considered critical infrastructure, and detailed load/consumer data sharing leads to privacy concerns. As a result,

very few actual networks are publicly available. This has driven the research community to primarily use the available test (benchmark) networks that have been published in the literature to date, as found in e.g. [68]–[73], even though the purposes they serve very often go beyond the original intentions of their creators as reported in [74]. To this end, one major requirement for the analysis is realistic grid models.

Furthermore, the loads and generators in the grid must be specified realistically. In the context of this thesis, we define any type of load or generator under the general term DER. However, the focus of this thesis lies on the evaluation of the residential heat demand, which is why distributed generators, such as PV, are neglected. The loads are represented by (i) household loads which are considered as fixed in the context of this thesis, and (ii) flexible loads such as HPs. Considering the fixed loads, corresponding time series are needed with a temporal resolution of 30 minutes to one hour. For residential heat demand, building data is required to properly model the thermal characteristics of buildings and the resulting heat demand profile. Directly related to this, the defined region inherently defines the underlying climate. In addition, the region also implies corresponding electricity prices. For the chosen region, the analysis, therefore, requires climate data and wholesale market energy prices.

The Dutch government is exceptionally progressive in making data available to the public in terms of their quantity and accessibility. That is why it is decided to move forward with a focus on the Netherlands. It is a representative country for continental Europe and most of the data needed for the analysis is provided directly or indirectly in several sources by the Dutch government or associated agencies. The following sections provide an overview of the raw data used in the remainder of this thesis.

3.2 Grid data

While the transmission grid in the Netherlands is mainly operated by TSO TenneT, which also owns and operates large parts of the German transmission grid, the distribution grid for both electricity and gas is mainly split among four large DSOs, namely Enduris, Enexis, Liander, and Stedin. Next to five additional smaller DSOs, their operational areas of the grid are separated as depicted on the map in Figure 3.1 with Enexis covering the largest share of the distribution grid in terms of area and total line length on both Low Voltage (LV)- and Medium Voltage (MV)-level, as can be seen in Table 3.2. Since the year 2019, Dutch DSOs agree to publish up-to-date spatial data on their electricity and gas grids and make it accessible through their open data platforms which can be found in [75]–[78] for the four largest DSOs, respectively.

In the context of this thesis, we are exclusively interested in the electricity grid. However, not all DSOs provide the same level of detail for their respective grid data. A comparison can be found in Table 3.1, with Enexis providing the highest level of detail in their dataset. Furthermore, the table also shows that none of the datasets contain information on the cable or the transformer types.

Figure 3.2 shows an example view of the spatial grid data provided by DSO Enexis. The image demonstrates the high level of spatial detail the dataset provides, as the exact paths of the cables of both MV- and LV-level are represented and the connections between line segments can be observed visually, which allows the potential derivation of a calculable network model.

Figure 3.1: Partition of the distribution grid in the Netherlands among the four largest DSOs

Table 3.1: Available information for the respective datasets

Data	Enexis	Enduris	Liander	Stedin
Location of line segments	✓	✓	✓	✓
Voltage levels of line segments	✓	✓	✓	✓
Line types	–	–	–	–
Location of transformers	✓	✓	–	✓
Transformer types	–	–	–	–
Location of distribution boxes	✓	–	–	–
Location of connection points	✓	–	–	–

Table 3.2 contains information on the total line length on each voltage level for the four major DSOs. For the cases of Enduris and Stedin, interestingly, the ratio between MV- and LV line lengths is almost equal to one, whereas for the other two DSOs the total length of LV lines is higher than that of MV lines, which is very typical as the LV lines branch out much more and therefore sum up to a very high line length. However, when looking at the map of the Netherlands, it becomes clear that both Enduris and Stedin operate grids in rather rural areas
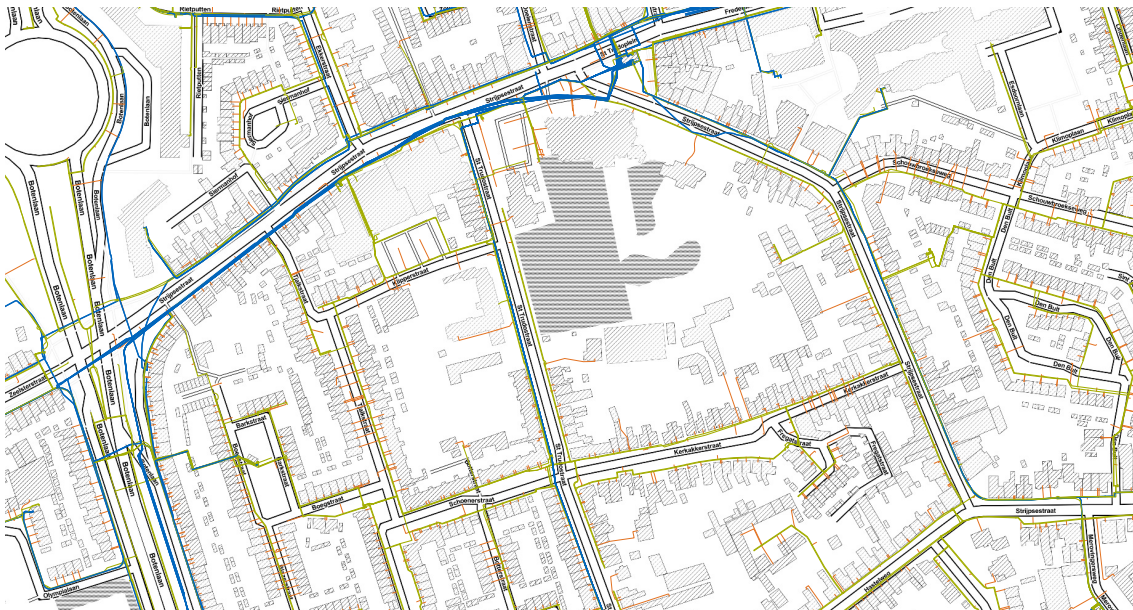
Figure 3.2: Example view of the spatial data provided by the Dutch DSO Enexis, with MV lines in blue, LV lines in green, connection cables in orange (map from [79], line data from [76])

(note that Rotterdam forms part of the Liander grid), and therefore LV lines are less frequent as the regions are less densely populated.

Table 3.2: Line length in kilometers of the available grid data [75]–[78]

DSO	Asset type	Length [km]
Enduris	MV lines	5664.6
	LV lines	5605.0
Enexis	MV lines	74847.0
	LV lines	105156.0
Liander	MV lines	38728.9
	LV lines	49506.5
Stedin	MV lines	15500.7
	LV lines	15659.6
	Total	**310668.3**

Altogether, the grid data allows an accurate representation of grid topology and line lengths. As we will later present in Chapter 5, for a small region, additional data on the line types have also been provided. However, the major part of the dataset does not include exact line type data, nor does it allow the conclusion of specific operation modes, such as radial or ring configurations, as the position and status of potential circuit breakers are not clearly identifiable. To this end, in Chapter 5 we will demonstrate the grid synthetization method that was applied to generate calculable and realistic grid models from the underlying dataset.

3.3 Building data

In this thesis, building data is used to model both electrical and thermal loads. In order to do so, we rely on several different datasets that provide information on building geometry, function, thermal properties, and individual electricity consumption profiles. The following subsections will briefly introduce these datasets and their respective sources.

3.3.1 BAG and 3dBAG dataset

The Basisregistratie Adressen en Gebouwen (BAG) (en: registry for buildings and addresses) is a publicly accessible database, which contains administrative and spatial data on property and the rights involved for roughly 10.2 million buildings in the Netherlands [80]. Among other information, it includes data on construction year, building function, and usable area. As for the building function definition, possible identifiers are listed in Table 3.3 in combination with some examples. Note that buildings that have a "cell" or "other" function are not further considered in this work, as their loads are either neglectable or their occurrence very rare. In addition, it should be noted that one building can indeed have more than one function, e.g. a shopping and residential function with the shop on the ground floor and dwellings above.

Table 3.3: Building functions as defined in the BAG dataset [80]

Building function	Examples
Meeting	Restaurants, religious buildings, exposition halls
Healthcare	Hospitals, dental centers
Office	Office space
Accommodation	Hotels
Educational	Schools, Universities
Sports	Sports centers, stadiums
Shopping	Shops, shopping malls
Residential	Households
Industrial	Factories
Cell	Prisons
Other	Every building not classified (Garages, sheds, etc.)

To get an overview of the building stock in the Netherlands, Figure 3.3 shows the distribution of construction years of all residential buildings contained in the dataset, which are the focus of this thesis and account for roughly 5.2 million buildings in total. For the sake of representation, only buildings that were constructed after the year 1700 are displayed. One can observe a high number of newly constructed buildings in the 1970's and 1980's. Furthermore, one can see the suspension of any construction during the Second World War. Finally, clear spikes can be observed in years that complete an entire decade, e.g. 1920, 1930, and so on. As this effect decreases over the years until the most recent buildings, it is safe to assume that these are based on imprecise documentation or assumptions, as the exact construction year was not well documented. However, as we will see later, a rough estimation of the year of construction suffices in the context of this thesis.

The dataset has been enhanced with detailed geometrical information about the height and shape of the buildings by researchers at TU Delft in [81], using aerial laser scanning. The
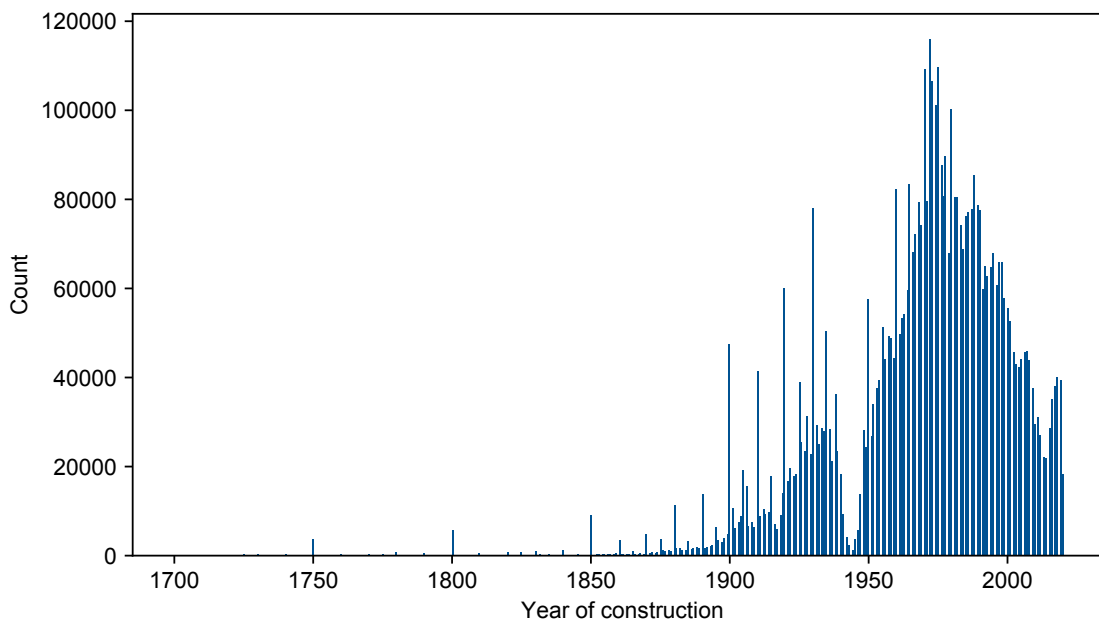
Figure 3.3: Number of residential buildings by year of construction in the BAG dataset [80]

dataset contains no definitive height data but rather statistical information on the raw measurement data. For constructions that are indicated to have flat roofs, the 95th percentile height is utilized, while for gable-roofed buildings, the 50th percentile serves to approximate the reduced volume of prismatic roofs. However, the data measurements are incomplete. Hence, the data quality is augmented by replicating missing values. To this end, omitted ground elevation is matched with the data linked to the nearest building. Missing rooftop data is inferred from a neighboring building if the two buildings are directly attached and joined by one wall. If missing data cannot be replicated, the building is dropped from further consideration.

When looking at the height distribution for residential buildings in Figure 3.4, one can reason that the majority of buildings can be assumed to be Single Family Houses (SFHs), with an average height of 7.4 m. The small spike on the far left of the histogram represents measurement errors or wrongful labeling. Consequently, these buildings will be discarded in our further discussions. Finally, Figure 3.5 represents the area of the geometrical footprint of all residential buildings. With an average area of roughly 90 m^2, this underlines our assumption that the majority of residential buildings are indeed SFHs.

In combination, this collection of data contains detailed information about the existing Dutch building stock concerning spatial, functional, and geometric properties. It allows generating detailed building geometries as depicted in Figure 3.6, which we will later use to parameterize a thermal building model. However, to fully parameterize such a model, information about the characteristics of the building material is needed. That is why the TABULA building typologies dataset was included in this thesis.
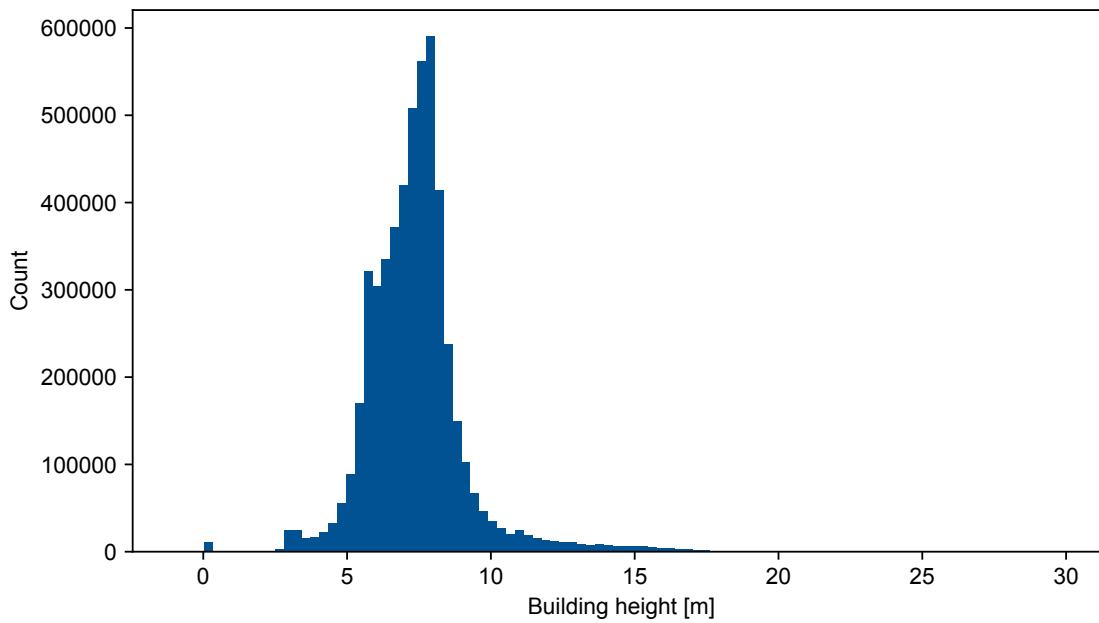
Figure 3.4: Number of residential buildings by height in meters in the BAG dataset [80]
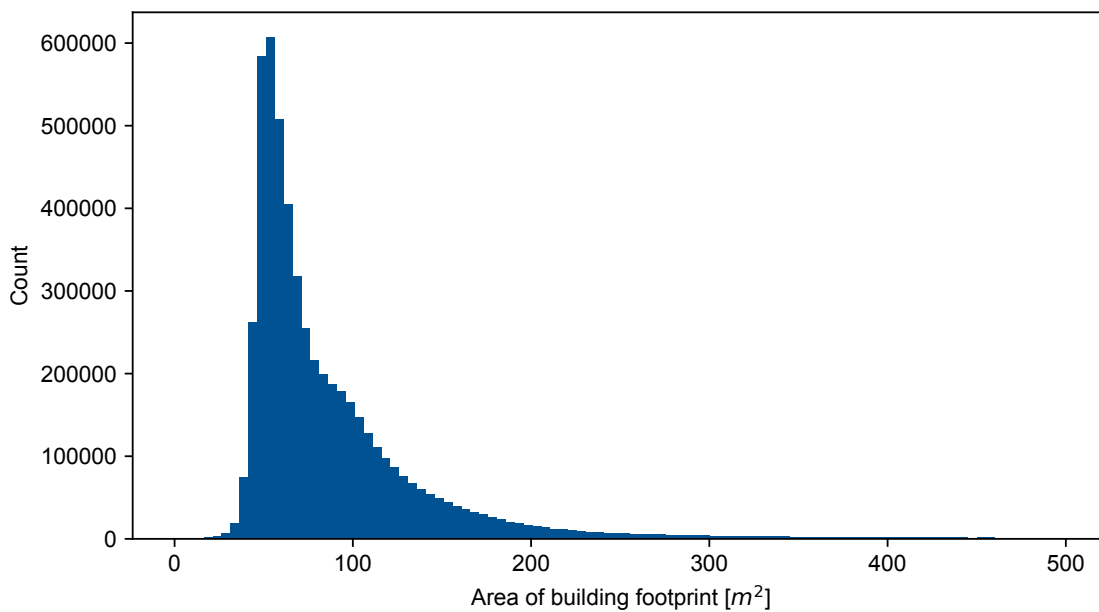
Figure 3.5: Number of residential buildings by area of their geometrical footprint in square meters in the BAG dataset [80]

3.3.2 TABULA building typologies

To fully parameterize a thermal building model, the geometry data is further enhanced using Typology Approach for Building Stock Energy Assessment (TABULA) Webtool, introduced in [82] and in the rest of this thesis referred to as TABULA. The publicly accessible dataset was
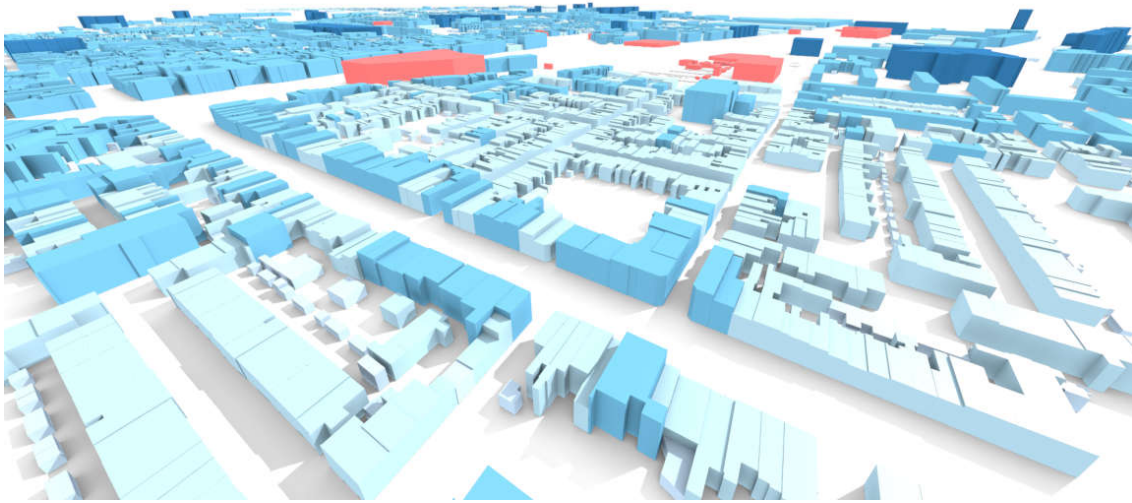
Figure 3.6: The 3dBAG dataset allows to generate 3-dimensional geometries enhanced with detailed building information [81]

created and maintained as part of the TABULA/EPISCOPE Project by the *Intelligent Energy Europe Programme* of the European Union. It contains information for 20 European countries, including the Netherlands, and classifies buildings according to their size, age, and additional parameters and a set of exemplary buildings representing these respective building types. It is enhanced with detailed information on materials used for specific construction elements (e.g. roofs, walls, etc.) and their characteristics in terms of thermal resistance and capacitance. This information is crucial for parameterizing thermal building models to derive their thermal demand profile over time. In addition, it classifies thermal supply systems and building reference areas, as well as typical annual energy consumption values. This will prove helpful for validating our thermal building model parameterization. Finally, the TABULA Webtool supports remote access through data endpoints which can be used for the automatic classification of buildings from the BAG dataset to the respective typology and its parameters from the TABULA dataset.

3.4 Electric loads

The detailed building data allows us to accurately represent the building's thermal demand and the respective electric demand, which we consider fixed in the context of this thesis. General practice is applying standard load profiles, as provided by the German Association of the Energy and Water Industry (BDEW) in [83]. However, as authors in [84] point out, for the case of residential loads, they cannot be used for the consideration of individual loads, but only for an aggregate observation of a minimum of 150 consumers together. To this end, we decide to choose two different approaches, for residential and all other loads. For all load profiles we use data from Germany, which we consider applicable to the Netherlands as well, given the socio-economic similarities between the two countries [85].

For the case of residential loads, we require a variety of different individual household loads. As publicly available consumer data is scarce, we rely on synthetic load profiles generated

based on public data applying the methods in [86] and kindly provided by the authors for use in this thesis. The dataset contains yearly load profiles of different household types synthesized through a bottom-up activity-based approach and validated based on aggregate statistics. It contains data for 1000 households of different types, which are listed in Table 3.4 in combination with their respective occurrence probability, which we derive from the information provided in [86]. Note that the probabilities sum up to only roughly 100%, as the profiles provided do not cover all possible combinations in [86]. However, these probability values can later serve in the realistic assignment of load profiles to residential buildings.

Table 3.4: Synthetic residential load profile types and their respective occurrence probability from [86]

Consumer type	Probability [%]
One full-time working man	10.90
One full-time working woman	16.35
One male retiree	4.90
One female retiree	3.55
One part-time working man	0.43
One part-time working woman	0.99
Two full-time working persons (m/f)	9.74
Two retirees (m/f)	14.62
One full-time working man, one part-time working woman	4.38
One full-time working woman, one part-time working man	3.18
Two full-time working persons (m/f) and one child	4.25
One full-time working man, one part-time working woman and one child	6.37
One full-time working woman, one part-time working man and one child	1.91
Two full-time working persons (m/f) and two children	3.06
One full-time working man, one part-time working woman and two children	4.59
One full-time working woman, one part-time working man and two children	1.38
Two full-time working persons (m/f) and three children	1.40
One full-time working man, one part-time working woman and three children	2.11
One full-time working woman, one part-time working man and three children	0.63

Like residential buildings, the electric power demand of commercial or industrial buildings follows characteristic profiles defined by, e.g. office hours or production schedules. To this end, we also represent commercial loads with fixed load schedules. Here, we rely on German standard load profiles, as provided by BDEW in [83], as the number of commercial buildings in our analysis is much smaller than that of residential buildings, and therefore, issues of load coincidence of non-residential buildings are not as significant. The BDEW standard load profiles serve DSOs in predicting power loads of various consumer groups, for example agricultural or industrial facilities. They define quarter-hourly load schedules for diverse commercial customer sub-categories with a normalized annual energy consumption of 1000 MWh, and are publicly available. Figure 3.7 shows the six BDEW standard curves that can potentially occur in this study. Table 3.5 contains the BDEW load profile IDs mapped to the respective building functions from the BAG dataset.
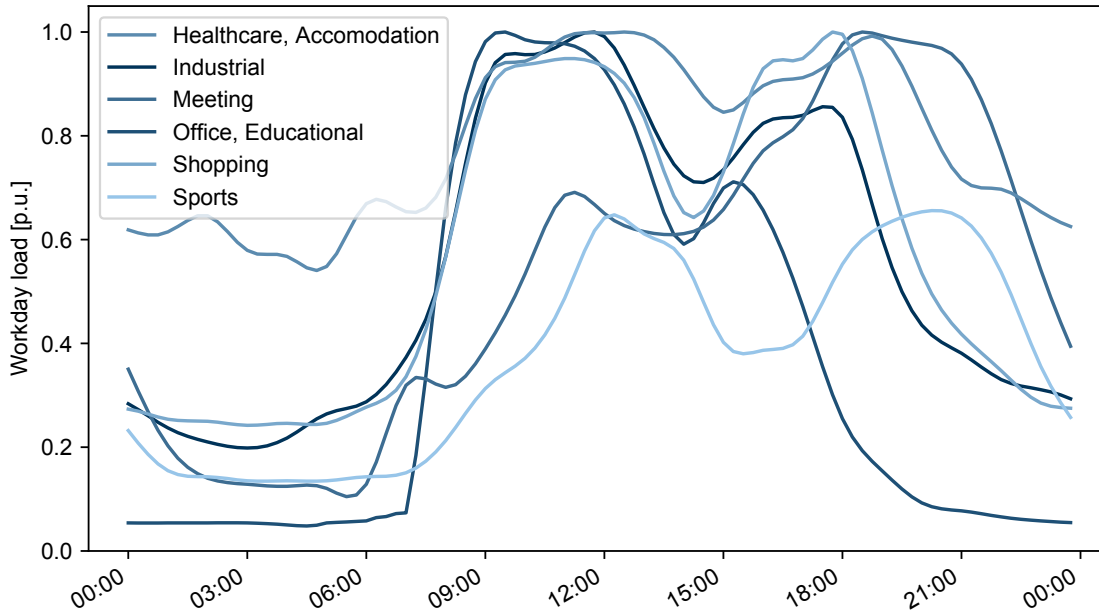
Figure 3.7: Workday load profiles in per unit of their peak load based on BDEW standard load profiles, as defined in [83]

Table 3.5: Mapping of building functions to BDEW standard load profiles from [83]

Building function	Load profile ID
Meeting	G2
Healthcare	G3
Office	G1
Accommodation	G3
Educational	G1
Sports	G6
Shopping	G4
Industrial	G0

3.5 Climate data

Interaction and heat transfer processes significantly determine the thermal behavior of a building with the surrounding environment. Most notably, this includes heat exchange due to a temperature gradient between ambient air and the inside of the building and heat input through solar irradiation. These two mechanisms can be modeled based on weather data time series. For the Netherlands, the Royal Dutch Meteorological Institute (KNMI) records multiple meteorological data measurements and provides datasets including historical time series, which are publicly accessible through web endpoints in [87]. For the parameterization of our building models, the dataset *Radiation - BSRN irradiance data at 1 minute interval at Cabauw* contains all relevant information. The measurements were performed in Cabauw in the province of Utrecht, with coordinates (Longitude, Latitude): 4.927734, 51.96828. We assume that it is applicable to most of the Netherlands. The irradiation data includes long- and short-wave downward irradiance, diffuse and direct irradiance, air pressure, relative humidity,
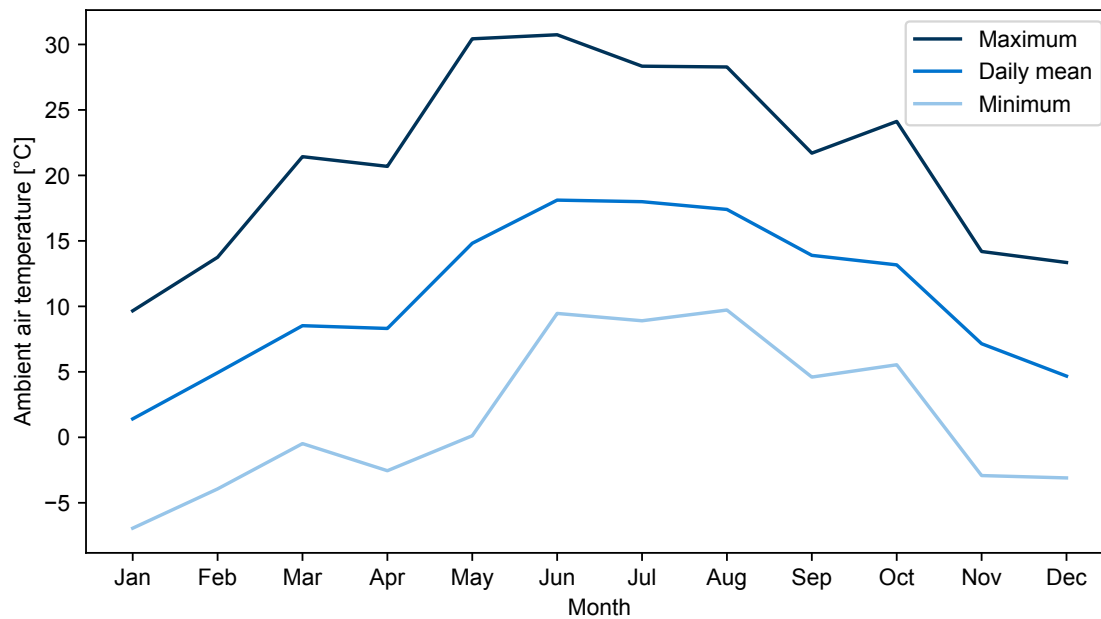
Figure 3.8: Ambient air temperature over the year 2017 as provided by [87]

and ambient air temperature. The data is provided in a high temporal resolution of 60 s intervals. Figure 3.8 shows the ambient air temperature as measured in Cabauw for the year 2017. As we can see, the Netherlands experiences moderately warm summers and cool winters with temperatures below zero degrees, which has a strong influence on the heating demand during the winter season.

3.6 Wholesale market data

In addition to the data required to parameterize realistic models of the power system and thermal buildings, wholesale price data is also required. For this purpose, historic market data from the *EPEX SPOT Power NL Day Ahead Market* is used, which was acquired through the European Network of Transmission System Operators for Electricity (ENTSO-E) Transparency Platform in [88]. The data contains the wholesale day-ahead electricity price for the Netherlands for the time period of 1st of January 2016 to 31st of December 2019. It reflects the hourly day-ahead prices for electricity derived in an auction process matching supply and demand on the transmission grid level. The mean wholesale price is depicted in Figure 3.9. From the light blue area we can observe wholesale prices reaching much higher maximum prices during winter season, especially in the colder winter months of January.
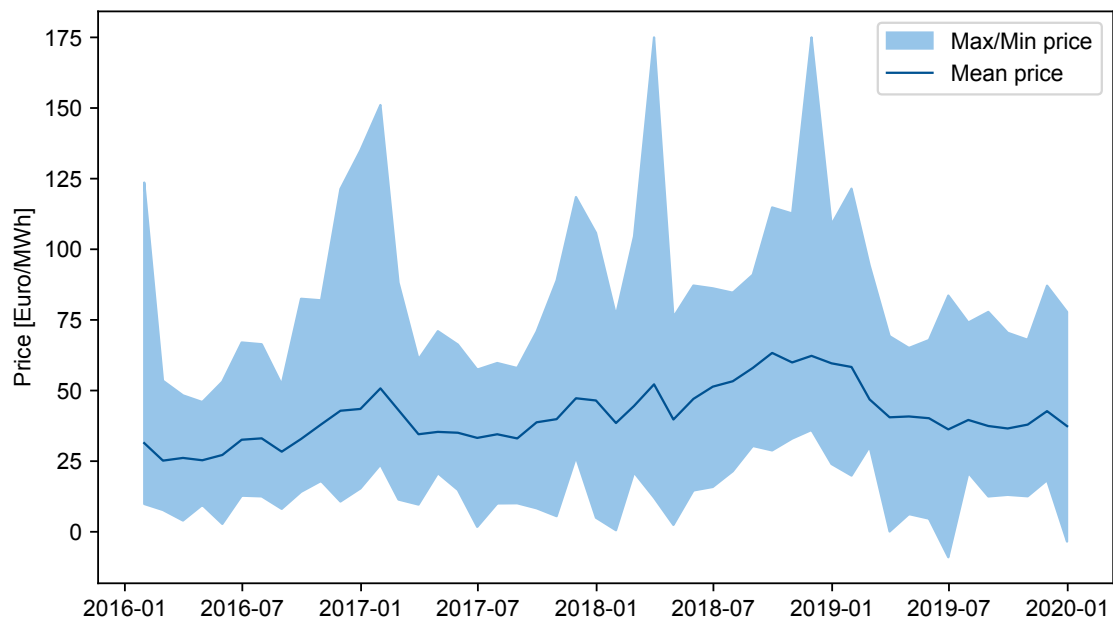
Figure 3.9: Mean electricity wholesale market from the *EPEX SPOT Power NL Day Ahead Market* in dark blue, with the light blue area indicating the price range in the respective month

Chapter 4

Electrification of the residential heat sector: A case study

Most of today's thermal demand must also be supplied from carbon-neutral energy sources for a consequent energy transition. The electrification of the residential heat sector, therefore, is a promising option. Representing a 26% share of final energy consumption in the European Union in 2018, of which 64% is used for heating, the residential sector can have a significant impact on the overall goal of net-zero emissions [89]. Given their high energy efficiency by using energy from its surrounding, electric HPs are a promising way of electrifying residential heating supply. In combination with attractive governmental subsidy schemes, there is a strong push for the installation of HPs in the residential sector in many European countries. Furthermore, given buildings' inherent storage capabilities, heat and its resulting electricity demand can be decoupled to a certain extent, which allows for a flexible operation of HPs. However, as mentioned before, high penetration of the distribution grid with these novel intermittent loads could put significant new strains on existing distribution systems. To this end, this chapter will help build an intuition about the impact of HPs on the individual and overall system load. In this context, we will furthermore look at the effect of a dynamic pricing signal on the coincidence of flexible HP loads. The subsequent section will briefly introduce HP technologies and their underlying principles to generate space heating from electric power. To analyze their impact on the system load, we then present the modeling and parameterization of the thermal building models. Finally, we investigate HP loads on an individual and aggregate system level.

4.1 HPs for residential space and water heating

In the building sector, electric HPs gain popularity as an alternative to common gas- or oil-fuelled heating systems. Although the overall sales of HPs has not gained the traction in the Netherlands as much as in other European markets, such as Norway, Sweden, or Estonia [90]. The overall number of HPs installed in the Netherlands, as presented in Figure 4.1, shows a clear increase in their installation and already exceeded 700,000 HPs under operation in the year 2019 [91]. There exist two major types of HP technologies, namely air and ground source HPs. Air source HPs extract energy from the ambient air outside of the building to heat the living space. Compared to ground source HPs, they are a relatively inexpensive
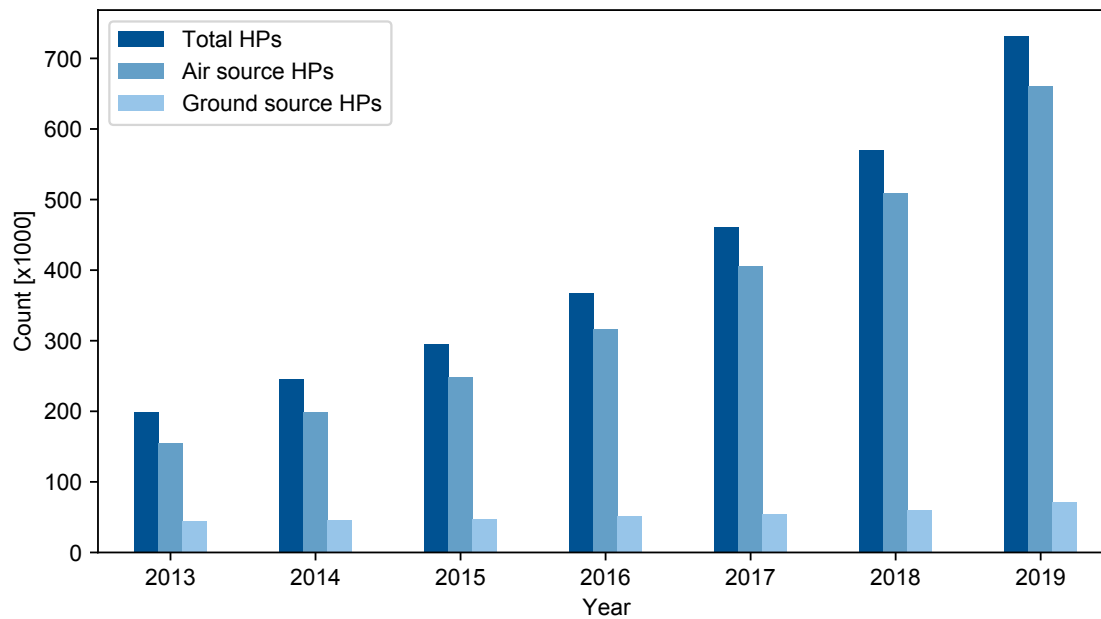
Figure 4.1: Development of the total number of HPs in the Netherlands [91]

option, which is why they are more common in the Netherlands, as can be seen in Figure 4.1. This is also because the Netherlands experiences a relatively mild winter, as air source HPs cannot operate efficiently at temperatures well below 0 °C. In this case, ground source HPs are the more suitable choice, as they extract energy from the soil or groundwater, which, at appropriate depth levels, maintains a relatively constant temperature well above the freezing point throughout the entire year. This increases their overall efficiency significantly. However, due to the vertical drilling needed and more complex heat exchanger setup, their installation is more costly than the one of air source HPs. Therefore, as air source HPs are more common in the Netherlands, the remainder of this case study and subsequent analysis in this thesis will focus on this type of technology [92].

In comparison to conventional household loads, such as for artificial lighting or other types of consumer electronics, HPs distinctly stand out in two properties: Firstly, their nominal electric power demand considerably exceeds typical residential loads, and their operation is not tied to a pre-determined schedule [93]. Secondly, the building's inherent thermal storage capacities enable the HP's electric load to be temporally decoupled from the time of final delivery of heat. This is further enhanced by additional sensible heat storage units, which commonly have a capacity of between 700 L and 1500 L [94]. HPs are therefore flexible in their operation. To exploit this type of flexibility, we must apply a thermal building model to accurately mimic the building's behavior and the resulting thermal energy demand over time.

4.2 Building model and parameterization

For convenience, we resort to the existing and validated Control-oriented Building Model (CoBMo) which was presented in [95] and is available in [96]. An additional advantage of this

model is the fact that it neatly integrates with the distribution grid simulation package, which we later apply in Chapters 6 and 7. CoBMo is specifically designed for model predictive control problems and implements linear, convex building model equations. It relates the operation of HVAC systems to indoor air climate and quality, considering interdependencies between building and internal as well as external influences, such as occupation, irradiation, and ambient temperature. The CoBMo software package can optimize the electric energy procurement costs subject to the occupants' individual thermal comfort limits. The following subsections introduce the model and the parameterization procedure, which we finally validate based on values from TABULA. In addition to the electric HP load, fixed loads are assigned to the buildings to finally be able to investigate the system load. The parameterization procedures are based on the works in [10], [97], [98].

Notation

Before introducing the model formulations, we must first establish a common understanding of the notation used throughout the remainder of this thesis. We define $\mathbb{R}$ the domain of real numbers. Non-bold letters x, X denote scalars in $\mathbb{R}^1$, while bold letters $\mathbf{x}$, $\mathbf{X}$ denote vectors and matrices in $\mathbb{R}^{n,m}$, with $n, m \in \mathbb{Z}$. Symbols $\mathbf{0}$ and $\mathbf{1}$ denote vectors, and matrices of zeros and ones of appropriate sizes. x_t (subscript t) denotes discrete expressions for time step t in the planning horizon $\mathcal{T}$ while $x(t)$ represents continuous expressions with $\dot{x}$ the derivative of $x(t)$ over time. All prices are in Euro and denoted by € or EUR.

4.2.1 Thermal building modeling

According to [95], the thermal building models in CoBMo are expressed in state-space form with vectors $\mathbf{x}$, $\mathbf{u}$, $\mathbf{y}$ and $\mathbf{d}$ the state, control, output and disturbance vector, respectively. A detailed presentation of the formulations in CoBMo is omitted at this point and can be found in [95]. In the following, a few specifics in the context of this thesis shall be pointed out.

The amount of heat delivered to a zone is defined through control vector $\mathbf{u}$. Disturbance variables influence the internal building climate and are captured in the disturbance vector $\mathbf{d}$. It links the ambient temperature T^{amb}, sky temperature T^{sky}, irradiation $\dot{q}_d^{irr}$, as well as internal gains $\dot{q}_z^{occ}$ to the climatic development in individual zones. Irradiation gains result from solar irradiation onto external surfaces (walls and roof) in relation to the surface orientation. Internal gains are heat inputs related to the occupation of zones, such as heat dissipation of occupants and thermal emission of internal devices. Disturbance data can be provided in the form of time series. The output vector $\mathbf{y}$ contains the electric power of the HP $P^{hp,el}$. We apply a simple gain factor for the conversion of electric to thermal power through the HP, which results in

$$P^{hp,el} = \frac{\dot{Q}_{th}^{gen,heat}}{COP_{HP}}, \tag{4.1}$$

with COP_{HP} the Coefficient of Performance (COP), which expresses the efficiency of a HP as the ratio of thermal energy $\dot{Q}_{th}^{gen,heat}$ provided per electric energy employed and which we assume to be constant, as explained further below.

By applying zero-order hold discretization, the continuous state-space formulation results in the following explicit discrete time-invariant system $\forall t \in \mathcal{T}$,

$$\mathbf{x}_{t+1} = \mathbf{A}\mathbf{x}_t + \mathbf{B}^u\mathbf{u}_t + \mathbf{B}^d\mathbf{d}_t, \tag{4.2a}$$

$$\mathbf{y}_t = \mathbf{C}\mathbf{x}_t + \mathbf{D}^u\mathbf{u}_t + \mathbf{D}^d\mathbf{d}_t, \tag{4.2b}$$

with vectors $\mathbf{x}_t$, $\mathbf{u}_t$, $\mathbf{y}_t$ and $\mathbf{d}_t$ the discrete time-invariant form of the state, control, output and disturbance vectors from above, $\mathbf{A}$ and $\mathbf{C}$ the state and output matrix and $\mathbf{B}^u$, $\mathbf{B}^d$, $\mathbf{D}^u$, and $\mathbf{D}^d$ the input and feed through matrices on the control and disturbance vectors, respectively.

4.2.2 Optimal operation problem

Under the assumption that all HPs are operated aiming at minimizing their electricity procurement cost, according to [10], [95], the optimal operation problem can be formulated as, $\forall t \in \mathcal{T}$,

$$\min_{P_t^{hp,el}} \quad \sum_{t \in \mathcal{T}} P_t^{hp,el} c_t \Delta t \tag{4.3a}$$

$$\text{s.t.}_{(\forall t \in \mathcal{T})} \quad (4.2), \tag{4.3b}$$

$$\mathbf{y}_t^- \leq \mathbf{y}_t \leq \mathbf{y}_t^+. \tag{4.3c}$$

with the objective to minimize the overall energy cost over time horizon $\mathcal{T}$, based on the product of the HP's electric power $P_t^{hp,el}$, the electricity cost c_t at time step t and the time interval Δt, subject to the state-space model equations from above and the output constraints. The latter consist of comfort temperature constraints in the form of time series, storage constraints and a maximum power output of the HP. The parameters in (4.2) and in the additional constraints in (4.3) are defined for each building individually based on the following paramaterization procedure.

4.2.3 Parameterization procedure

This subsection describes the parameterization procedure of the CoBMo model, which is performed on individual residential buildings in the study area. For this purpose, we again rely on the data introduced in Chapter 3, which is further enhanced with data from additional sources required to populate the CoBMo models accurately. The overall procedure is depicted in Figure 4.2. Its steps are explained in more detail in the following paragraphs.

Geometry simplification

The building geometries required for the characterization of the thermal building model are derived from the 3dBAG dataset in [81]. In order to match the required input data format, the building shapes are simplified to cuboids based on their geometrical footprint and height information, and their orientation is aligned with the geographic north/south and east/west axes. Following the procedures in [10], the ratio of floor area and circumference are preserved. A detailed description is omitted here and can be obtained from [10]. The cuboids are treated as homogeneous constructions, meaning the entire construction is assumed to be a single room, and hence only one zone is defined per building, neglecting any interior structures. Considering the size of most of the buildings, this is deemed a fair assumption.
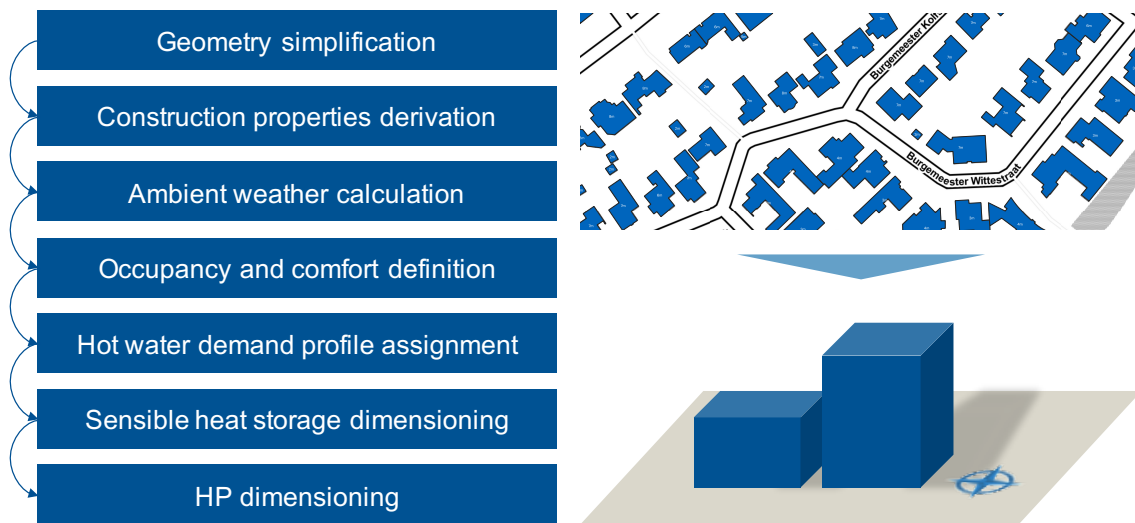
Figure 4.2: Parameterization procedure for populating accurate individual thermal building models with CoBMo
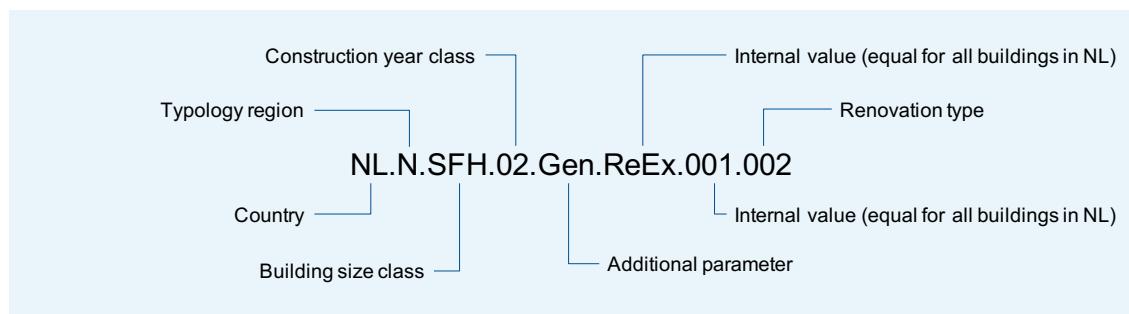
Figure 4.3: Exemplary typology code from the TABULA dataset

Construction properties derivation

Based on the spatial information and additional data from [80], the TABULA dataset introduced in Chapter 3 is now used to classify each building by matching the respective building attributes with TABULA's characteristic classes. The dataset holds thermal building properties for representative typologies, which are defined through four different attribute classes in the form of a code. Figure 4.3 presents an exemplary code and its decomposition details. The following paragraphs explain how these typology codes are derived from the data at hand.

Building size class distinguishes SFHs, Terraced Houses (THs), Multi Family Houses (MFHs), and Apartment Blocks (ABs) to identify the type of building. The size classes are uniquely defined by the number of units in a building, stories, neighbors, and a separate indicator for terraced end houses. Using the information from the BAG dataset and based on further spatial analysis, each building is assigned to a building size class based on the scheme presented in Table 4.1. The number of units is extracted from the BAG dataset, while the number of stories s is estimated using the building's height and an average story height of 2.5 m for all buildings. To identify terraced (end) houses, the spatial data from [81] is utilized to identify neighboring buildings and to determine the number of attached neighbors. The attached

neighbors are defined as buildings that share at least one common wall. This is determined by evaluating the intersections and proximity of spatial shapes. When multiple buildings are sequentially interconnected, i.e., at least one has two other buildings attached, the construction is considered a TH. Indicator variables are set to denote this feature, as well as an indication for the houses located at the end of a row of THs, as they have one more surface facing the ambiance directly. This information about joint walls is utilized to identify adiabatic surfaces. It is assumed that walls bridging two buildings do not participate in heat transfer processes and exchange with the ambient air, as the temperature gradient between buildings is neglectable.

Table 4.1: TABULA building size classification scheme

Building size class	Number of dwellings d	Number of stories s	Number of attached neighbors n	Terraced end house
SFH	$1 \leq d \leq 3$	$1 \leq s \leq 4$	$0 \leq n \leq 1$	–
TH	$1 \leq d \leq 3$	$1 \leq s \leq 4$	$1 \leq n \leq 2$	✓
MFH	$d \geq 4$	$1 \leq s \leq 4$	$n \geq 0$	–
AB	$d \geq 10$	$s \geq 5$	$n \geq 0$	–

The construction year class classifies buildings by age in six categories (01–06). The corresponding class is determined based on the construction year known from the BAG dataset. The classes are assigned as indicated in Table 4.2.

Table 4.2: TABULA construction year class segmentation

Construction year class	First year	Last year
01	–	1964
02	1965	1974
03	1975	1991
04	1992	2005
05	2006	2014
06	2015	–

The renovation type value defines the Energy Performance Level (EPL). For the Netherlands, EPL1 (existing state) denotes the original state with no alterations or enhancements to the building thermal properties since its construction. EPL2 (standard refurbishment) represents refurbishment according to current practices, while EPL3 (ambitious refurbishment) describes buildings that have been upgraded to the highest energy performance levels. Note that two buildings with identical renovation type, do not show identical thermal behavior, as the renovation type is based on the individual building's original state and makes few explicit definitions of thermal values. The BAG dataset contains no information on the refurbishment status of individual buildings. Therefore, we allocate the individual renovation types of buildings based on statistical building stock data, depending on its construction year class and the probability distribution that is provided in Table 4.3 and derived from actual data on the distribution of refurbishment levels within the Dutch residential building stock in [99], [100].

Table 4.3: Refurbishment status distribution in the Dutch residential building stock, based on [99], [100]

Renovation type	Construction year class		
	01–03	04–05	06
EPL1	0.68	0.53	0.96
EPL2	0.32	0.43	0.00
EPL3	0.00	0.04	0.04

The TABULA dataset provides thermal parameters for each typology utilized for the parameterization of building zones and surfaces in the CoBMo model. To parameterize the building zone types in the CoBMo model, the internal zone heat capacity per m^3 reference volume, as well as the infiltration rate, i.e., the volumetric flow rate of outside air into a building, are obtained from TABULA reference values. Here, TABULA distinguishes between the air change rate by, e.g. opening windows and doors, and the air change rate by infiltration, which is dependent on the general tightness of the building. In CoBMo, the infiltration rate represents the sum of these two values. Table 4.4 summarizes the final values for the model parameterization, which were adapted during validation process. The values depend on the individual building's construction year class and renovation type and are assigned to the zone types.

Table 4.4: Chosen infiltration rate values, adapted based on [82]

Construction year class	Renovation type	Infiltration rate [1/h]
01	EPL1	1.50
01	EPL2	1.00
01	EPL3	0.50
02	EPL1	1.35
02	EPL2	1.06
02	EPL3	0.50
03	EPL1	1.35
03	EPL2	1.00
03	EPL3	0.50
04	EPL1	1.05
04	EPL2	1.00
04	EPL3	0.50
05	EPL1	1.12
05	EPL2	1.05
05	EPL3	0.50
06	EPL1	1.10
06	EPL2	1.00
06	EPL3	0.90

For the parameterization of the building surfaces, each TABULA typology specifies additional construction elements that are to be considered in the thermal model. Most importantly, this includes window types assigned to each surface and linked through window-to-wall-area ratios. The TABULA dataset furthermore contains representative heat transfer coefficients per building typology. For a full thermal characterization of building surfaces (i.e., walls, windows, and roofs), additional property attributes are required, which are not provided by TABULA. These

include absorptivity and emissivity factors, as well as the specific heat capacity of certain materials. Table 4.5 provides an overview of the chosen values and the respective sources.

Table 4.5: Additional parameters which are not provided in TABULA

Name	Symbol	Value	Sources
Surface emissivity	ϵ_{wall}	0.9	
	ϵ_{roof}	0.9	[101], [102]
	ϵ_{window}	0.95	
Absorptivity factors	α_{wall}	0.6	
	α_{roof}	0.65	[103]– [106]
	α_{window}	0.45	
Heat capacities	c_{wall}	$459.0\,kJ/m^2K$	[107], [108]
	c_{roof}	$200.0\,kJ/m^2K$	

Ambient weather calculation

The thermal behavior of a building is significantly determined by its interaction with its surroundings, most notably, temperature gradients between ambient air and building and heat input through solar irradiation. These two mechanisms are reflected in CoBMo based on weather data time series. Using the weather data presented in Chapter 3 and following norm DIN EN ISO 52016-1, the sky temperature T_t^{sky} is approximated applying a temperature delta of $\Delta T^{sky,amb} = 11K$ [109], so that we end up with, $\forall t \in \mathcal{T}$,

$$T_t^{sky} = T_t^{amb} - \Delta T^{sky,amb}. \tag{4.4}$$

Based on the ambient air temperature T_t^{amb}, relative humidity, and air pressure data, the absolute air humidity is calculated employing the thermophysical property library CoolProp [110]. Based on this data, we can derive the absolute air humidity ratio defined as

$$r = \frac{m_{water}}{m_{air}}, \tag{4.5}$$

with m_{water} and m_{air} the mass of water and air, respectively.

Ultimately, the irradiance onto all surfaces (horizontal, north, east, south, and west orientations) is calculated. According to [111], the global horizontal irradiance GHI_t is derived from diffuse horizontal irradiance DHI_t, direct normal irradiance DNI_t, and the solar zenith angle $\theta_{z,t}$ in the relationship, $\forall t \in \mathcal{T}$,

$$GHI_t = DHI_t + DNI_t \cdot \cos \theta_{z,t}. \tag{4.6}$$

Angle $\theta_{z,t}$ is obtained using the time and position information in the pvlib toolbox from [112], which implements a set of functions for simulating the performance of PV energy systems, using the respective time and geographic position of the weather data.

Occupancy and comfort constraints definition

The demand for thermal energy is furthermore dependent on occupancy and individual comfort constraints. As the focus of this study lies on the flexible operation of HPs, only upper and
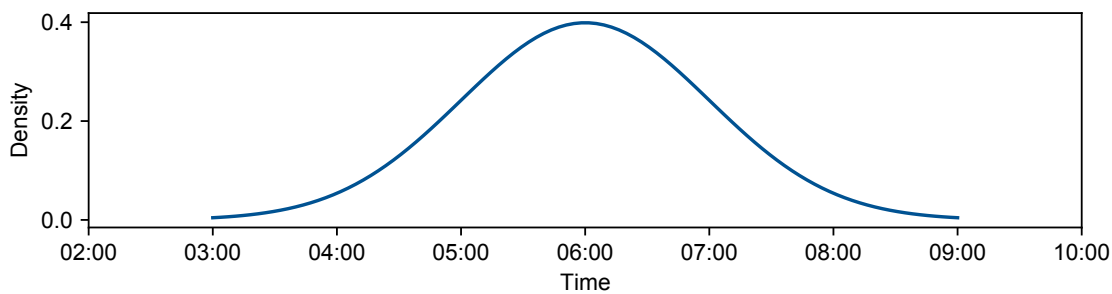
Figure 4.4: Night interval end distribution, with the mean end time at 6:00h in the morning

lower temperature constraints are enforced, disregarding air quality. We define temperature constraints based on a temperature range endorsed by the World Health Organization [113]. The comfort range is set to be 20–22 °C during the day and 18–22 °C at night. The nighttime interval is set to be six hours long. During away periods (such as working hours), which are set to be six hours long as well, the upper temperature limit is raised to 25 °C, while the temperature is allowed to drop to 18 °C, which is in the spirit of the works in [114] and allows for potential pre-heating periods during low-price hours to exploit the building's thermal inertia. The away period starts only on weekdays and four hours after the nighttime interval has ended. To generate individual constraint schedules for all buildings, we vary the end of the night interval based on a normal distribution with a mean night interval end time at 06:00h in the morning and a standard deviation of one hour. The resulting density curve is depicted in Figure 4.4.

Domestic hot water demand assignment

The domestic hot water demand is commonly served by the same thermal unit providing space heating in a building. Including this type of thermal power demand in our thermal building models is therefore essential. Hot water demand in CoBMo is modeled as an internal gain. Peak thermal heating power is given in relation to the zone area, and the demand schedules specify the corresponding hot water demand rate for the given time step. We assign each building a unique schedule, which is generated using the tool UrbanHeatPro, which was introduced in [115]. UrbanHeatPro was designed to simulate the heat demand profiles of buildings in urban areas. Besides space heating demand, it generates hot water demand curves for residential buildings, which we isolate from the space heating demand. Conveniently, the tool is equally based on the TABULA dataset so that the hot water demand schedules are uniquely generated for each building using consumption profile distributions as characterized in VDI 3807-3 [116].

Sensible heat storage

The thermal building model includes a sensible heat storage model, which further increases the building's inherent storage capabilities. The storage capacity of the sensible heat storage is defined relative to the building size and living area. Therefore, the same storage type is assigned to each building as it varies with the individual size. The storage self-discharge rate

is neglected. Its parameterization is based on the work in [117], [118] and is defined with the parameters given in Table 4.6.

Table 4.6: Sensible heat storage model parameterization

Model parameter	Value	Unit
Storage capacity per zone area	0.005	m³/m²
Round-trip efficiency	80.0	%
Sensible temperature delta	10.0	K
Self-discharge rate	0.00001	%/h
Initial state of charge	50	%

HP dimensioning

Depending on the season and temperature gradient between interior and exterior, the COP of a HP may vary. However, in the context of this thesis, we define a constant value for $COP_{HP} = 2.2$ for all buildings, based on data from TABULA. As buildings differ in zone size, thermal properties, and hot water demand, the power delivery capacity of the HPs must be defined individually for each building. Following [118], [119], the HP's initial nominal electric heating power $P_{init}^{hp,el}$ is approximated as

$$P_{init}^{hp,el} = \frac{Q_{th}^{heating}}{t_{fullload}} \cdot \frac{1}{COP_{HP}}. \tag{4.7}$$

The total annual thermal heating demand $Q_{th}^{heating}$ is derived from TABULA. The reference value for the full-load hours of heating systems $t_{fullload}$ is obtained from VDI 2067-2 and given as 2000 to 2100 h/a for residential buildings [119]. This yields rough estimates for the installed nominal heating power required by the individual HPs. However, this approximate value might not suffice in some cases, which would lead to infeasibilities. To this end, we slightly adapt (4.3) by introducing a slack variable $s_t^{hp,el}$ to the output constraint on the electric power $P_t^{hp,el}$ in combination with a compensation term in the objective, so we end up with an adapted version for the HP's optimal operation problem, which allows us to properly dimension the HPs, $\forall t \in \mathcal{T}$,

$$\min_{P_t^{hp,el}} \quad \sum_{t \in \mathcal{T}} (P_t^{hp,el} + s_t^{hp,el}) c_t \Delta t \tag{4.8a}$$

$$\text{s.t.}_{(\forall t \in \mathcal{T})} \quad (4.2), \tag{4.8b}$$

$$\mathbf{y}_t^- \leq \mathbf{y}_t \leq \mathbf{y}_t^+. \tag{4.8c}$$

$$P_t^{hp,el} - s_t^{hp,el} = P_{init}^{hp,el} \tag{4.8d}$$

$$s_t^{hp,el} \geq 0 \tag{4.8e}$$

Note that we isolate the power output $P_t^{hp,el}$ from the output vector $\mathbf{y}_t$. Instead of defining a firm power output constraint, we let the slack variable compensate for any "missing" power, in case the required electric power, defined by (4.8b) and (4.8c), exceeds the initial capacity dimensions, which we estimated as $P_{init}^{hp,el}$. We furthermore force the HP to operate at least

at $P_{init}^{hp,el}$. We will end up with the minimum additional capacity needed. The nominal power for the respective HP is consequently set to be equal to the sum of our initial guess and the maximum value of the slack variable as, $\forall t \in \mathcal{T}$,

$$P_{nom}^{hp,el} = P_{init}^{hp,el} + max_t\{s_t^{hp,el}\}. \tag{4.9}$$

The corresponding reactive power value is computed based on (5.10) assuming a fixed power factor of 0.9 for all HPs. We solve the above problem for the first three weeks of a year, as these represent the coldest time of the year and will therefore require the maximum power output. The energy cost in (4.3a) is set to a flat price $c_t = 1$ €/MWh, $\forall t \in \mathcal{T}$, and the time interval $\Delta t = 1$h.

4.2.4 Validation of model parameters

To validate the model parameterization, in a similar fashion as for the HP dimensioning procedure from above, we solve the optimal operation problem (4.3) with a flat energy cost for an entire year $c_t = 1$€/MWh, $\forall t \in \mathcal{T}$. The resulting total heating demand per m^2 is then compared to the respective TABULA reference values of required annual thermal energy for each building individually.

As a study area for the validation, we focus on the residential neighborhoods of Eindhoven defined in section 5.3.1, as it consists of a large number of residential buildings. Figure 4.5 shows the resulting building stock in which the distribution of building size classes and renovation types is depicted. It becomes clear that most buildings are relatively old in this area. As the renovation types were assigned based on the probability distribution from Table 4.3, we can observe the same patterns here. In terms of building size classes, the majority of buildings are THs, which is a reasonably common housing type in the Netherlands.

Based on the simulation and reference heat demand, the relative deviation is calculated. The original infiltration rates from TABULA were adapted to the values in 4.4, so that a satisfactory result is realized, as seen in Figure 4.6. The building model parameterization appears to be a valid and accurate representation of the actual building stock in the study area, as the majority of results are off by no more than 10% in either direction. However, as authors in [120] point out, since the static TABULA calculation is itself a simplified approximation of the demand, there is no final answer to which value is more accurate. Just like in [120], the CoBMo simulation results seem to be rather sensitive to infiltration rates. No further adaption to these values was done to finally preserve similar air volumes and system efficiencies as used in the TABULA typology. To this end, the obtained parameterization was further validated by inspection and comparison with characteristic literature values for heating power [118], [121] and for annual domestic hot water demand [116], [122]. Overall, the building parameterization reflects the estimated thermal energy demand of residential buildings closely. The chosen parameter sets are therefore deemed suitable for further analysis.

4.2.5 Fixed residential household loads

To evaluate the system load and the interplay of the additional electric load from HPs with typical residential loads, we further assign individual domestic electric power load profiles to all
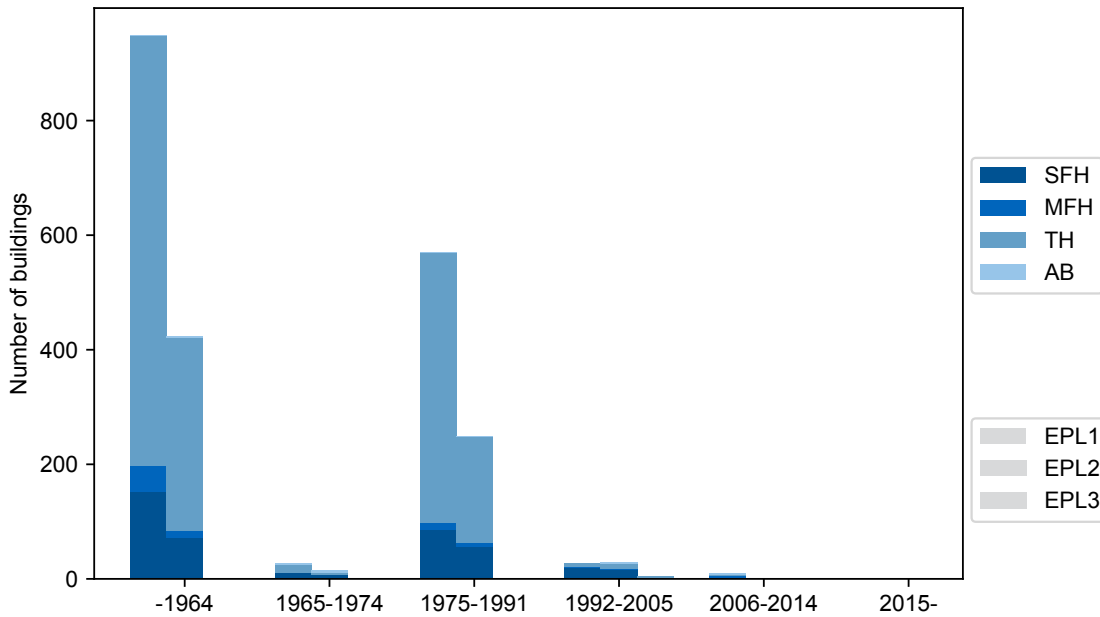
Figure 4.5: Original building stock in the study area of Eindhoven
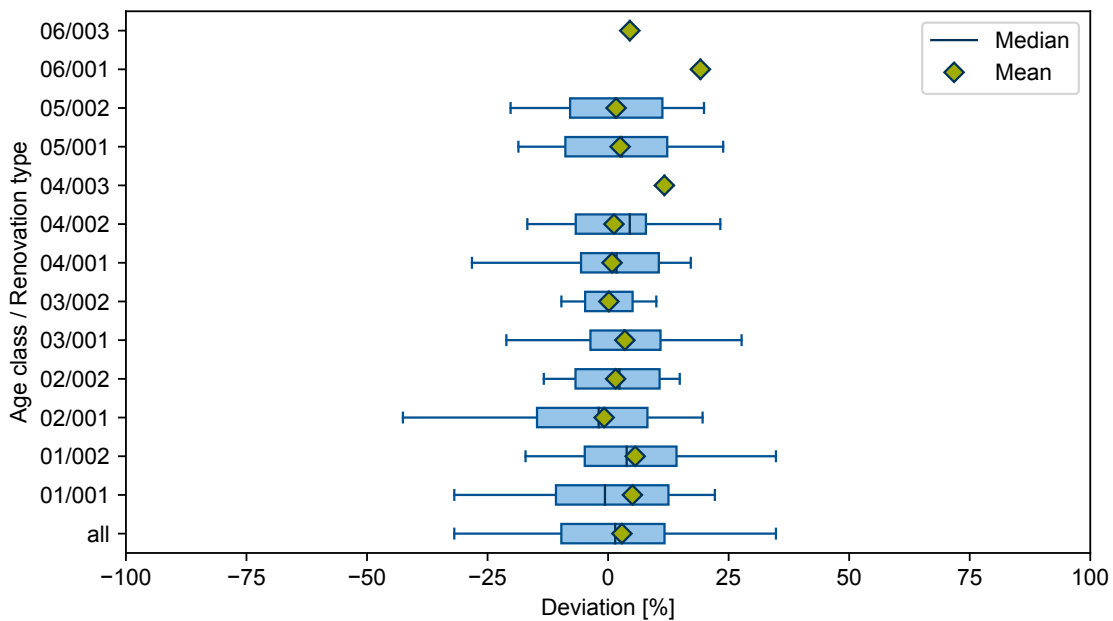
Figure 4.6: Relative deviation of CoBMo annual heating demand per m² from the average heat demand in TABULA

buildings. In the spirit of statements in [60] about low price elasticity of end consumers, we assume all residential loads to follow fixed profiles, as the load profile of electrical devices in residential buildings is determined by the daily routines of the residents and environmental factors, such as the usage of artificial lighting in response to nightfall, and there exists a negligible willingness to change this behavior.

To this end, we assign the synthetic load profiles from section 3.4 to individual buildings based on the probability distributions from Table 3.4. These synthetic electric load profiles are generated using a simulation model for private households in Germany. As the derived load schedules represent average German settlements, they can be assumed to not differ significantly from Dutch residential profiles.

4.3   Analysis of the electric heating demand

In this section, we perform a case study on the defined study area of Eindhoven with the aim to investigate the impact of a high HP penetration from the perspective of the (i) individual, (ii) coincident, and (iii) absolute system load under a constant and temporally dynamic pricing scheme, which we denote as Volumetric Block Pricing (VBP) and Real Time Pricing (RTP), respectively. The subsequent subsections will first briefly introduce the scenario design, followed by the results for (i)–(iii).

4.3.1   Scenario design

We adopt the assumption from TABULA and authors in [120], [123], that HPs can be installed in buildings built before 1995 only after prior refurbishment measures have been taken. As these buildings lack modern thermal insulation, their heat load is much higher, and they fail to meet the requirements of low-temperature systems, such as HPs. Younger buildings can already be equipped with a HP, even in their original state (EPL1). In terms of scenario design, we consequently assume that all buildings of construction year class 03 or older (classes 01 and 02) have been refurbished at least according to refurbishment type EPL2 and have consequently been equipped with a HP. Contrary to the studies in [120], we furthermore assume all housing types to be potentially equipped with a HP, instead of SFHs only.

We again use the study area of Eindhoven, where we end up with a renovated building stock represented in Figure 4.7 consisting of 2307 residential buildings. We can see that no building constructed before 1992 is now still in its original state (EPL1) and can consequently be equipped with a HP. This is necessary, as this case study aims at evaluating an extreme HP penetration scenario, in which all residential buildings are equipped with HPs.

Concerning the underlying price signal, in the case of VBP, the electricity price is set to $c_t = 1$€/MWh, $\forall t \in \mathcal{T}$, while for RTP, c_t follows the time series of the historical wholesale market data that we introduced in section 3.6. Under the assumption of the highest expected heating demand in winter, we run the simulation for the entire month of January for the year of 2017, which experienced below-average temperatures. The corresponding price time series is depicted in Figure 4.8 over all days of the month, with a mean price that reaches its peak during the afternoon hours at 17:00h and 18:00h.

We define the time interval $\Delta t = 1$h, to match the time interval of the day-ahead wholesale price. It is important to note that this flattens potential peak load effects in both the fixed and HP load profiles, while the overall energy demand (the area below the load curve) remains unchanged. However, for the sake of the later evaluation of a local energy market that integrates with the wholesale market, we deem this time interval more practical.
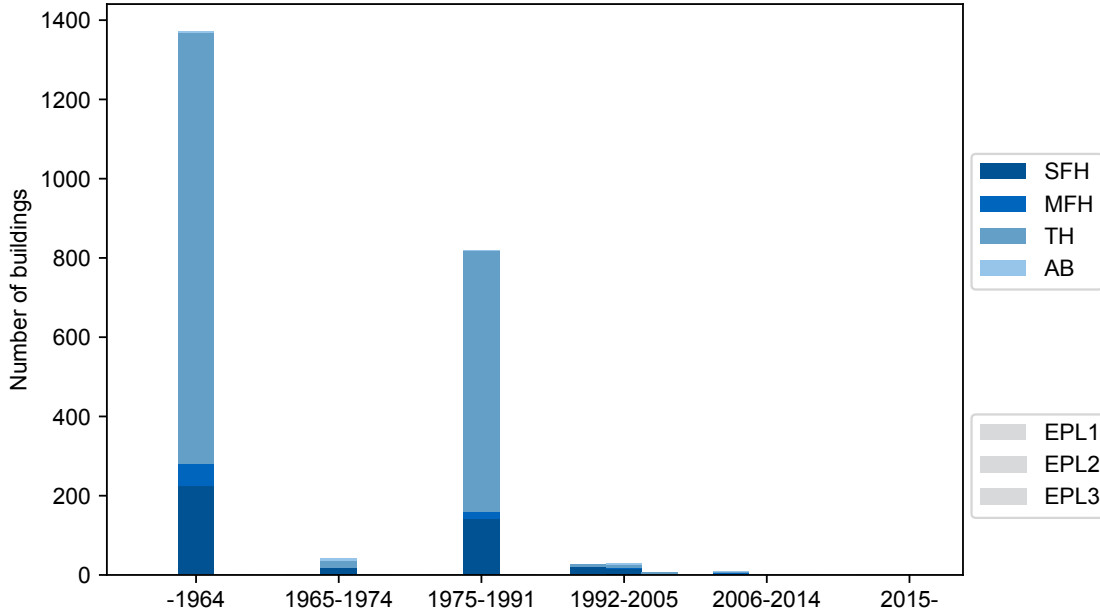
Figure 4.7: Building stock of the case study

4.3.2 Individual household load

We first observe the individual load profiles in Figure 4.9 for an arbitrary workday and building in the building stock. In the bottom graph the load profiles represent the HP load under VBP and RTP, respectively. Under VBP, the HP operates rather constantly and drops its consumption slightly during the early afternoon hours, when the thermal input from the surroundings, e.g. through solar irradiation, is the highest. It becomes clear that not only does the load under RTP vary significantly more over the day, but the overall peak load also increases significantly, especially in the early morning hours, when the HP pre-heats its storage capacities to avoid the typically increasing prices in the morning. The same effect can also be observed in the late afternoon hours, where we also typically observe a price increase after lower prices in the afternoon. After investigating the individual load, we now evaluate the effect of several price-following HPs together under the RTP signal at a time in more detail.

4.3.3 Load coincidence

For this part of the analysis we resort to the concept of Coincidence Factors (CFs). They are a measure for the temporal correlation of the peak load of n individual end consumers within a certain time interval Δt_{CF}, which is typically one full day [124]. For calculating them based on time series data, they can be defined as the ratio of the maximum of the accumulated load demand over the sum of the respective individual maximum load demand P_x of n consumers

$$CF(n) = \frac{max_{\Delta t_{CF}}\{\sum_{x=1}^{n} P_x\}}{\sum_{x=1}^{n} max_{\Delta t_{CF}}\{P_x\}}. \tag{4.10}$$

To calculate the coincidence curves based on (4.10) with $n = \{1, 2, ..., 100\}$, we apply the methods in [124] which are based on a Monte-Carlo approach in which we randomly iteratively
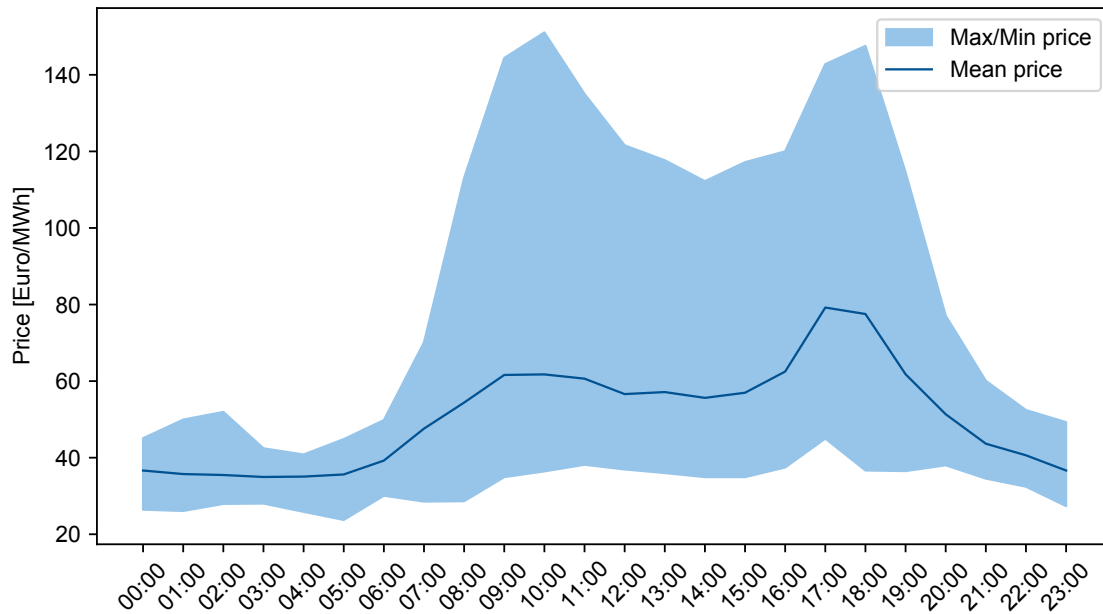
Figure 4.8: Mean electricity wholesale price from the *EPEX SPOT Power NL Day Ahead Market* in dark blue, with the light blue area indicating the price range in the respective hour for January 2017
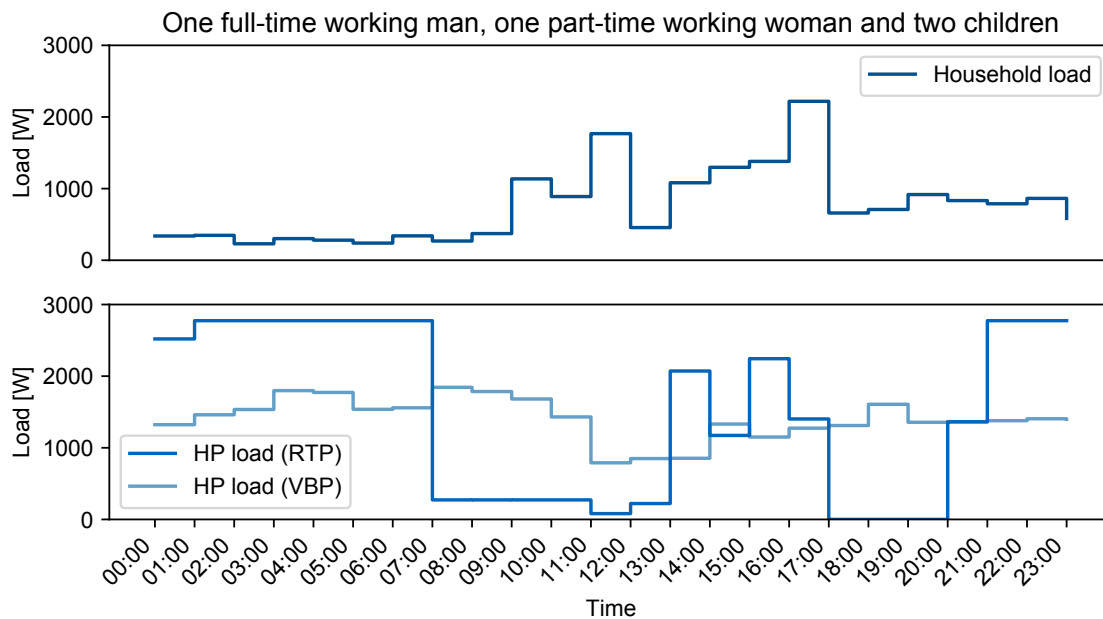
Figure 4.9: Individual electric load (top) and HP load (bottom) based on VBP and RTP, respectively, of an exemplary household for an arbitrary workday in January 2017

pick load profiles. The detailed procedure is omitted here and can be found in [124]. Due to the lower number of load profiles in our base population, we choose a maximum number of Monte-Carlo iterations of 1000.

The resulting curves in Figures 4.10 to 4.12 show a clear convergence of the individual CFs.
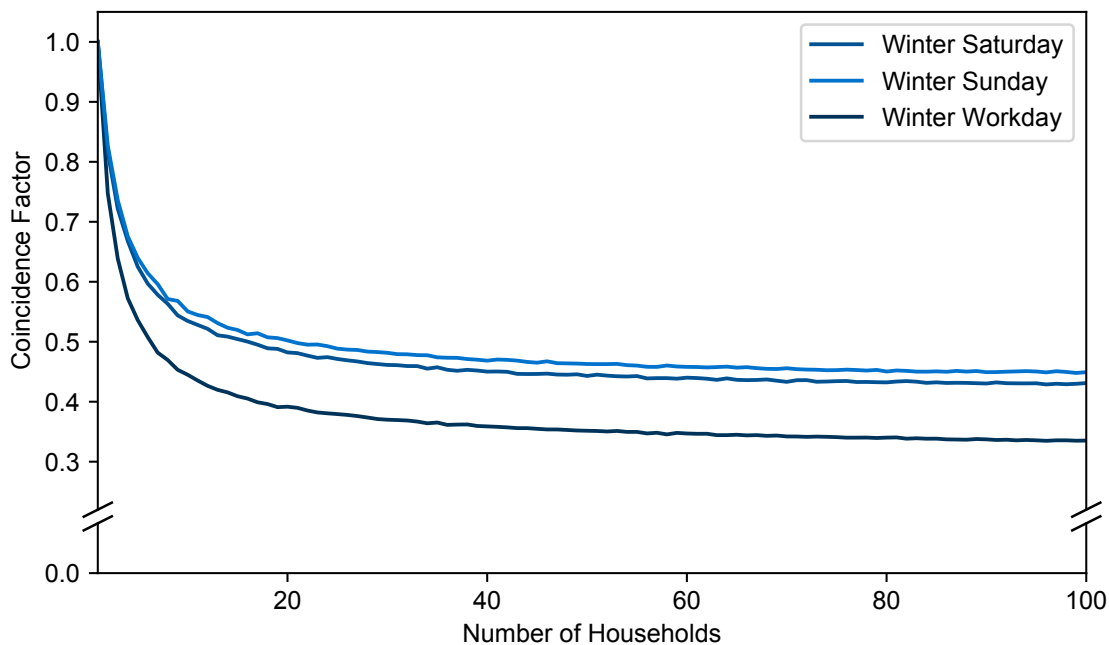
Figure 4.10: Coincidence curve of fixed residential loads

The graphs furthermore distinguish between workdays and weekend days as residential energy demand is typically higher during weekends due to a higher occupancy, which consequently influences the thermal demand from HPs. The coincidence curve for VBP shows a typical exponential decay with an increasing number of households, while the overall coincidence is already significantly higher than the one of residential loads, which is depicted in Figure 4.10. For large time intervals of one hour, the coincidence factor of our residential load profiles ranges between 0.4 to 0.5 for 100 households, which is in line with calculations in [124]. The higher coincidence can be explained based on the fact that all buildings in the study area under investigation are exposed to the same, or very similar, external factors, such as temperature of the surrounding or solar irradiation. Furthermore, on winter days, HPs are typically operated over the entire day with only short intervals of downtime and close to their nominal power output making use of the storage capacities as a buffer for the varying thermal load [125].

When we now consider the coincidence curve of the HPs following a dynamic RTP signal, we can observe a dramatic increase in the overall load coincidence. This can easily be explained by looking at the optimal operation problem (4.3) again, which minimizes the total cost of energy for the operation of the HP. This time, not only the external environmental factors are more or less equal for all buildings, but also the underlying price signal and its corresponding price peaks and valleys. Using their flexibility potential to their fullest, all HPs consequently shift their load to times of low prices and minimize their consumption during times of high prices as much as possible.

This effect becomes clear when we add a time dimension to this observation by looking at the heat maps in Figure 4.13 which compare the CFs of both price signals at a number of households of $n = 100$. We can observe that the load coincidence of the RTP signal is very
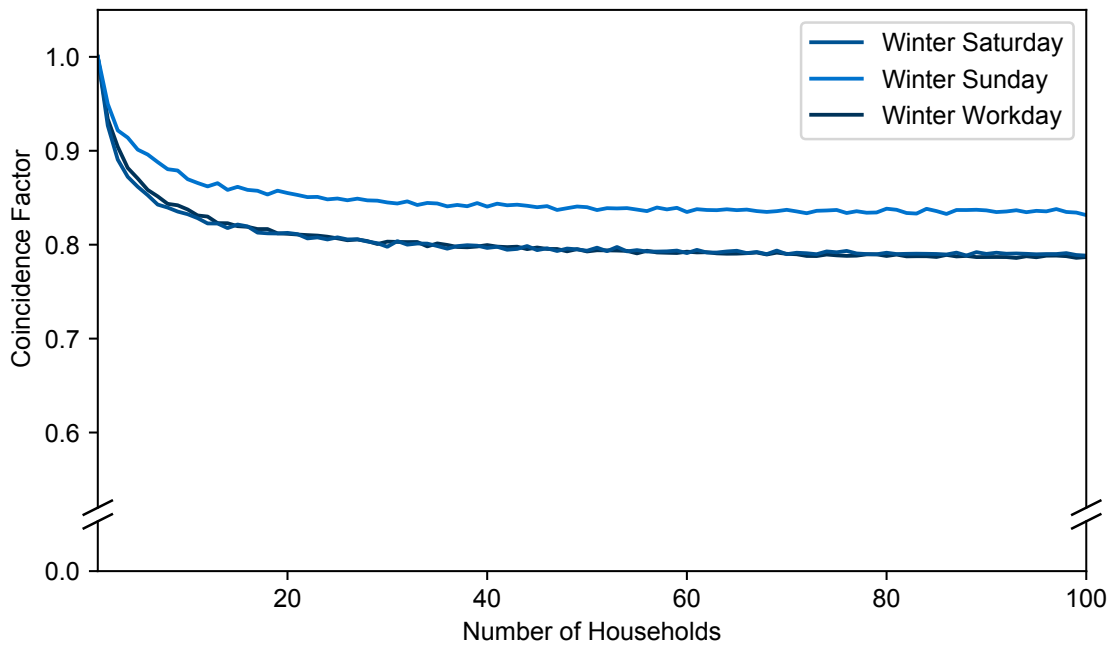
Figure 4.11: Coincidence curve of the HPs under VBP
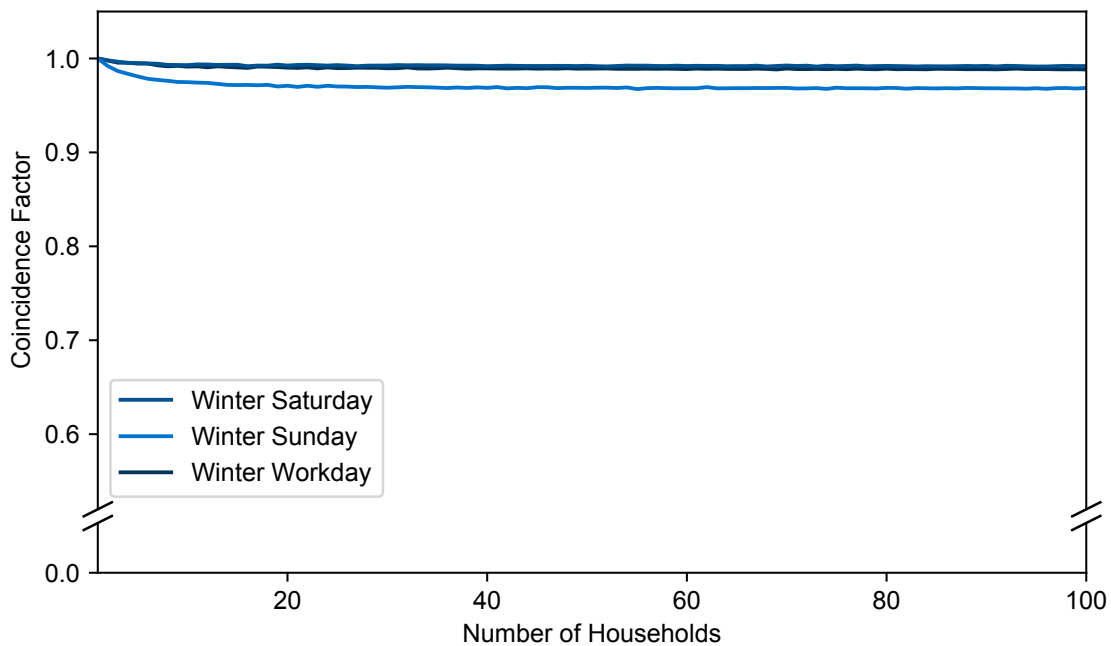
Figure 4.12: Coincidence curve of the HPs under RTP

high during times of low prices, which typically occur during nighttime and early morning hours, as can be seen in Figure 4.8. The contrary can be observed in the late afternoon when wholesale prices are typically relatively high.

One must note that this effect depends on the underlying price signal, which would adapt
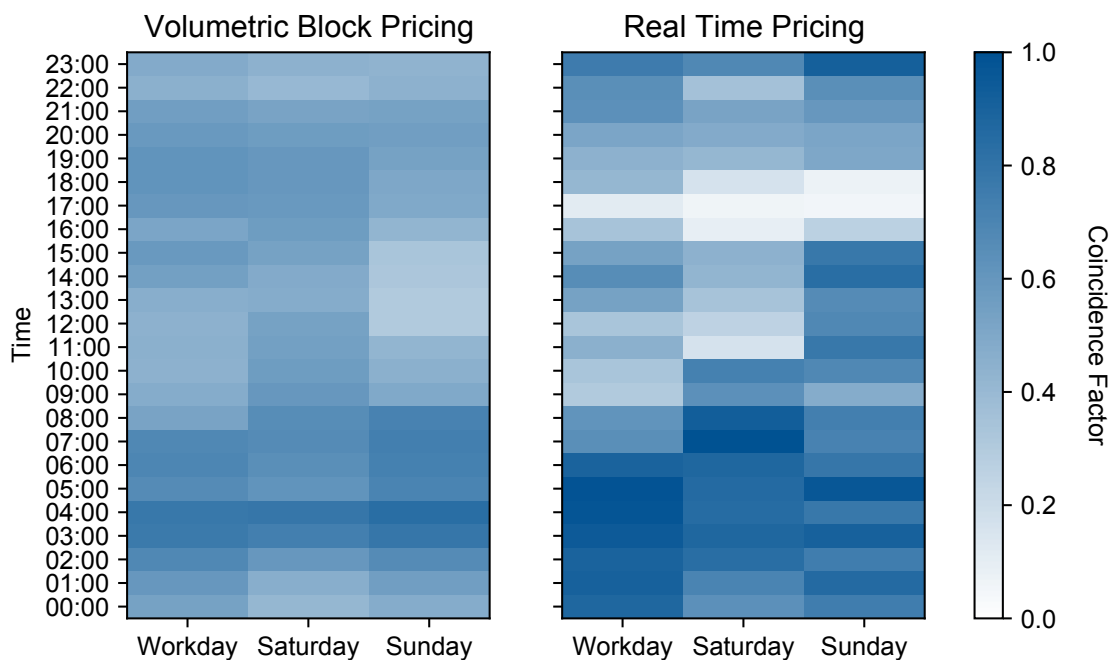
Figure 4.13: Comparison of load coincidence for a flat and a dynamic price signal with values of zero meaning no HP load and one all HPs at their individual maximum power

accordingly due to the higher demand. However, with higher penetration of RESs in the market, which produce at nearly zero marginal cost, it can be expected that especially price valleys will be more and more decoupled from the demand and are instead defined by an oversupply.

4.3.4 System load

Finally, we investigate the overall system load. Figure 4.14 shows the system load of all residential fixed loads under observation in the study area for typical January winter days. We can observe the "duck curve" in the shape, which is very typical for residential power demand.

Figure 4.15 shows the system load of the HPs under the two respective price signals. Note that all residential buildings in the study area have been renovated to be equipped with a HP. We can observe that the aggregated HP load under both pricing schemes adds a significant peak power demand at almost all times to the system that multiplies the traditional peak demand roughly by factor eight. Interestingly, the HP system load under RTP behaves complementary to the fixed residential load curve, as the main HP load concentrates on the night time when residential load and power prices are the lowest. However, the maximum HP system load is significantly higher than the load under VBP.

4.4 Discussion and conclusion

In this case study, we investigated the effect of a full electrification of the residential heat sector based on HP technology on the individual and system load under a constant and a temporally
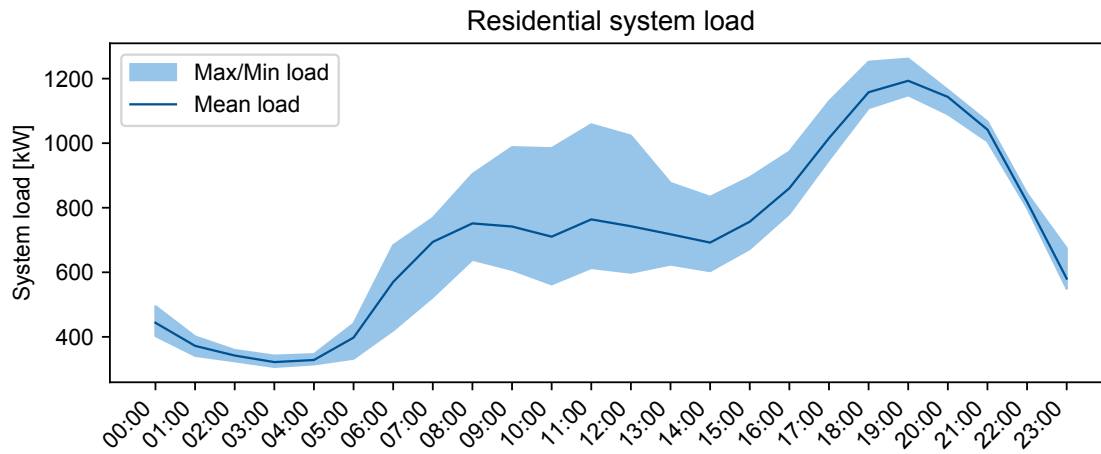
Figure 4.14: Typical "duck curve" shape of fixed residential loads over a day for the case of Eindhoven
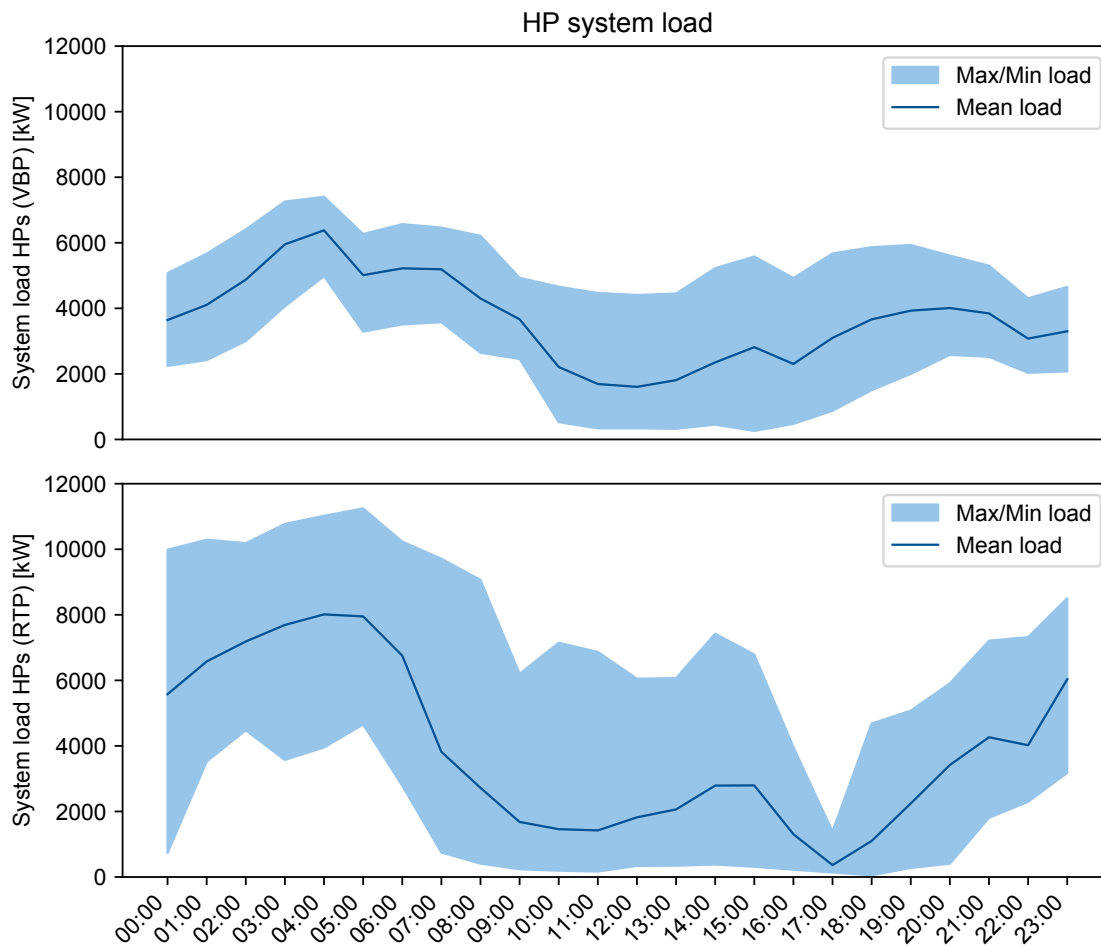
Figure 4.15: Comparison of aggregate HP load over a day for the month of January under VBP and RTP for the case of Eindhoven

variable energy tariff, namely VBP and RTP. In summary, this case study revealed the following issues:

– A high HP penetration will increase individual and overall system load significantly
– HPs generally show a high load coincidence, as all buildings in a defined area are exposed to very similar external conditions
– However, the load coincidence of price-following HPs under RTP is even higher, as flexibility is fully exploited
– From a system perspective, price-following HPs behave complementarily to the residential loads
– HP system load under RTP is significantly higher than under the constant VBP

It is important to note that the assumption of a one hour time interval has an impact on the results under consideration. As mentioned above, this flattens potential peak moments, which would additionally increase the peak demand. Furthermore, the operation of current HPs is based on a full load or no load logic, which means that they are either turned on or off but are not continuously variable as assumed in this study. However, this is a relic from the past and is expected to change as RTP becomes more and more widespread. Finally, as authors in [126] argue, it cannot be expected that all consumers would opt for a dynamic pricing scheme such as RTP. However, this represents an extreme case for analysis purposes and is, therefore, suitable to investigate the maximum impact on the system.

Based on the results of this case study, it becomes clear that the impact on the grid should not be neglected to evaluate if a coordinating mechanism based on the overall grid state might be needed. Highly granular DLMPs are a price signal that promises to coordinate flexible DERs in line with grid conditions in a decentral manner. However, realistic distribution grid data is usually unavailable. Based on the data from Chapter 3, the following chapter will present a method for the generation of realistic distribution grid models, which we later use in a systematic analysis of price signals.

Chapter 5

Distribution grid model synthesis

The analysis of DLMPs requires realistic distribution grid models that accurately mimic the behavior of the underlying system. However, as illustrated in the data requirement section 3.1, the availability of realistic distribution grid models is limited due to security and privacy concerns. Therefore, based on the spatial data at hand from Dutch DSOs, this chapter introduces a synthetization methodology that we apply to obtain realistic distribution grid models. Note that this chapter has been partially published in a joint scholarly work, in which Antoine Bidel contributed roughly 60% of the work, particularly the implementation and detailed conceptualization of the methodology, the author of this thesis contributed the initial idea and overall concept, as well as the general project administration (roughly 40%), while Thomas Hamacher contributed with valuable feedback and supervision. The full paper is available in [127].

5.1 Literature review

Due to the lack of real distribution power system data, there exists a great attention for the synthetization of distribution grid models based on publicly available data in the research community. Most of the distribution grid synthetization procedures found in literature rely on available street data, mainly from OpenStreetMap, in combination with census statistics to identify load centers and estimate peak loads [128]–[133]. They commonly use the street network as a reference for possible line paths of the electricity grid. In addition, substations are positioned either by using the street network or clustering techniques, such as in [132]. In [133], the authors use similar approaches for the case of Italy, while authors in [129] build on the work of [128] to generate statistically plausible grid models for the United States. Authors in [134] follow a different synthetization approach by formulating a cost-minimization problem to include economic considerations in the model, while the technical limitations are introduced through mixed-integer conic load flow constraints. Contrary to this, the work of [135] follows a heuristic method for dimensioning the grid assets by iteratively correcting violations with grid planning measures until a functioning solution for the grid properties is reached that obeys the grid's operational limits.

To the best of our knowledge, no work in current literature proposes to process the spatial datasets presented in section 3.2 to generate synthetic grid models. Therefore, this chapter's objective is to develop a methodology allowing the generation of synthetic distribution grid

Figure 5.1: The methodology can be decomposed into three main steps

models for defined sections of the Dutch distribution grid, using the data at hand. The synthetic grid models will form the basis for the analysis of this thesis.

5.2 Methodology

The developed methodology comprises three main steps (i) to (iii), as depicted in Figure 5.1:

  (i) Line data processing (see 5.2.1) aims at identifying and defining proper connections between the line segments as well as the position of the substations and distribution boxes.
 (ii) Load estimation and allocation (see 5.2.2) estimates individual peak loads for each building and allocates them to the grid. CFs are applied to calculate the expected loads. This results in the generation of a calculable radial grid model.
(iii) Line dimensioning (see 5.2.3) determines a proper selection of the type of each line through a heuristic approach based on successive AC power flow calculations.

The steps are subsequently explained in further detail and finally result in a radial distribution grid model for power flow calculations on a defined study area.

5.2.1 Line data processing

For a selected study area, which is defined by a geographical polygon, all MV and LV line segments from the raw spatial data that are located within or intersect the edge of the study area's polygon are considered. Every line segment is composed of two nodes. The configurations encountered at each of these nodes are characterized and processed by corresponding algorithms to generate a first version of the grid model, including the substations' location. The following subsections present the major challenges encountered during the line data processing step and the procedures implemented to tackle them.

Grouping of line segments

An extensive range of the line segments is superimposed, which means that they show identical geometries. For better manipulation, these line segments are therefore grouped and are consequently characterized by their unique geometry, their voltage level (MV or LV), and the number of individual line segments included in the group.
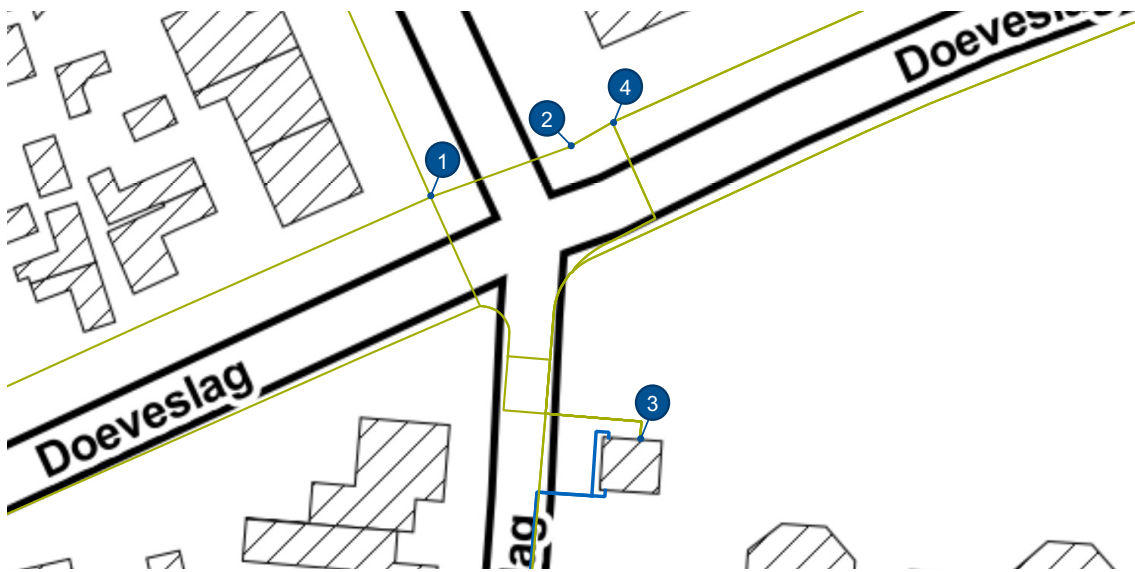
Figure 5.2: Example of different line configurations, with MV and LV lines in blue and green, respectively (map from [79], line data from [76])

Categorization of nodes

The observation of the raw line data using a Geographic Information System (GIS) highlights the need to characterize the nodes. Indeed, many of the observed node and line configurations visually suggest connections between line segments that would not exist in reality, or that can be simplified. Figure 5.2 exhibits a sample of the line data provided by DSO Enexis [76]. Based on the arrangement of the line segment groups that meet at a certain node, we can classify nodes according to the following categories: *Intersection nodes* correspond to the intersection or crossing of lines without any actual connection. Node 1 in Figure 5.2 represents such a situation. They can be recognized at the junction of four line segment groups that can be paired. Two line segment groups are considered pairable if they have the same voltage level and include the same number of line segments. To properly connect the line segment groups at an intersection node, angles are calculated, and the configuration showing the flattest angle between the groups is selected. *Intermediary nodes* are points used to define the connection between two pairable line segment groups. Node 2 in Figure 5.2 represents such a case. These nodes are not necessary for the definition of the grid model as they serve a purely geometrical purpose. The line segments connected to these nodes can therefore be merged, and the *intermediary nodes* deleted. *End nodes* correspond to the open ends of a line, as seen for example at node 3 in Figure 5.2. Finally, *dispatch nodes* represent all other cases, for instance, a group A of x line segments branching in a group B of y line segments and another group C of $x - y$ line segments, with $0 < y < x$ and all of the same voltage level. The x line segments of group A are associated one by one with the ones of groups B or C. Node 4 in Figure 5.2 represents such a case. In this example, the line segment group coming from the bottom of the clipping (group B), continues the path within the line segment group leaving the clipping's frame on the upper right edge (group A), while another line segment group (group C) that passes through node 2 also continues in this direction. In this case, we can only guess which line segments of groups B and C are associated with which line segments of group A.
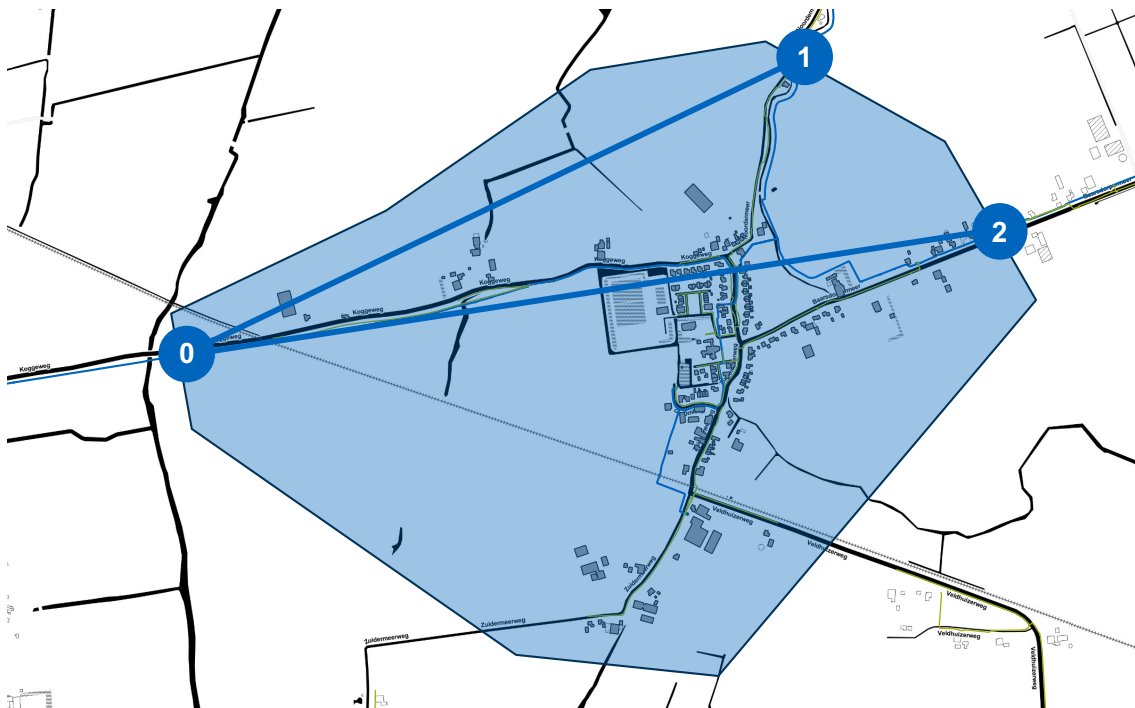
Figure 5.3: Point 0 defines the slack node, while points 1 and 2 are connected to the slack node with lines of zero length (map from [79], line data from [76])

Therefore, we choose to connect them sequentially until all are connected.

Recognition of MV/LV substations and distribution boxes

If one or more LV *end nodes* are located within a defined range of a MV *end node*, the corresponding line segment groups of the LV nodes are connected to this MV node, and a MV/LV substation is created at the location. One substation can later contain one or more individual transformers. Figure 5.2 shows such a situation at the bottom around node 3. Similarly, if two or more *end nodes* of the same voltage level are close enough to each other, the line segment groups related to these nodes are connected, and a distribution box is created. These node types are important for the synthetization process, as they represent a potential location of circuit breakers. In order to finally generate a radial distribution grid, we assume that the grid is usually split at nodes with a distribution box or a substation, as we consider circuit breakers to be opened to form strictly radial grids.

Definition of the slack node of the power grid model

For power flow calculation purposes, a unique slack node must be defined for the MV grid at the border of the area selected. To allow the processing of the area as an independent distribution grid, even in case the area is supplied from the outside by distinct systems, the MV nodes laying at the border of the study area are all artificially connected to this slack node by adding zero-length line segment groups between them. Consequently, they all share the same voltage magnitude of the slack node. Figure 5.3 depicts this procedure. In this example, the

chosen study area is connected with three MV lines entering or leaving the polygon. They are cut at points 0 to 2, and the lines 0-1 and 0-2 are added with zero length, which simulates them all being connected to the same slack bus.

Additional processing

The observation of the raw line data reveals the rare existence of odd connections between lines, particularly problematic when they are located close to the slack node or the substations. These lines are processed or deleted. For the sake of brevity, we omit a detailed discussion as these cases are rare and highly individual. Note that the line data processing step reduces the number of total line segments due to the simplification process and deletion of isolated line segments by 10% to 20% depending on the study area. This only concerns line configurations that do not allow the identification of the correct configuration with high certainty and are therefore simplified. As we will later see in the validation process, this procedure yields adequate results.

At the end of the line data processing step, we have a first version of a calculable network graph G

$$G = (V, E), \tag{5.1}$$

with nodes (vertices) V and a set of line segment groups (edges) E

$$E \subseteq \{\{x, y\} | x, y \in V\}, \tag{5.2}$$

where x and y are the respective start and end nodes of a line segment group. We have furthermore identified transformers and distribution box locations and associated them to nodes of our graph. The next step now allocates electric loads to the nodes in G and reduces it to a radial graph G'.

5.2.2 Load estimation and allocation

Based on the building data from section 3.3 and on peak load statistics for different types of buildings from literature [136]–[139], we estimate an individual peak load for each building and allocate buildings' loads to the grid. Meanwhile, to allow an appropriate sizing of the grid, CFs for the different sub-grids within the study area are determined. To simplify the allocation of the loads to the substations and the calculation of these coefficients, but also because these configurations are widely observed in practice, we decide to generate radial grid configurations only. This way, loads and the respective CFs can be associated explicitly to individual sub-grids. In further detail, we apply the following steps.

Splitting of the loads per type of building

The buildings in the BAG dataset can have $n_f \geq 1$ functions, such as a shop with dwelling units above. The buildings are consequently partitioned per function. The total usable area, obtained by multiplying the building's geometric footprint's area A_f with its estimated number of stories $n_{stories}$, derived from the building's height, is therefore split equally among the partitions, to obtain an individual usable area A_b as

$$A_b = \frac{A_f \cdot n_{stories}}{n_f}. \tag{5.3}$$

Estimation of the individual peak loads

To estimate individual peak load P_b for each non-residential building partition, we multiply their individual usable area A_b with specific peak load value P_s, so we finally end up with

$$P_b = P_s \cdot A_b. \tag{5.4}$$

Authors in [136] provide a list of typical peak loads per square meter for a diverse set of load types which we map to the building functions from the BAG dataset, as presented in Table 5.1.

Table 5.1: Typical peak load per square meter for building functions as defined in the BAG dataset, inspired by [136]

Building function	Peak load per square meter [W/m²]
Meeting	45.7
Healthcare	36.0
Office	18.9
Accommodation	30.9
Educational	7.4
Sports	29.4
Shopping	45.7
Industrial	79.0

For the case of residential buildings, we assume a peak load value P_b of 30 kW for a fully electrified household (without electric heating), which we base on information provided in [139] and [138]. This value is independent of the usable area. The number of units/dwellings in a building is extracted from the BAG dataset. It is important to note that the peak load of a residential building with multiple dwellings is not assumed to be the sum of individual peak loads. However, we later apply a CF to the loads, which is explained further below.

Connection of the loads to the power grid

Subsequently, the loads are connected to the grid. It is assumed that all buildings are connected to the LV grid, except for the industrial buildings, which are assumed to consume power at MV level. For each building of a specific type, the closest line of the suitable voltage level is selected. Since this line is defined as a series of points, its closest point to the building is used. If this geographical point corresponds to an existing node, the building is connected to this node. Otherwise, the selected line is split in two, and a node is created at the junction.

Generation of a radial power grid graph

The methodology for generating a radial power grid is based on the single-source shortest path problem, which yields a reduced set of line segment groups (edges) E' which connect the source node via the shortest path to every node in the grid. Line segments outside of the set of lines in the shortest paths are consequently deleted, so we end up with the radial graph G'

$$G' = (V, E'), \tag{5.5}$$

which contains the same nodes (vertices) with a new set of line segment groups (edges) E'

$$E' \subseteq E. \tag{5.6}$$

As the original graph G contains both LV and MV line segments, it must be ensured that the shortest paths only include line segments of the same voltage level. For the MV grid of the study area, all shortest path searches are realized from the slack node. The *end node* of the path is then a node assigned with MV loads or a substation. For the LV sub-grids, the start nodes of the shortest paths are always their respective substation, while the *end nodes* can be nodes assigned with LV loads or distribution boxes. As mentioned before, these are typical points where circuit breakers are located to switch between topological configurations. These points are used to form strictly radial grids by opening adequate circuit breakers.

In practice, the line weight used for the shortest path search is the line resistance, defined as the product of their length with their resistance per meter. However, the conductors in the line segment groups of E are not dimensioned yet, so their properties are assumed to be uniform over the entire grid. The weight chosen for the shortest path determination is, therefore, the line length. Finally, each load is allocated to a single substation (or to the slack node). The sub-grids can therefore be defined and used for the calculation of CFs.

Estimation of the coincident peak loads

In practice, all individual power demands do not reach their peak at the same moment in time. Considered together, the load profiles of consumers fed by the same line or transformer compensate each other, and the total maximum load observed for a neighborhood is significantly lower than the sum of the individual peak loads [140]. To consider this effect, known as load coincidence, a CF is applied to each load fed by the same substation or source. The value of this coefficient then depends on the number of loads fed by this element. As defined in [139], the coincident load of a group of n consumers, denoted $P_p(n)$, is thus the product of the CF for this group $CF(n)$ with the sum of the individual peak loads $P_{b,n}$ as

$$P_p(n) = CF(n) \cdot \sum_n P_{b,n}. \tag{5.7}$$

For residential loads, the following equation proposed in [138], [139] is used, defined as

$$CF(n) = CF_\infty + (1 - CF_\infty) \cdot n^{-3/4}, \tag{5.8}$$

where n is the number of households and CF_∞ the CF for an infinite number of households. For a typical fully electrified household without electric heating, the value of CF_∞ is between 0.06 and 0.07 [138]. For other types of loads, we apply the following more conservative equation from benchmark evaluations in [73] which is defined as

$$CF(n) = 0.6 \cdot (1 + n^{-1}), \tag{5.9}$$

with n the number of consumers. For each sub-grid and for each building type, a CF is therefore calculated and applied to the corresponding loads. For the AC power flow calculations,

a corresponding reactive power load Q_p is also needed. Here, we rely on the following relationship

$$Q_p = \tan\left(\cos^{-1}\left(\cos(\theta)\right)\right) \cdot P_p, \tag{5.10}$$

with $cos(\theta)$ the power factor, with typical values for $cos(\theta) = \{0.95, 0.8\}$ for residential and all other types, respectively.

Dimensioning of the transformers

After estimating the coincident load of each building in the LV sub-grids, the total coincident apparent load assigned to each substation can already be calculated and compared to the nominal apparent power of selected benchmark transformers. Considering a 20% safety margin, the smallest possible transformer type among the common types listed in Table 5.2 is chosen for each substation. If the total coincident load assigned to a substation is higher than the nominal apparent power of a transformer including margins, additional transformers are added to the substation, and the load is shared.

Table 5.2: List of common local network transformers and their characteristics [141]

Trafo type	Vol. prim. side [kV]	Vol. sec. side [kV]	Nom. power [MVA]	Resistance [%]	Reactance [%]
Type 1	10	0.4	0.25	1.2000	4.0
Type 2	10	0.4	0.40	1.3250	4.0
Type 3	10	0.4	0.63	1.0794	4.0

5.2.3 Line dimensioning

Before dimensioning the lines in the radial graph, the line segment groups are separated again into individual line segments, which are added to the graph in parallel to the original line segment group to preserve the coherence of the model. Then, the individual line segments are dimensioned by choosing the appropriate line type among a set of selected standard line types. The following subsections present the approach in further detail.

Selection of common line types

In addition to the publicly available datasets from the DSOs presented in section 3.2, an extended dataset for the city of Doetinchem in the province of Geldernland was kindly provided by DSO Liander upon a personal request to the four largest DSOs. Apart from the location and voltage levels, this dataset also includes the cable types of the line segments. As a result, we can identify a large number of unique cable types installed in this area, that is to say 176 different types on the LV-level and 34 on the MV-level. Against the background of the historical development of the electricity grid over many decades, this large number of different cable types can be easily explained, as technological progress, falling costs, and changing electricity demand forecasts had a significant influence on the cable types used throughout the years. Furthermore, one major differentiator among this large variety of cable types is the type of insulation used, while cross-sections do not vary as much. Among the cable types used, the most observed cross-sections in this extended dataset can be found in Table 5.3.

Table 5.3: Most used cross-sections for cable types per voltage level in the extended dataset from Liander for the city of Doetinchem

Voltage level	Cross-sections [mm^2]
LV	2.5, 6, 10, 16, 50, 95, 150
MV	50, 95, 150, 240

On the LV-level, we can observe from the locational information that the smallest cross-sections essentially correspond to building connections and are therefore disregarded for further investigations, as they are not available for other datasets and do not play such an important role in the discussion of this thesis. In combination with additional data sources [73], [138], [142] and from standard line types defined in the tool PandaPower [141], we then derive a set of common line types, which is presented in Table 5.4.

Table 5.4: List of selected cable types and their characteristics [73], [138], [141], [142]

Cable type	Cross-section [mm^2]	Resistance [Ω/km]	Max. current [A]
NA2XS2Y 1x70 RM/25 6/10 kV	70	0.443	217
NA2XS2Y 1x95 RM/25 6/10 kV	95	0.313	249
NA2XS2Y 1x120 RM/25 6/10 kV	120	0.253	280
NA2XS2Y 1x185 RM/25 6/10 kV	185	0.161	358
NA2XS2Y 1x240 RM/25 6/10 kV	240	0.122	416
NAYY 4x50 SE (LV)	50	0.642	142
NAYY 4x120 SE (LV)	120	0.225	242
NAYY 4x150 SE (LV)	150	0.208	270

Line type dimensioning heuristic

The following methodology is inspired by the heuristic methods proposed in [135]. The lines are dimensioned by performing successive AC power flow calculations and checking at each step for violations of technical limits, followed by incrementally decreasing line cross-sections. With the costs of an electric line increasing significantly with its cross-section, the targeted solution is a line type with minimal cross-section for the lines satisfying the operation within the technical limits for the entire power grid. We apply common technical limits based on [139], namely a voltage deviation of maximum ±10% of the rated voltage and a line flow of maximum 80% of the line flow reference value S_{ref}, defined by the value of the thermal limiting current I_{max} and expressed as

$$S_{ref} = I_{max} \cdot V_1 \cdot \sqrt{3}, \tag{5.11}$$

with nominal voltage V_1 at the start node of the line and $\sqrt{3}$ for the single-phase equivalent for balanced distribution grids.

The dimensioning procedure is first performed on the individual LV sub-grids. A radial directed subgraph is associated with each sub-grid defined by a substation, which represents its source, and a set of nodes and directed lines, which may also be parallel. Line types are only changed for each sequence of lines located between two *dispatch nodes* or distribution boxes, or

between one of these two types of elements and an *end node*. This assumption is made since a network planner is more likely to change a line over an entire section whose extreme nodes are connection points between several lines. Moreover, the dimensioning of the line sequences is realized hierarchically, starting with the closest lines to the source. Indeed, a change of line type impacts the power flow results of all the lines downstream of this line.

For each LV sub-grid, a list L of all the *dispatch nodes* and distribution boxes is generated. Applying a breadth-first search algorithm, the *end nodes*, defined as nodes with no successors in the directed subgraph, are also added to this list. Then, the closest predecessor node contained in L is determined for each node of the subgraph. Couples of nodes from L are then formed, and the lines included between each couple of nodes are collected to form a line sequence. A depth level is calculated for each couple in the subgraph and associated with the corresponding line sequence.

For each LV sub-grid and each line sequence, starting with the ones with the lowest depth level, a power flow calculation is performed on a grid model combining the MV grid and the LV sub-grid involved. This simplification is done to speed up the computation, and the MV grid is kept in order not to redefine the slack node, which would significantly affect the results. A correction factor must be added to the security margins to take into account the overall load reduction. The results of the power flow calculation are analyzed and, if no violations are detected in the line sequences downstream of the line sequence under investigation, its line type is changed to a smaller type from Table 5.4. A second power flow calculation is then performed to verify that this cross-section reduction does not cause new violations on the line sequences downstream. However, if violations are indeed detected, the line type is changed back to the previous one. Otherwise, the new line type is kept. This procedure is repeated as many times as there are possibilities of changing the line type to a smaller one.

A similar method is applied to dimension the MV grid. However, the power flow calculations are not only performed on the MV grid but the entire system. Indeed, the line type chosen for a MV line sequence affects the power flow on the MV line sequences downstream as well as the LV line sequences connected to the lines through a substation.

5.3   Test cases and validation

The validation of the generated synthetic grid models is based on Complex Network Analysis (CNA) methods which aim at identifying statistical properties in the grid structure represented as a graph [143]. This section presents the results of the statistical analysis conducted on two different study areas for a rural and larger suburban/urban case with mostly residential buildings. The methodology is implemented using Python in combination with the spatial PostGIS relational database mentioned in Chapter 3. All power flow calculations are performed using the software package Multi-Energy System Modeling and Optimization (MESMO) [144] applying a fixed-point solution methodology, which is also used in the analysis part of this dissertation and is explained in more detail in section 6.4.3. The two grid models are finally used in the analysis, partially in a reduced form.
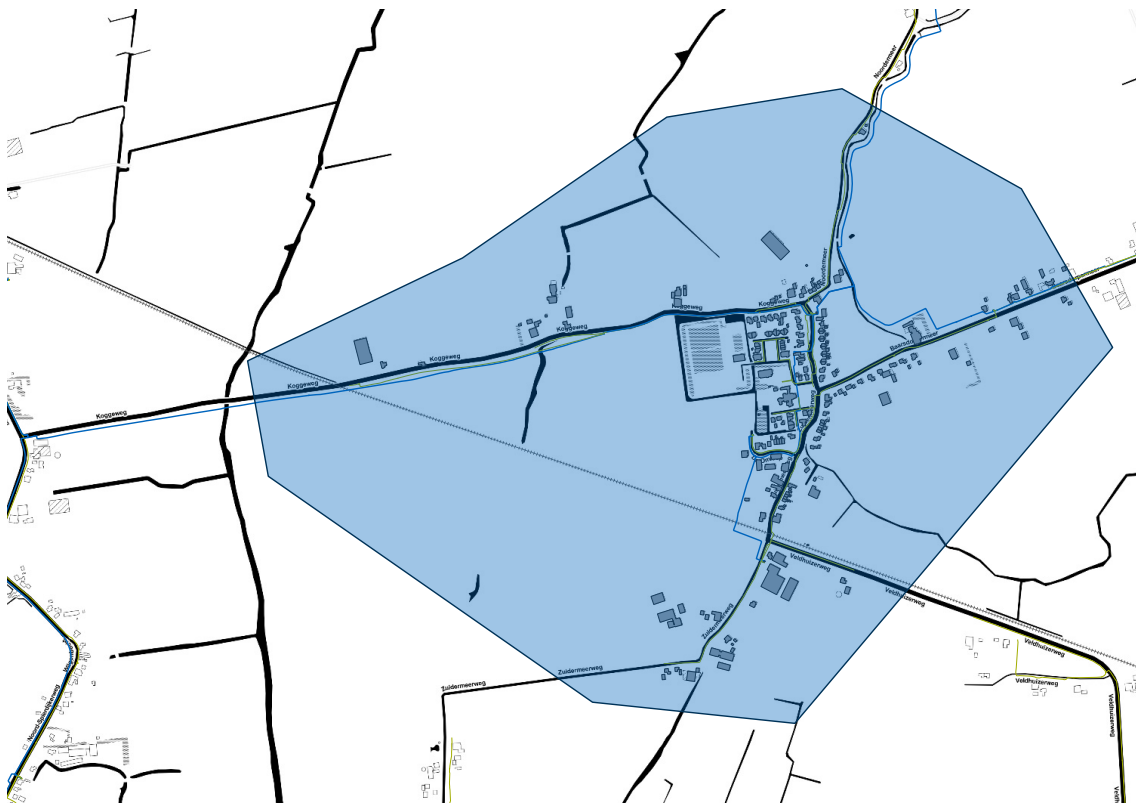
Figure 5.4: Study area for the rural town of Zuidermeer with MV lines in blue, LV lines in green (map from [79], line data from [76])

5.3.1 Study areas

To validate the grid synthetization routines' applicability to different types of regions, two fairly distinct study areas are analyzed, as distribution grids vary in their complexity depending on their locality, as explained in section 3.1. To this end, we apply the methodology to a rural and suburban/urban residential case.

Rural case: Zuidermeer

Zuidermeer in the Dutch province North-Holland is a rural village due to its low-density population and strictly radial distribution grid topology with fairly high line lengths. The grid is operated by DSO Enexis. The town has 540 inhabitants [145], roughly 150 residential buildings in the town's center, around 30 commercial, mostly agricultural establishments, and a few social, communal facilities [81]. Figure 5.4 presents the corresponding polygon that is applied to select the appropriate data points from the raw dataset.

Suburban/urban case: Eindhoven

We define the second study area as a portion of the municipality of Eindhoven, as seen in Figure 5.5, corresponding to a suburban/urban case. The study area includes portions of the neighborhoods Schouwbroek (1530 inhabitants), Philipsdorp (3095 inhabitants), Eliasterrein-
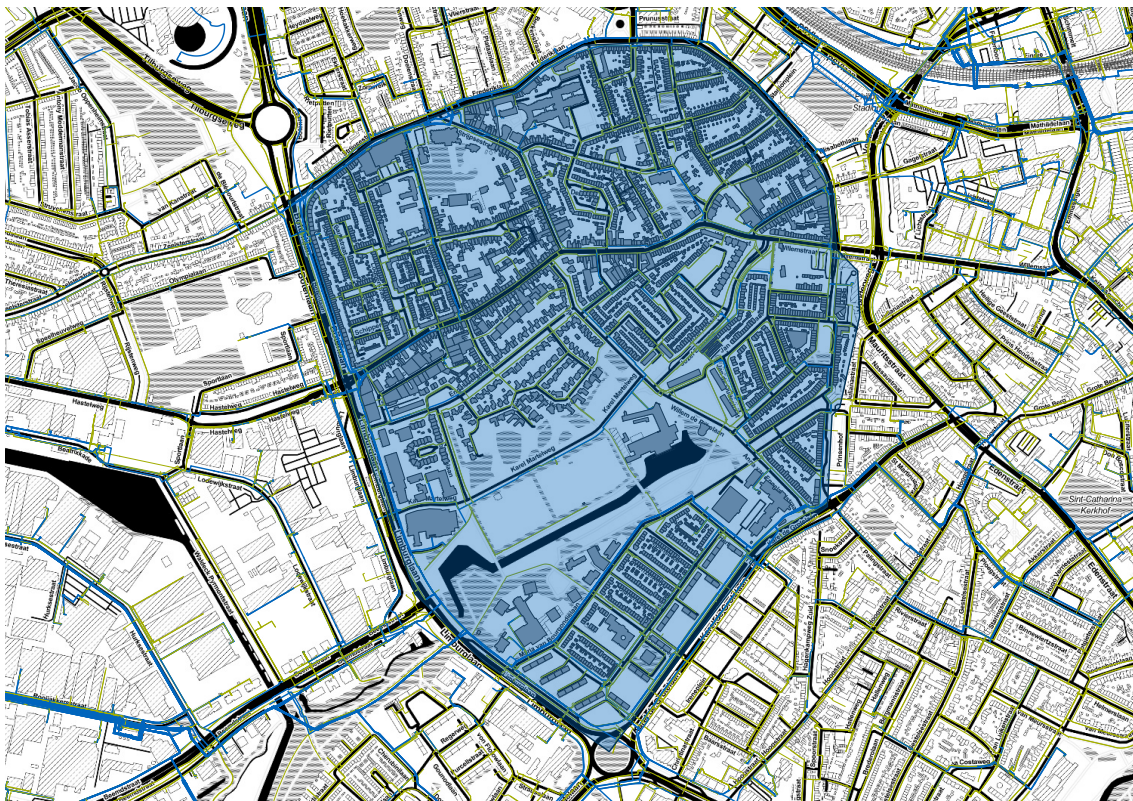
Figure 5.5: Study area for a portion of the city of Eindhoven with MV lines in blue, LV lines in green (map from [79], line data from [76])

Vonderkwartier (3165 inhabitants), Engelsbergen (635 inhabitants) and Hagenkamp (1180 inhabitants) [146]. The municipality is located in the province of Noord-Brabant, and its distribution grid is equally operated by DSO Enexis.

5.3.2 Validation

For test case Zuidermeer (Eindhoven), the generated grid model comprises 156 (2569) nodes, 151 (2993) lines, and 5 (31) substations. For the validation, a statistical analysis is performed on both test cases. The statistical results are then compared to the patterns observed in real European distribution systems based on the works of [143] and [147]. The subsequent subsections present three different properties that were analyzed, which describe topological characteristics of the grid model as a graph and its edges' properties, i.e., the chosen line types.

Hop distance distribution

To validate the topological characteristics of the radial synthetic grid models, authors in [147] suggest the measurement of the hop distance distribution. We measure the hop distance as the distance of a node to the root node, represented by a substation or the source node. According to the authors, in the context of a radial grid, each node's one path of interest is the one between itself and the substation (source node). The distance is measured as the number
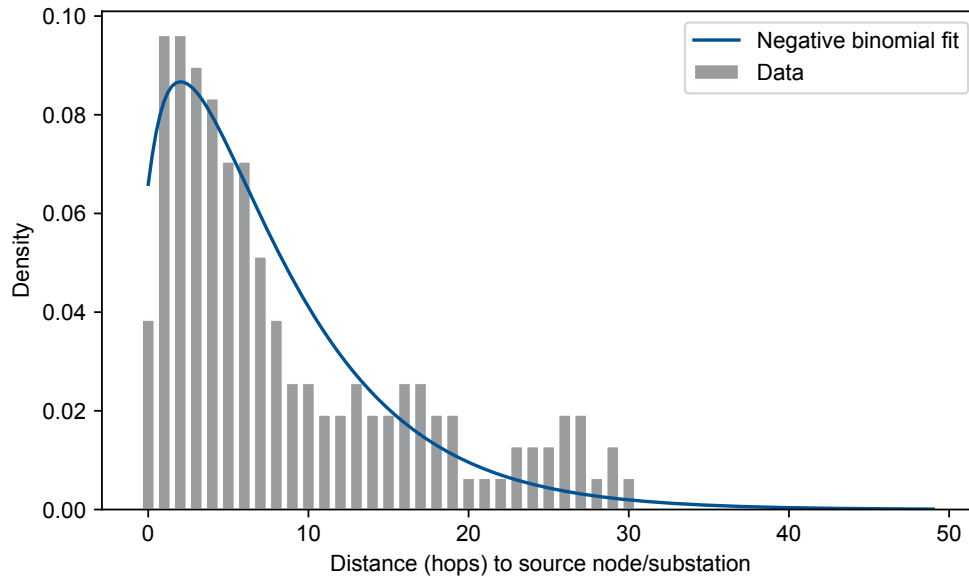
Figure 5.6: Hop distance distribution for Zuidermeer and the corresponding negative binomial fit

of edges (line segments) to the root node. For the case of the LV sub-grids, the individual root nodes correspond to the respective substations while the slack node plays this role for the MV grid. Based on their statistical analysis, authors in [147] suggest that the hop distance distribution should follow a negative binomial curve, which is given as

$$P(x, r, p) = \frac{\Gamma(r + x)}{x! \Gamma(r)} \, p^r \, (1 - p)^x, \tag{5.12}$$

with positive coefficient $r > 0$, integer value p, as $0 \leq p \leq 1$, hop distance $x = 0, 1, ..., \infty$, and Γ being the Gamma function. For our two study areas, the hop distance distributions and the corresponding fitting curves are presented in Figures 5.6 and 5.7. As can be observed in both figures, the hop distance distributions for our resulting synthetic grids closely follow a negative binomial distribution. However, the Zuidermeer example seems to achieve a less accurate fit, which could be related to the fact that it is a much smaller grid. We can conclude from this analysis step that our methodology performs well in identifying the distribution boxes, which results in cutting ring structures at the correct places to make the grid strictly radial.

Normalized weighted characteristic path length

As suggested in [143], the weighted characteristic path length (WCPL) L_{wcpl} is a defining property of a graph and is given by the number of weighted steps that are necessary on average for connecting any two nodes within a graph. According to [143], it is defined as the median for all nodes $(v_i, v_j) \in V$ of the distance that is defined as

$$d_w(v_i, v_j) = \sum_{e_{s,t}} e_{w_{s,t}}, \tag{5.13}$$
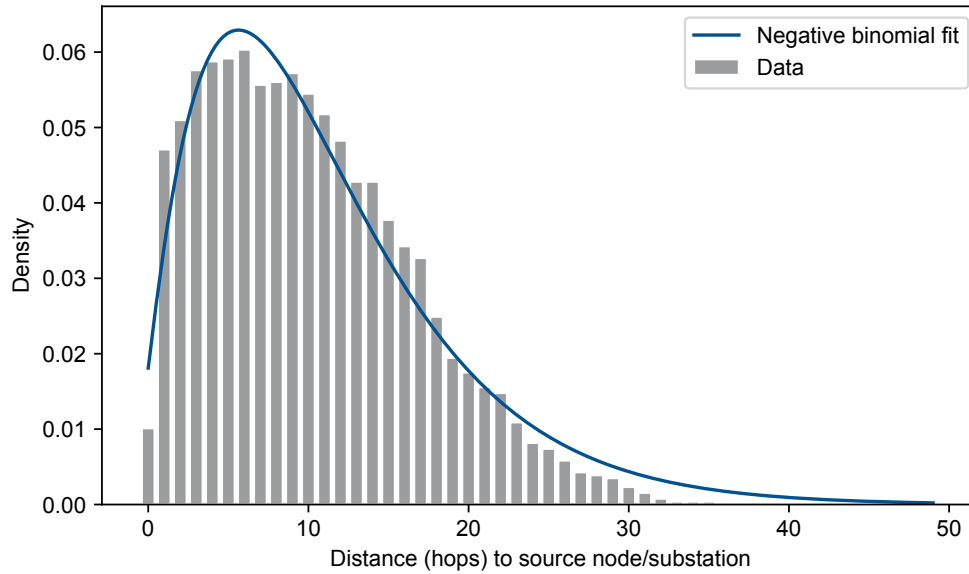
Figure 5.7: Hop distance distribution for Eindhoven and the corresponding negative binomial fit

with $e_{w_{s,t}}$ an edge in the minimum weighted path between nodes v_i and v_j. The weight of an edge is defined as the resistance of the line segment multiplied with its length. For comparability, the normalized weighted characteristic path length (NWCPL) is obtained by dividing L_{wcpl} by the average weight of the edge belonging to the same data sample. Tables 5.5 and 5.6 present the values for our synthetic grids. We can observe that results obtained for the NWCPL for both cases range between $[3.08, 18.42]$ and are within a similar range as the values provided in [143], which are given as $[5.5, 20.6]$. Authors in [143] point out that typical values for MV lines are high since they span over larger geographical areas. We observe the contrary effect for our MV grids, which is due to the fact that lines are cut by the defined polygon of the study area.

Table 5.5: NWCPL for the synthetic grid generated for the case of Zuidermeer, with the root ID describing the source node of each sub-grid

Rood ID	Voltage level	NWCPL
1	MV	3.08
152	LV	6.96
153	LV	6.00
154	LV	4.73
155	LV	8.55
156	LV	3.20

Ratio of estimated current over thermal limiting current

Finally, the distribution of the ratio of the estimated current I_{est} in the lines over their thermal limiting current I_{max}, as defined in [147], also yields satisfying results. This measure serves as

Table 5.6: NWCPL for the synthetic grid generated for the case of Eindhoven, with the root ID describing the source node of each sub-grid

Rood ID	Voltage level	NWCPL
1	MV	9.44
2552	LV	15.36
2553	LV	9.69
2554	LV	10.13
2555	LV	18.42
2556	LV	14.52
2557	LV	7.32
2558	LV	8.78
2559	LV	12.92
2563	LV	16.79
2564	LV	15.20
2566	LV	7.39
2567	LV	6.20
2568	LV	13.54
2569	LV	9.99
2570	LV	3.96
2571	LV	17.76
2572	LV	13.16
2573	LV	3.33
2575	LV	8.42
2576	LV	6.08
2577	LV	8.52
2582	LV	13.09
2583	LV	6.80
2584	LV	12.33

an indicator for the quality of our line dimensioning process, as the thermal limiting current is a function of the line characteristics, given as

$$I_{est} = \frac{S_1}{V_1 \cdot \sqrt{3}}. \tag{5.14}$$

Using equation (5.11), we can then derive the ratio

$$x = \frac{I_{est}}{I_{max}} = \frac{S_1}{S_{ref}}. \tag{5.15}$$

Plugging in ratio x, authors in [147] suggest the distribution $f(x)$ to follow an exponential decay, formulated as

$$f(x) = \mu e^{-\tau x}, \tag{5.16}$$

with parameters μ and $\tau > 0$. The exponential decay indicates that most lines are operated far below their operating limits. Figure 5.8 shows that the distribution indeed follows an exponential decay for increasing ratio x, with similar trends for tail values, which is in line with statements in [147]. When looking at the case of Zuidermeer, however, as depicted in Figure 5.9, the distribution shows a significant mismatch. This can be explained by the smaller area and number of lines for the rural case. Recall that for x, no values above 0.8 can be expected, as
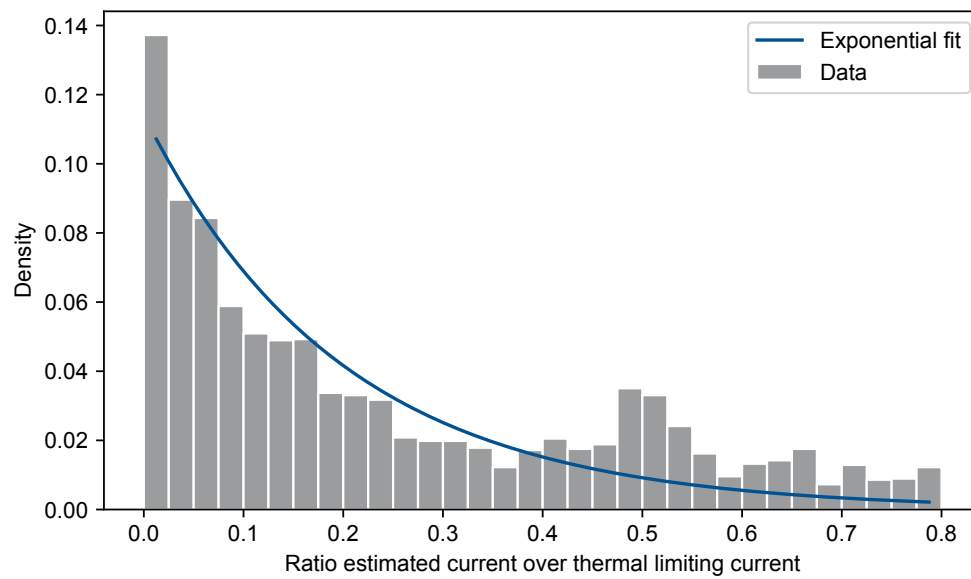
Figure 5.8: Current ratio distribution for Eindhoven and the corresponding exponential fit
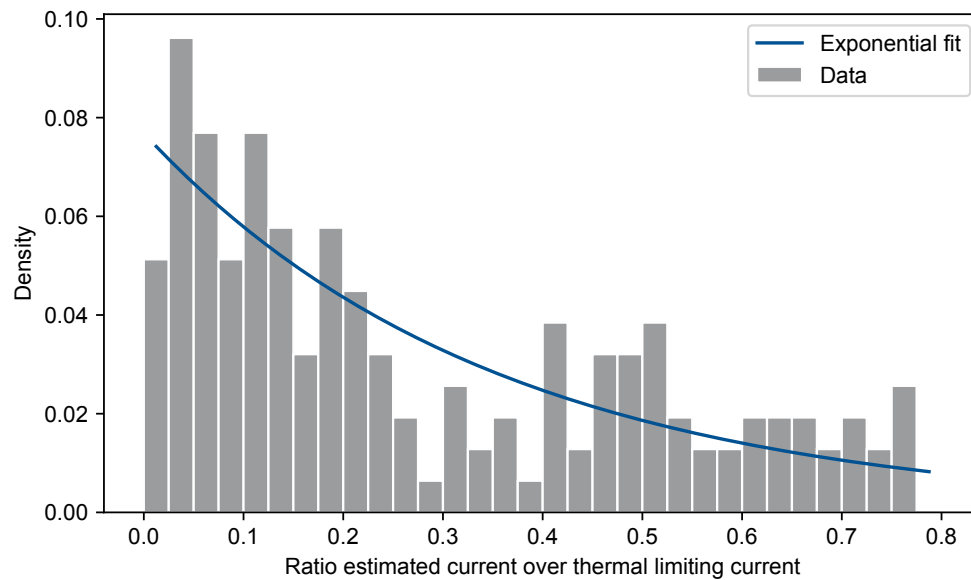
Figure 5.9: Current ratio distribution for Zuidermeer and the corresponding exponential fit

we applied a 20% safety margin in the line dimensioning process. Curiously, there exist lines in both cases that experience no current. These were identified manually and removed where possible, as they can cause numerical problems in the optimal power flow calculations that we perform in the analysis of this thesis.

5.4 Conclusion

In conclusion, the synthetic grid of Eindhoven shows a high validity based on the applied validation methodology by comparing the grids to statistical patterns. On the other hand, for the rural case of Zuidermeer, we identified some mismatches between the synthetic grid and targeted patterns. They can be explained by the smaller area and the lower number of nodes and lines. However, given the small study area, it is possible to manually verify its topological validity easily by comparing it to the raw data, as the study area contains very few superimposed lines and has a relatively simple topology. To this end, we can deem both synthetic grid models realistic and therefore suitable for the application in our analysis, which follows in the subsequent chapter.

Chapter 6

Price signal analysis framework

As explained in Chapter 2, nodal prices provide the highest level of spatial and temporal granularity and therefore represent the optimal price signal in terms of economic efficiency. To exploit the full potential of DERs and to prevent the system from potential overloading (or voltage violations), efficient economic price signals are needed. To this end, researchers have proposed DLMPs as presented in section 1.3. However, current research fails to provide a systematic analysis of their applicability and of the actual need for a price signal defined on such a high granularity level. Therefore, this thesis applies a systematic approach for identifying the impact of different price signals, and in particular DLMPs, and their respective influence on social welfare as a measure of efficiency. This chapter will therefore lay out the methodology of the analysis applied in this thesis. The first section will present the models and the problem formulation. Subsequently, the analysis flow and calculation routines are introduced, represented as a sequence of different optimization problems. Then, the dimensions of the techno-economic analysis are presented. The final section derives the implementation requirements and presents the resulting software environment.

6.1   Problem formulation and models

Based on the intuition we have built on electricity markets and price discovery in Chapter 2, the analysis conducted in this thesis rests upon two central principles: (i) Electricity markets aim at maximizing social welfare, which is the sum of the surplus of individual market participants; (ii) price granularity increases when representing the grid characteristics in the welfare optimization, yielding individual prices at different locations of the grid, termed nodal prices or DLMPs. Therefore, the following subsections introduce the local distribution grid market organization and the welfare formulations and models. These are used throughout the analysis routines, which are presented subsequently.

6.1.1   Welfare definitions

For our local distribution grid market, we assume a radial grid being fed from the transmission grid at the source node at wholesale market price c_t^{ref}. Note that we assume a reactive power price at the source node equal to zero at all times. On the supply side, the source node
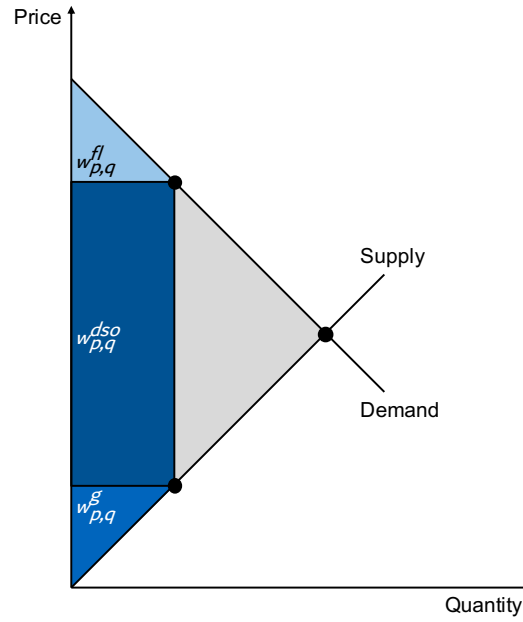
Figure 6.1: Social welfare is defined as the sum of the colored areas $w_{p,q}^{fl}$, $w_{p,q}^{g}$, and $w_{p,q}^{dso}$, the consumer, producer, and merchandising surplus, respectively

represents the only generating source in the context of this thesis. However, the following formulations can easily be generalized for an arbitrary number of distributed generators, such as PV or wind turbines. Concerning the demand side, we consider DERs as flexible loads (superscript fl) in the form of HPs as introduced in Chapter 4. As we have learned in Chapter 2, we can understand the market-clearing of energy markets as an optimization problem, which maximizes social welfare. The following paragraphs define social welfare and surplus formulations for the market participants, to then formulate the optimization problem in its entirety.

Social welfare

Recall from the simple example in section 2.1.1 that for an unconstrained (single-node) system, social welfare is defined as the sum of consumer and producer surplus. In the constrained case, the market operator yields a merchandising surplus from its economic activity as a spatial arbitrager for energy. This leads to market splitting and different prices at different nodes. For convenience, we are repeating an adapted version of the social welfare graph from section 2.1.1 in Figure 6.1. For the unconstrained case, the merchandising surplus equals zero, and the entire area between the supply and demand curves in Figure 6.1 is filled with consumer and producer surplus. In the constrained case, the system operator gains a surplus, and the grey area in the same figure is the welfare decrease that the system experiences.

To now formalize the social welfare, we define it over the planning horizon $\mathcal{T}$ as

$$w_{p,q}(\mathbf{p}_t, \mathbf{q}_t) = w_{p,q}^{fl}(\mathbf{p}_t^{fl}, \mathbf{q}_t^{fl}) + w_{p,q}^{g}(p_t^0, q_t^0) + w_{p,q}^{dso}(\mathbf{p}_t, \mathbf{q}_t), \tag{6.1}$$

with $w_{p,q}^{fl}$, $w_{p,q}^{g}$, and $w_{p,q}^{dso}$ the consumer, producer, and merchandising surplus, respectively,

and general injection variables $\mathbf{p}_t := [p_t^0, \mathbf{p}_t^{fl\mathsf{T}}]^\mathsf{T}$ and $\mathbf{q}_t := [q_t^0, \mathbf{q}_t^{fl\mathsf{T}}]^\mathsf{T}$ that collect the active and reactive power injections at the source node p_t^0, q_t^0 and at all nodes with flexible loads $\mathbf{p}_t^{fl}$, $\mathbf{q}_t^{fl}$.

Consumer surplus

The consumers are represented by aggregators, that collect several DERs and participate for them collectively in the local market. They can aggregate all types of DERs, which can both generate and consume electricity. However, in the context of this thesis, they merely consist of flexible loads in the form of HPs. Assuming that aggregators are acting economically rational, their (individual) surplus equals the aggregate benefit of flexible loads from their active and reactive power procurement over the planning horizon $\mathcal{T}$ defined as

$$w_{p,q}^{fl}(\mathbf{p}_t^{fl}, \mathbf{q}_t^{fl}) = \sum_{t \in \mathcal{T}} \left(\mathbf{U}_t^{fl}(\mathbf{p}_t^{fl}, \mathbf{q}_t^{fl}) \right), \qquad (6.2)$$

with $\mathbf{U}_t^{fl}(\mathbf{p}_t^{fl}, \mathbf{q}_t^{fl})$ the utility from consuming active and reactive power at time step t. In the context of this analysis, the utility is modeled as the negative cost of consuming active and reactive power, which is a common assumption in literature [29], so we claim, $\forall t \in \mathcal{T}$,

$$\mathbf{U}_t^{fl}(\mathbf{p}_t^{fl}, \mathbf{q}_t^{fl}) = -\mathbf{C}_t^{fl}(\mathbf{p}_t^{fl}, \mathbf{q}_t^{fl}), \qquad (6.3)$$

with $\mathbf{C}_t^{fl}(\mathbf{p}_t^{fl}, \mathbf{q}_t^{fl})$ the procurement costs for active and reactive power.

Remark 6.1. Following definitions from [29], for all market participants procuring active/reactive power $y \in \{p, q\}$, costs are defined as $\mathbf{C}_t(\mathbf{y}_t) := \mathbf{c}_{y,t} \cdot \mathbf{y}_t$, where marginal cost is of the form $\mathbf{c}_{y,t} := \mathbf{a}_{y,t} + \mathbf{B}_{y,t} \cdot \mathbf{y}_t$, with a positive price per unit vector $\mathbf{a}_{y,t} \in \mathbb{R}^n$ (in €/kWh) and symmetric, positive definite matrix $\mathbf{B}_{y,t} \in \mathbb{R}^{n \times n}$ of small positive price sensitivity coefficients (in €/kWh^2), with n being the number of nodes considered. This turns the social welfare equations introduced in this chapter strictly convex, which is a prerequisite for the derivation of DLMPs.

Producer surplus

Recall that we assume the only generator being located at the source node in the form of the transmission grid connection. The producer surplus is thus defined as the profit resulting from the revenue $\mathbf{R}_t^g(p_t^0, q_t^0)$ from selling active and reactive power p_t^0, q_t^0 minus the cost of producing/supplying active and reactive power at the source node, so we can define for the producer surplus over the planning horizon $\mathcal{T}$ as

$$w_{p,q}^g(p_t^0, q_t^0) = \sum_{t \in \mathcal{T}} \left(\mathbf{R}_t^g(p_t^0, q_t^0) - \mathbf{C}_t^g(p_t^0, q_t^0) \right). \qquad (6.4)$$

However, the wholesale market price is considered inelastic, which means that regardless of the power demand at the source node, the price remains unchanged. Apart from the negligible price sensitivity required to keep the optimization problem strictly convex, the supply curve is approximately horizontal. This assumption allows no surplus to be generated and, as $\mathbf{R}_t^g = \mathbf{C}_t^g$, consequently the producer's surplus can be considered zero over the entire planning horizon $\mathcal{T}$

$$w_{p,q}^g(p_t^0, q_t^0) = 0. \qquad (6.5)$$

Merchandising surplus

The market operator is a neutral third party that clears the market and whose role is assigned to the DSO, which is in the spirit of the role of the TSO in nodal pricing-based wholesale markets and common practice in literature [7], [30]–[32]. The DSO can therefore aggregate a merchandising surplus. Along the lines of the individual producer's surplus formulation and over the planning horizon $\mathcal{T}$ we end up with

$$w_{p,q}^{dso}(\mathbf{p}_t, \mathbf{q}_t) = \sum_{t \in \mathcal{T}} \left(\mathbf{R}_t^{dso}(\mathbf{p}_t^{fl}, \mathbf{q}_t^{fl}) - \mathbf{C}_t^{dso}(p_t^0, q_t^0) \right), \tag{6.6}$$

with $\mathbf{R}_t^{dso}(\mathbf{p}_t^{fl}, \mathbf{q}_t^{fl})$ the revenue from selling active and reactive power to flexible loads at either a uniform or a nodal price for active and reactive power, respectively, and $\mathbf{C}_t^{dso}(p_t^0, q_t^0)$ the cost from purchasing the power required at the source node from the wholesale market at the wholesale market price. Recall that we consider the wholesale market price for reactive power to be zero at all times.

6.1.2 DSO as the market operator

As the market operator, the DSO aims at maximizing social welfare. We know that the DSO's revenue from selling active and reactive power to the flexible loads at a uniform or nodal price must equal the sum of their individual cost for active and reactive power procurement, which results in, $\forall t \in \mathcal{T}$,

$$\sum_{t \in \mathcal{T}} \left(\mathbf{R}_t^{dso}(\mathbf{p}_t^{fl}, \mathbf{q}_t^{fl}) \right) = \sum_{t \in \mathcal{T}} \left(\mathbf{C}_t^{fl}(\mathbf{p}_t^{fl}, \mathbf{q}_t^{fl}) \right). \tag{6.7}$$

In combination with (6.2), (6.3), and (6.5) as well as zero reactive power cost at the source node, we can simplify the social welfare formulation over the planning horizon $\mathcal{T}$ to

$$w_{p,q}(\mathbf{p}_t, \mathbf{q}_t) = \sum_{t \in \mathcal{T}} \left(-\mathbf{C}_t(p_t^0) \right), \tag{6.8}$$

with the active power demand at the source node p_t^0. Note that in the case of a single-node market (unconstrained case), p_t^0 simply equals the aggregate active power demand from the flexible loads, as no losses are reflected in the market, so that we can write, $\forall t \in \mathcal{T}$,

$$p_t^0 = \mathbf{1}^\mathsf{T} \mathbf{p}_t^{fl}. \tag{6.9}$$

In this case, social welfare equals the aggregated consumer surplus from (6.2). Equation (6.8) defines the objective function of the social welfare maximization problem, which we formulate and solve for different prices and scenarios throughout the analysis. In order to now formulate the entire optimization problem, the following section covers the modeling of the electric grid and DERs.

6.1.3 Models

The following two subsections introduce the linear electric grid model and DER formulations that are embedded in the optimization problem formulations for modeling and optimizing power flow and DER dispatch quantities in the analysis.

Electric Grid Model

We consider a radial, balanced distribution grid of *n* nodes, which is served through a source node that is connected to the transmission grid and with DERs $d \in D$. We assume an unconstrained active and reactive power supply at the source node. The electric grid is formulated as a linear approximate model, as presented in full detail in [29], [114], and defined as

$$\mathbf{v}_t = \mathbf{v}^{ref} + \mathbf{M}^{v,p}\Delta\mathbf{p}_t + \mathbf{M}^{v,q}\Delta\mathbf{q}_t, \tag{6.10a}$$

$$|\mathbf{s}_t^f|^2 = |\mathbf{s}^{f,ref}|^2 + \mathbf{M}^{s^f,p}\Delta\mathbf{p}_t + \mathbf{M}^{s^f,q}\Delta\mathbf{q}_t, \tag{6.10b}$$

$$|\mathbf{s}_t^t|^2 = |\mathbf{s}^{t,ref}|^2 + \mathbf{M}^{s^t,p}\Delta\mathbf{p}_t + \mathbf{M}^{s^t,q}\Delta\mathbf{q}_t, \tag{6.10c}$$

$$p_t^{ls} = p^{ls,ref} + \mathbf{M}^{p^ls,p}\Delta\mathbf{p}_t + \mathbf{M}^{p^ls,q}\Delta\mathbf{q}_t, \tag{6.10d}$$

$$q_t^{ls} = q^{ls,ref} + \mathbf{M}^{q^ls,p}\Delta\mathbf{p}_t + \mathbf{M}^{q^ls,q}\Delta\mathbf{q}_t. \tag{6.10e}$$

Vector $\mathbf{v}_t \in \mathbb{R}^n$ in (6.10a) is the voltage magnitude at the grid nodes $n \in N$, while the vectors $|\mathbf{s}_t^f|^2, |\mathbf{s}_t^t|^2 \in \mathbb{R}^l$ in (6.10b) and (6.10c) define the squared branch flow in "from" and "to" direction at lines $l \in L$ for time step $t \in \mathcal{T}$. Equations (6.10d) and (6.10e) express the total active and reactive losses in the grid for time step $t \in \mathcal{T}$. Symbol $(\cdot)^{ref}$ denotes the reference point for each of the above properties, which is chosen to be the nominal operation point of the electric grid. The vectors $\Delta\mathbf{p}_t, \Delta\mathbf{q}_t \in \mathbb{R}^d$ are the change in active and reactive power, respectively, at DERs $d \in D$ for time step t and are expressed as $\Delta\mathbf{p}_t = \mathbf{p}_t^d - \mathbf{p}^{ref}$, $\Delta\mathbf{q}_t = \mathbf{q}_t^d - \mathbf{q}^{ref}$ with $\mathbf{p}_t^d, \mathbf{q}_t^d \in \mathbb{R}^d$ the absolute active and reactive power injections of *d*. The vectors $\mathbf{p}^{ref}, \mathbf{q}^{ref}$ are the active and reactive power injections reference which is chosen to be the individual nominal (installed) power of the DERs *d*. The matrices $\mathbf{M}^{v,p}, \mathbf{M}^{v,q} \in \mathbb{R}^{n,d}$, $\mathbf{M}^{s^f,p}, \mathbf{M}^{s^f,q}$, $\mathbf{M}^{s^t,p}, \mathbf{M}^{s^t,q} \in \mathbb{R}^{l,d}$, and $\mathbf{M}^{p^ls,p}, \mathbf{M}^{p^ls,q}, \mathbf{M}^{q^ls,p}, \mathbf{M}^{q^ls,q} \in \mathbb{R}^{1,d}$ describe the sensitivity of the respective properties to the active and reactive power change.

The reference properties for the linear approximate model in (6.10) can be obtained by solving the reference power flow problem as shown in [29], [114]. This is achieved by applying a fixed-point solution methodology and a local approximation for the sensitivity matrices as a function of the reference properties, which is then updated in an iterative fashion using a trust-region algorithm, which is later explained in more detail. However, for the sake of brevity, the complete model formulation is omitted in this work and can be found in [29], [114].

DER Models

DER models in the context of this thesis are defined in linear state-space format. For our flexible HPs, we apply the same explicit discrete time-invariant system known from the formulations in 4.2.1 and repeated here for convenience for a set of DERs $d \in D$ and $\forall t \in \mathcal{T}$,

$$\mathbf{x}_{d,t+1} = \mathbf{A}_d\mathbf{x}_{d,t} + \mathbf{B}_d^u\mathbf{u}_{d,t} + \mathbf{B}_d^d\mathbf{d}_{d,t}, \tag{6.11a}$$

$$\mathbf{y}_{d,t} = \mathbf{C}_d\mathbf{x}_{d,t} + \mathbf{D}_d^u\mathbf{u}_{d,t} + \mathbf{D}_d^d\mathbf{d}_{d,t}, \tag{6.11b}$$

with vectors $\mathbf{x}_{d,t}, \mathbf{u}_{d,t}, \mathbf{y}_{d,t}$ and $\mathbf{d}_{d,t}$ the state, control, output and disturbance vectors, $\mathbf{A}_d$ and $\mathbf{C}_d$ the state and output matrix and $\mathbf{B}_d^u, \mathbf{B}_d^d, \mathbf{D}_d^u$, and $\mathbf{D}_d^d$ the input and feed through matrices on the control and disturbance vectors, respectively. This general formulation for DERs

allows convenient customization and expansion of scenarios as all DER models follow the same type of logic. Only the respective vectors and matrices must therefore be defined. For the fixed loads in our scenarios, this reduces the above representation (6.11) to a fixed output vector $\mathbf{y}_{d,t}$.

6.1.4 Optimization problem formulation

All market participants are assumed to be economically rational. Hence they seek the maximization of their individual economic surplus. Following our definition in section 6.1.2, we consider the DSO as the independent system and market operator, which maximizes the social welfare of the system subject to the operational constraints of the electric grid and the DERs. We repeat the objective from (6.8) for convenience. We can then formulate the DSO's full problem, $\forall t \in \mathcal{T}$,

$$\max_{\mathbf{p}_t^d, \mathbf{q}_t^d} \quad \sum_{t \in \mathcal{T}} \left(-\mathbf{C}_t(p_t^0) \right) \tag{6.12a}$$

$$\text{s.t.}_{(\forall t \in \mathcal{T})} \quad (6.10), \ (6.11), \tag{6.12b}$$

$$\mathbf{v}^- \leq \mathbf{v}_t \leq \mathbf{v}^+ \quad :\mu_t^{v^+}, \mu_t^{v^-}, \tag{6.12c}$$

$$|\mathbf{s}_t^f|^2 \leq |\mathbf{s}^{f,+}|^2 \quad :\mu_t^{s^{f,+}}, \tag{6.12d}$$

$$|\mathbf{s}_t^t|^2 \leq |\mathbf{s}^{t,+}|^2 \quad :\mu_t^{s^{t,+}}, \tag{6.12e}$$

$$p_t^0 - \mathbf{1}^\mathsf{T}\mathbf{p}_t^d = p_t^{ls} \quad :\lambda_t^{p^{ls}}, \tag{6.12f}$$

$$q_t^0 - \mathbf{1}^\mathsf{T}\mathbf{q}_t^d = q_t^{ls} \quad :\lambda_t^{q^{ls}}, \tag{6.12g}$$

$$\mathbf{y}_t^{d-} \leq \mathbf{y}_t \leq \mathbf{y}_t^{d+}, \tag{6.12h}$$

with active power injection at the source node $p_t^0 = \mathbf{1}^\mathsf{T}\mathbf{p}_t^{fl} + p_t^{ls}$ known from above and general DER active and reactive power injection variable $\mathbf{p}_t^d$ and $\mathbf{q}_t^d$, which only include flexible loads in the context of this thesis, hence $\mathbf{p}_t^d = \mathbf{p}_t^{fl}$ and $\mathbf{q}_t^d = \mathbf{q}_t^{fl}$ as known from above. Equality constraints in (6.12b) represent the linear electric grid model and DER state-space equations, respectively. Vectors $\mathbf{v}^-, \mathbf{v}^+ \in \mathbb{R}^n, |\mathbf{s}^{f,+}|^2, |\mathbf{s}^{t,+}|^2 \in \mathbb{R}^l$ in (6.12c)–(6.12e) describe the electric grid voltage and branch loading limits. Equality constraints (6.12f), (6.12g) represent the active and reactive global power balance, respectively. Note that active and reactive power injections are defined positive for generation and negative for consumption. Inequality constraint (6.12h) defines the respective operating and output limits of the DERs, such as, for example, the comfort limits of the thermal flexible building model in the form of temperature intervals. Finally the vectors $\mu_t^{v^+}, \mu_t^{v^-}, \mu_t^{s^{f,+}}, \mu_t^{s^{t,+}}$, and scalars $\lambda_t^{p^{ls}}, \lambda_t^{q^{ls}}$ are the Lagrangian multipliers, i.e. dual variables, associated to the respective (in)equality constraints, which we will use for the derivation of grid DLMPs.

Recall from the previous section that in the single-node case, in which the grid is not represented, the DSO's social welfare maximization problem turns into the aggregate consumer surplus problem, which is the aggregate sum of the individual aggregator's utility. In this case,

the optimization problem reduces to, $\forall t \in \mathcal{T}$,

$$\max_{\mathbf{p}_t^d, \mathbf{q}_t^d} \quad \sum_{t \in \mathcal{T}} \left(-\mathbf{C}_t(p_t^0) \right) \tag{6.13a}$$

$$\text{s.t.}_{(\forall t \in \mathcal{T})} \quad (6.11), \tag{6.13b}$$

$$\mathbf{y}_t^{d-} \leq \mathbf{y}_t \leq \mathbf{y}_t^{d+}, \tag{6.13c}$$

with $p_t^0 = \mathbf{1}^\mathsf{T} \mathbf{p}_t^{fl}$ the aggregate demand from flexible loads, as no losses are reflected, and again $\mathbf{p}_t^d = \mathbf{p}_t^{fl}$, $\mathbf{q}_t^d = \mathbf{q}_t^{fl}$ for flexible loads only.

6.1.5 DLMP derivation and decomposition

According to [55], [148], electricity markets revolve around duals incentivizing market participants to realize individual surplus, which in turn also enables maximum social welfare. Even though the production/consumption schedules obtained from (6.12) cannot be enforced on the aggregators, there exists a price which can autonomously help achieve the optimal behaviors from market participants. These prices are termed DLMPs and can be derived from the dual variables of the grid constraints in the social welfare maximization problem (6.12). Following the derivation formulations in [29], we can decompose the active power grid DLMP vector $\boldsymbol{\pi}_{p_t}^{Grid}$ into its energy $\boldsymbol{\pi}_{p_t}^{E}$, loss $\boldsymbol{\pi}_{p_t}^{L}$, congestion $\boldsymbol{\pi}_{p_t}^{C}$ and voltage $\boldsymbol{\pi}_{p_t}^{V}$ components as

$$\boldsymbol{\pi}_{p_t}^{Grid} = \boldsymbol{\pi}_{p_t}^{E} + \boldsymbol{\pi}_{p_t}^{L} + \boldsymbol{\pi}_{p_t}^{C} + \boldsymbol{\pi}_{p_t}^{V}, \tag{6.14}$$

with its individual components determined with the help of the sensitivity matrices as, $\forall t \in \mathcal{T}$,

$$\boldsymbol{\pi}_{p_t}^{E} = c_t^{ref} \mathbf{1}^n, \tag{6.15a}$$

$$\boldsymbol{\pi}_{p_t}^{L} = -(\mathbf{M}^{p^{ls},P})^\mathsf{T} c_t^{ref} - (\mathbf{M}^{q^{ls},P})^\mathsf{T} c_t^{ref}, \tag{6.15b}$$

$$\boldsymbol{\pi}_{p_t}^{C} = -(\mathbf{M}^{s^f,P})^\mathsf{T} \mu_t^{s^f,+} - (\mathbf{M}^{s^t,P})^\mathsf{T} \mu_t^{s^t,+}, \tag{6.15c}$$

$$\boldsymbol{\pi}_{p_t}^{V} = (\mathbf{M}^{v,P})^\mathsf{T} (\mu_t^{v^+} - \mu_t^{v^-}), \tag{6.15d}$$

with c_t^{ref} the cleared wholesale market price at the source node. This is done for reactive power DLMPs accordingly. Under the assumption of economically rational behavior and perfect foresight, it can be shown that, when exposing the DER aggregators to the DLMP price signal, its optimal dispatch schedule from maximizing its individual surplus yields the same result as intended by the DSO in its optimal operation (social welfare maximization) problem for the entire system, as DLMPs implicitly reflect grid conditions [29].

6.2 Calculation routines and flow of the analysis

The analysis in this thesis follows an iterative approach analyzing the impact of different levels of temporal and spatial price granularity with varying DER penetration levels in the grid. This is depicted on the two axes in Figure 6.2. In the context of this thesis, three different levels of temporal and spatial granularity are under observation: (i) VBP, (ii) RTP, and (iii) LV-DLMPs, where (i) represents a signal with no granularity in both space or time which is traditionally applied for residential and smaller industrial consumers. (ii) only varies over time; in practice,
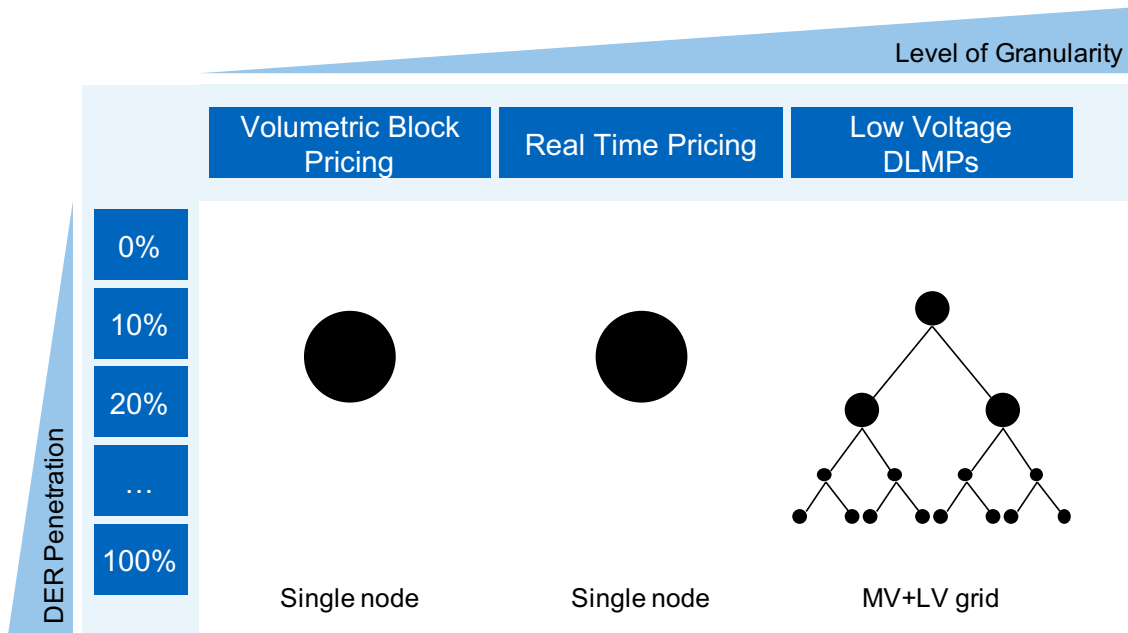
Figure 6.2: The analysis sequentially increases the price granularity for different DER penetration levels and scenarios

for the consumer, this often means a direct or adapted exposure to the wholesale spot price. Prices in (iii) also vary over space in addition to time and are termed nodal prices.

As explained above, from a mathematical perspective, the increase in spatial granularity of the price signal is equivalent to increasing the granularity of the underlying grid model in the social welfare maximization problem solved by the DSO, which is indicated by the simplified grid representation in Figure 6.2. For price signals (i) and (ii), the underlying grid model is reduced to a single node, which means that the grid does not have any effect on the dispatch quantities and the DSO's results equal the sum of the aggregators' joint surplus as obtained by the problem formulated in (6.13). With an increasing price signal granularity, the underlying grid model is defined up to its highest level of detail, i.a. all LV lines are represented and taken into account in the optimal power flow calculations. The corresponding social welfare maximization problem is formulated in (6.12).

On the vertical axis of the graph in Figure 6.2, the level of DER penetration is incrementally increased to evaluate the effect that the different price signals have on the underlying grid and potential violations of line flow constraints or voltage limits.

The overall analysis flow is presented as pseudo-code in Algorithm 6.1. The two outer loops increase the DER penetration and change the underlying price type, respectively, which is then translated into one of the two types of social welfare maximization problems in the If-statement and subsequently solved. Finally, the power flow calculation results are tested for any grid violations, i.a., if any line is operating beyond its allowable line flow limits or if the voltage level at any node is outside of its allowable boundaries. This information is saved and passed on to the techno-economic analysis.

```
1  for all levels of DER penetration do
2      Step 1: randomly assign DERs to respective share of all residential buildings
3      for all price types do
4          if price type has no spatial granularity then
5              Step 2a: formulate problem with grid as single-node equivalent as in (6.13)
6          else
7              Step 2b: formulate problem respecting underlying grid quantities as in (6.12)
8          end if
9          Step 3: solve the optimization problem
10         Step 4: run power flow on the entire grid based on resulting DER schedules
11         Step 5: check for grid violations and save the results
12         Step 6: increase price granularity level
13     end for
14     Step 7: increase DER penetration level
15 end for
```

Algorithm 6.1: Logical flow of the analysis

6.3 Techno-economic analysis

The techno-economic analysis can be separated into two interconnected steps: First, the technical effectiveness of DLMPs compared to the other price signals is evaluated by analyzing the grid states and energy balances, more specifically, the line loading and voltage levels with a particular focus on violations of the allowable limits. Furthermore, it includes a comparison of line losses and DER dispatch quantities. The main driver for differences between price signals in the technical analysis is expected to be the load coincidence that we introduced in Chapter 4 to motivate the overall problem.

The second step concerns the evaluation of economic efficiency, in which the different components of the welfare definition from section 6.1.1 are analyzed in detail. The interaction of flexible DERs with the local electricity market is expected to invoke changes in individual consumer surplus as defined in (6.2). Based on insights into the decomposition of price signals, the changes are deduced and reasoned. These observations lead to the analysis of aggregated and individual consumer surplus and the overall social welfare of the local electricity market. Subsequently, it is possible to derive and link the impact of price signals on the social welfare in (6.1) to dispatch quantities under the respective price signal. The relative change in social welfare and thus the welfare loss in comparison to RTP in particular, is assessed as an indicator of the overall efficiency decrease, as any corrective measure for alleviating congestion or voltage violations would be at least as costly.

Equity and fairness of the nodal prices are furthermore evaluated. The main objective is to understand how nodal prices are distributed over the grid and how much they differ from the RTP values. This leads to a change in individual surplus. This will help understand the impact of the pricing scheme and highlight potential outliers that are disproportionately affected compared to other market participants and carry the largest part of the changes in social welfare and the merchandising surplus in particular.

Note that in terms of economic efficiency, we can adequately compare only RTP and DLMPs, as VBP is not comparable because the prices are constant and time-invariant. Based on our assumption for the individual surplus, this means that electricity can arbitrarily be priced under this pricing scheme without any impact on dispatch quantities as only the overall energy consumption is minimized. For this reason, VBP is disregarded in the economic efficiency analysis and therefore limited to solely the impact of DLMPs presented in comparison with RTP. However, VBP will still be regarded in the technical analysis step, as it promises interesting insights when compared to variable price signals.

6.4   Simulation environment

This section presents the simulation environment that was implemented for the chosen analysis approach. To provide an overview of the functionality, the first subsection defines the requirements, while the subsequent subsections describe the overall environment setup.

6.4.1   Requirements for the simulation environment

The simulation environment that implements the above routines laid out in section 6.2 must combine several general functionalities and requirements that are summarized in this section. In order to provide an accurate description of flexible load modeling, one of the main requirements for the simulation environment is a multi-period implementation. In the context of distribution grids, static, aggregated load modeling as often chosen in transmission grids might not be accurate enough when being closer to the actual consumption [2]. The inter-temporal constraints regarding storage capacities and cost-minimization (or profit maximization) must be accurately represented in the chosen simulation environment. Furthermore, the fact that we are dealing with the distribution grid creates another barrier in the analysis of DLMPs, as power flow in the distribution grid is typically highly nonlinear. Unlike in the transmission grid, where a flat voltage level can be assumed and thus a DC load flow approximation can be applied to gain reliable solutions [149], [150], the voltage levels within a distribution grid can vary significantly, especially against the background of emerging intermittent flexible loads such as HPs. To this end, a simulation environment is needed that reliably solves a linear approximation of the AC load flow in the distribution grid, which is a prerequisite for the derivation of robust DLMPs, as defined in the previous sections. Several open-source and commercial software tools are available for performing such tasks, such as MATPOWER, OpenDSS, or DigSilent. However, as a final requirement, the chosen underlying load flow simulation tool must be modular to be flexibly applied to the different problems. This means that the mathematical foundation of the software should be well documented, accessible, and adaptable to the needs of this analysis.

In summary, the software environment must provide (i) multi-period capabilities, (ii) a high accuracy in solving optimal power flow problems for distribution grids, and (iii) a modular architecture for a high degree of flexibility. The capabilities provided by the open-source software package MESMO fulfill requirements (i)-(iii), and it was therefore chosen to form the basis for modeling and simulating DERs and the electric grid model in the context of this analysis. The following subsection will present the tool in further detail.
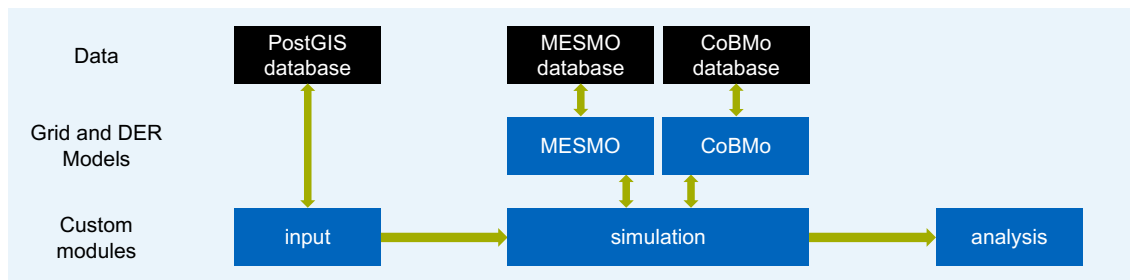
Figure 6.3: Setup of the simulation environment and interaction of the modules

6.4.2 The simulation software MESMO

MESMO or Multi-Energy System Modeling and Optimization was introduced in [144] and is available open-source in [151]. It is a simulation toolbox that combines active distribution grid operation with classical power flow studies by providing multi-period optimal power flow solutions in solving a combination of fixed-point iteration for the power flow and local/global linear approximation. With this, it provides the possibility of deriving decomposable grid DLMPs, as defined above. In addition to these optimal power flow capabilities, it allows full control over its calculation routines, as it follows a strict modular architecture based on rigorously defined interfaces and standards. This facilitates a comfortable extension with custom DER models, which go beyond the variety of already implemented models. The MESMO toolbox interfaces with the thermal building model CoBMo that we already applied in Chapter 4. All mathematical models introduced in this chapter are implemented in MESMO.

6.4.3 Implementation

Using the power flow optimization toolbox provided by MESMO as a basis, the above calculation routines and the presented models are all implemented in different modules using the programming language Python. This section will provide an overview of the module setup and how they interact with each other, while it also covers the solution algorithms used for solving the optimization problems, as the power flow approximations do not allow a straightforward approach.

Simulation environment setup

The overall setup of the simulation environment that was implemented for the purpose of this thesis is depicted on a conceptual level in Figure 6.3. The custom elements of the simulation environment are divided into three separate modules *input*, *simulation*, and *analysis*, following the overall flow of generating the input for the subsequent simulation of the models and final techno-economic analysis. On the data level, the modules interact with several databases, containing the necessary information for parameterizing all models and settings for relevant simulation parameters. The *input* module generates the respective scenarios for the simulation and implements several classes that allow the convenient management of all the simulation-related input data. The *simulation* module heavily makes use of both MESMO and flexible building model CoBMo and exploits their modular structure to implement the custom calculation routine that is showcased in Algorithm 6.1. The results of all iterations are saved and passed

onto the *analysis* module, which implements the analysis steps discussed in section 6.3. However, before moving on to the following chapter, the final subsection will now cover some technicalities of solving the optimization problems.

Optimization solution algorithm

The quadratic programs formulated above can be solved in a straightforward fashion by applying off-the-shelf solution algorithms. Therefore, we solve them using the commercial solver GUROBI. However, due to the non-linearities of the power flow, we apply an iterative approach using a trust-region algorithm in combination with GUROBI for the full DSO optimization problem (6.12), as the approximation of grid quantities may lead to inaccuracies and infeasibilities. The solution progress and the chosen parameters are explained in the following paragraphs.

As described above, we perform a linear approximation of the power flow to be used in the DSO's optimization problem. The reference properties for the linear approximate model in equation (6.10) are obtained by solving a reference power flow problem as shown in [29] for every time step. This is achieved by applying a fixed-point solution methodology and a local approximation for the sensitivity matrices as a function of the reference properties, which are then updated in an iterative fashion using a trust-region algorithm.

The trust-region algorithm supports in moving towards the optimal solution without violating grid quantities by improper approximations and large changes in power injections [152]. The authors in [29] propose to use the steady-state nominal power injection values for the initial linearization step of the first trust-region iteration. However, as the injections can vary significantly in every time step, this can yield inadequate approximate solutions for the linear power flow. Consequently, this can lead to an infeasible optimization problem, which is then wrongfully labeled as infeasible due to improper grid quantities. To solve this, we apply a first best guess for the power injections based on the solution of (6.13) and the resulting schedules of the DERs which is then used for the first linear approximation step. Under the assumption that most of the final DER schedules will not deviate much from the DSO's solution, we obtain accurate reference operation points for the local approximation in each time step.

Table 6.1: Trust-region parameters

Parameter	Value	Description
δ	1.0	Initial radius
δ_{max}	4.0	Maximum allowable radius
γ	0.25	Factor by which δ is decreased
η	0.1	Approximation evaluation parameter
τ	0.1	Solution acceptance threshold
ϵ	10^{-4}	Minimum control error

The trust-region algorithm then updates these reference power flow quantities in every accepted iteration to finally obtain the optimal solution under accurate power flow representation. This requires setting adequate parameters for the solution algorithm. The final trust-region parameters are listed in Table 6.1 for the sake of completeness. One important issue with this method is defining the size of the region δ in which the variables in the linearized model

are allowed to move during each iteration. If the region is too large, the linearized model will not accurately reflect the nonlinear model, as discussed above. If the region is too small, the convergence rate will be very slow, or wrongful infeasibilities can occur. As a result, it is desired that the size of the region starts relatively large so that fast progress can initially be made, and then decrease in size as the algorithm approaches the optimal solution [152]. As we normalize almost all variables to a per-unit value, the chosen initial radius of $\delta = 1.0$ allows the maximum movement of the majority of variables. The other parameters were chosen based on the works in [152], [153] and adapted applying a trial-and-error strategy that eventually led to the most robust and efficient behavior of the solution algorithm. The actual trust-region algorithm routine is explained in full detail in [152], [153].

Chapter 7

Simulation and results

This chapter presents the results of the techno-economic analysis illustrated in detail in section 6.3 of the previous chapter. In the first section of this chapter, the scenario design and the three defined scenarios are showcased. Subsequently, the results are presented, closely comparing the three scenarios to each other according to the dimensions of the techno-economic analysis framework. Finally, the chapter concludes with a discussion of the results and the assumptions that were taken. The simulations were performed on a Linux system running Ubuntu with 10 Intel "Xeon Gold 6148" CPUs at 2.4 GHz each and a total of 45 GB of memory.

7.1 Scenario design

The scenario design is separated into three steps: First, adequate study areas are chosen based on the data at hand, the synthetic grids from Chapter 5, and the context definitions from section 3.1. Then, an approach for the systematic HP assignment for the different DER penetration levels in the simulation routine is chosen. Finally, an adequate simulated time frame and the respective wholesale market price are defined.

7.1.1 Study areas

The analysis approach described in the previous Chapter 6 is performed on three different study areas that represent different behavior concerning the grid and building characteristics according to the remarks made in Chapter 3.1 on the defined context for this analysis. Recall that the locality of the underlying study area significantly influences grid architecture and the types of loads encountered in the distribution system. For the urban and suburban case, two adequate sub-grids are extracted from the large synthetic grid from the Eindhoven area, which can be seen in Figure 7.1. In combination with the rural study area from Chapter 5 we end up with a rural, suburban, and urban case, which are presented in Figure 7.2. All grids are fully radial.

One highly distinguishing aspect of the rural case compared to the two other cases is that it includes some industrial and agricultural loads, while the other two areas are purely residential. Table 7.1 summarizes the three study areas. Most notably, the suburban scenario does not
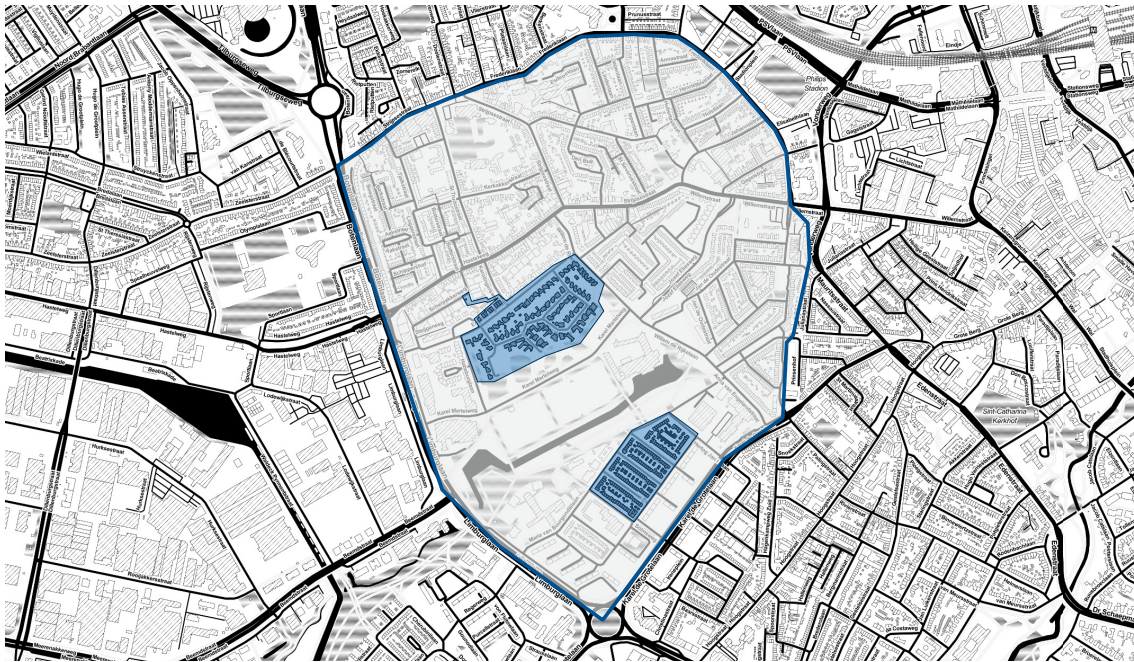
Figure 7.1: The two reduced urban and suburban study areas within the larger Eindhoven study area (map from [79])
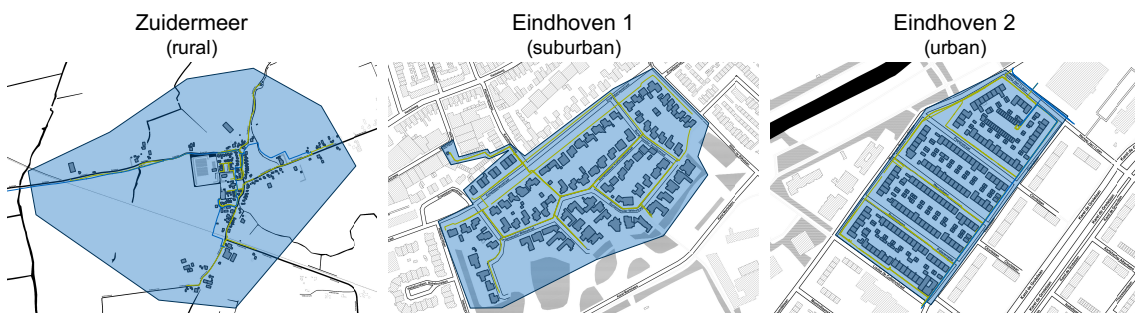
Figure 7.2: The three defined study areas for a rural, suburban and urban scenario (map from [79], line data from [76])

contain any MV lines, and the entire area is served through just one transformer station, which is located on the upper left side of the study area. In contrast, the other two study areas consist of four and five transformer stations, respectively, which means that the respective LV line lengths per feeder are significantly higher in the suburban scenario. Consequently, we can expect higher voltage drops and losses for this case.

Furthermore, the number of residential buildings is of interest. They range from fewer yet larger SFHs in the rural and suburban case to a higher number of THs in the urban case. For the electrification of their heat demand in this analysis, a systematic approach is chosen to assign HPs to the residential buildings in the different DER penetration levels.

Table 7.1: Study area statistics

	Rural	Suburban	Urban
Number of residential buildings [–]	130	92	154
Number of transformers [–]	5	1	4
Total line length (LV) [km]	4.4	2.8	2.7
Total line length (MV) [km]	3.3	0.0	1.2

7.1.2 HP assignment

For the assignment of HPs, two distinct approaches are evaluated, namely a random Monte-Carlo-based approach and a systematic approach based on assumptions. In a Monte-Carlo approach, the HPs are assigned randomly to the buildings, and simulation runs are repeated several thousand times with different configurations until convergence is reached. However, it was deemed impossible to apply a Monte-Carlo approach in a reasonable time frame due to a very high calculation cost. Furthermore, the overall benefit from such an approach is expected to be relatively low. This is because potential grid violations are expected to only occur in very high DER penetration scenarios (>70%), in which the potential number of variations in HP assignment is already quite low. That is why we opt for a systematic assignment of HPs. Thus, the number of buildings with installed HP is increased systematically by electrifying the heat demand from youngest to oldest buildings. The underlying rationale assumes that younger buildings are either already equipped with a HP or are more likely to fulfill the insulation criteria based on the minimum required renovation type EPL2 from section 4.2.3. Furthermore, it is assumed that pressure on property owners for thermal renovations will increase over time and will result most costly for older properties, which is why their heat demand will be electrified last.

7.1.3 Wholesale price and time frame

Along the lines of the scenario design in Chapter 4, for VBP, the electricity price is defined as $c_t = 1€/MWh, \forall t \in \mathcal{T}$, while RTP follows the time series of the historical wholesale market data that we introduced in section 3.6. As described above, the DLMPs are a result of the DSO's optimization problem (6.12) and are directly related to the RTP signal. Concerning the selected time frame, again, under the assumption of the highest expected heating demand in winter, we run the simulation for a random weekday in January for the year of 2017. In accordance with the day-ahead wholesale market, we define the time interval $\Delta t = 1$h. While the analysis concentrates on one entire day, the simulation is performed for three consecutive days, of which only the middle day is analyzed to avoid ramp-up and ramp-down effects.

7.2 Technical effectiveness

In this first result section, we investigate the effect that different price signals have on the operation of individual HPs and the electric grid as a whole to assess the overall strain that the additional residential heat load potentially puts on the grid. In this context, the effectiveness of the congestion and voltage management capabilities of DLMPs, as well as their loss reduction

potential, are analyzed. Therefore, we first consider an arbitrary HP's operation under the different price signals to understand the effects of the price signals on individual consumers, to look at the system load and asset utilization subsequently.

Note that for the suburban scenario, there are no values for 90% and 100% DER penetration levels under the DLMP price signal, as the optimization problem could not be solved. The infeasibility of the optimization problems of these two cases is because no feasible solution exists, as some assets would consistently be violated. However, the power flow linearization that is performed based on a reference value can also lead to approximation errors, which not even the trust-region algorithm can resolve. Inevitably, this issue of missing result data for these DER penetration levels persists throughout the remainder of the results chapter.

7.2.1 Individual building operation

Figure 7.3 presents the HP operation of an arbitrary building in the suburban scenario at 80% DER penetration for the three price types under investigation. Note that the constant VBP is not represented in the upper price curves, as it has been set to an arbitrary constant value and consequently cannot be compared to the other two price types. Concerning electric power consumption, we can see a direct correlation between power drops and price peaks. One example of the effect of the DLMP price signal can be seen between 4:00h and 6:00h in the morning, where, due to a higher DLMP price signal compared to the RTP, the power demand drops by roughly 50%.

It can be noted that under RTP, the storage was filled during the low nighttime prices. Under DLMP this operation is postponed. For VBP, there exists no incentive to use the storage, as the cost of energy does not vary, and due to inefficiencies of the sensible storage, it makes more sense to directly heat the building if possible, instead of using stored heat. Note that the storage in this example remains at its initial state of charge of 50%. As this represents "free" energy, the storage content is actually fully used towards the end of the last simulated day (out of three days), which is omitted in the analysis, as explained above.

Concerning the zone temperature in the lower plot, it can be observed that the lower zone temperature limits are fully exploited by all price signals to minimize energy procurement costs. Most notably, both time-varying price signals avoid the high electricity price peak in the afternoon by pre-heating the building and thus using its inherent storage capabilities when comparing to the constant VBP price signal.

7.2.2 System load and losses

After having inspected the individual operation of an exemplary building, we now investigate the energy consumption and losses in the entire system. The graphs in the top row of Figure 7.4 show the respective sum of all active power loads over the entire day for the different DER penetration levels and scenario types (rural, suburban, urban). Furthermore, it must be mentioned that the overall energy consumption values do not include active power losses. It becomes clear that the overall load increases with time-varying price signals and especially with increasing DER penetration in the system. This effect can be related to the fact that, while the aggregators of HPs all aim at minimizing their power procurement costs, in the time-varying
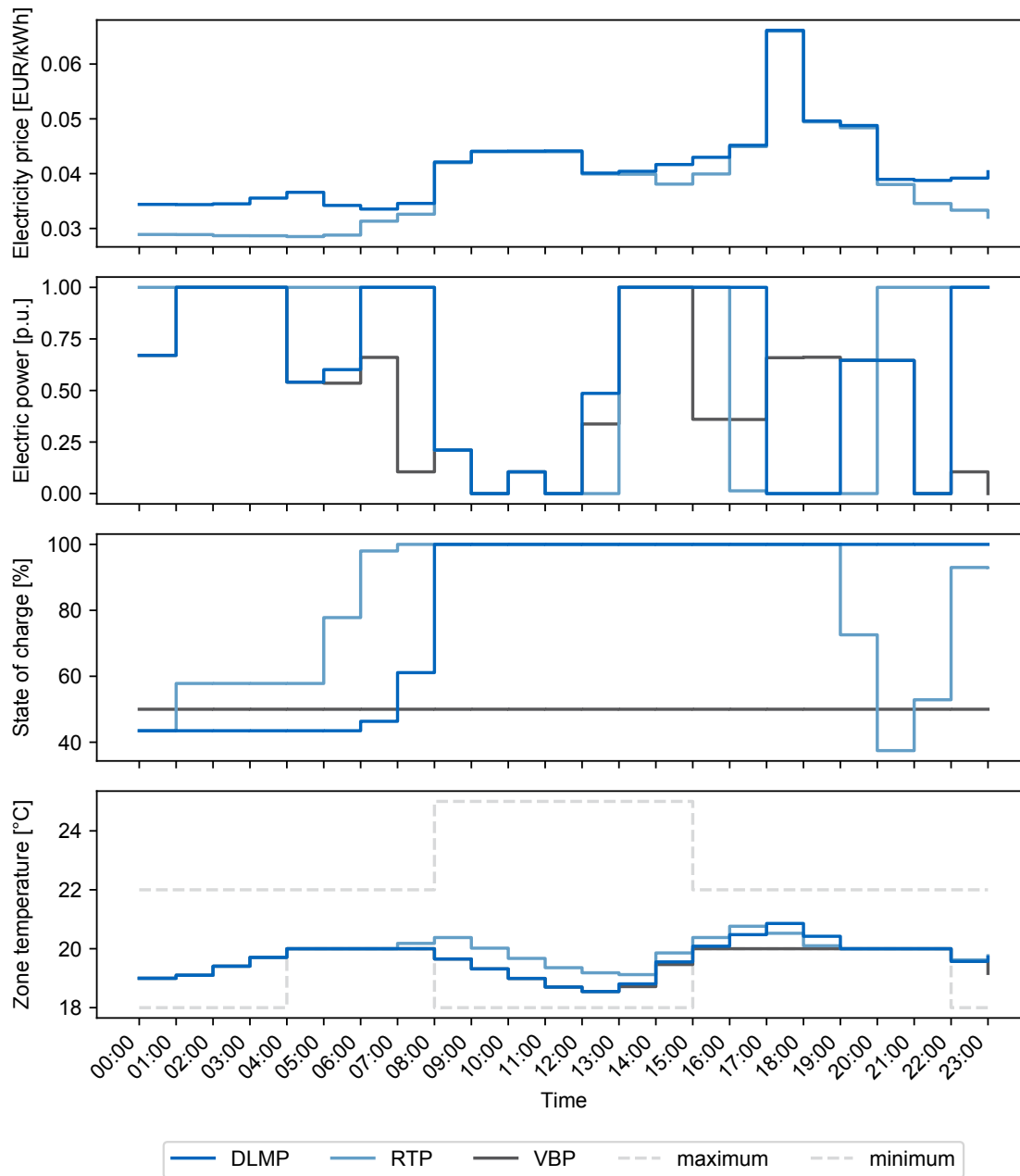
Figure 7.3: Arbitrary HP and storage operation over a full day at 80% DER penetration for the suburban scenario in Eindhoven

cases, they try to exploit storage capabilities of the integrated sensible heat storage and the building itself. In doing so, the amount of heat being lost through storage inefficiencies and dissipation through building walls increases. This explains the delta between the VBP values and the respective RTP and DLMP values.

When looking at the bottom row of the same Figure 7.4, it becomes clear that under the constant VBP price signal, the system active power losses are significantly lower than under
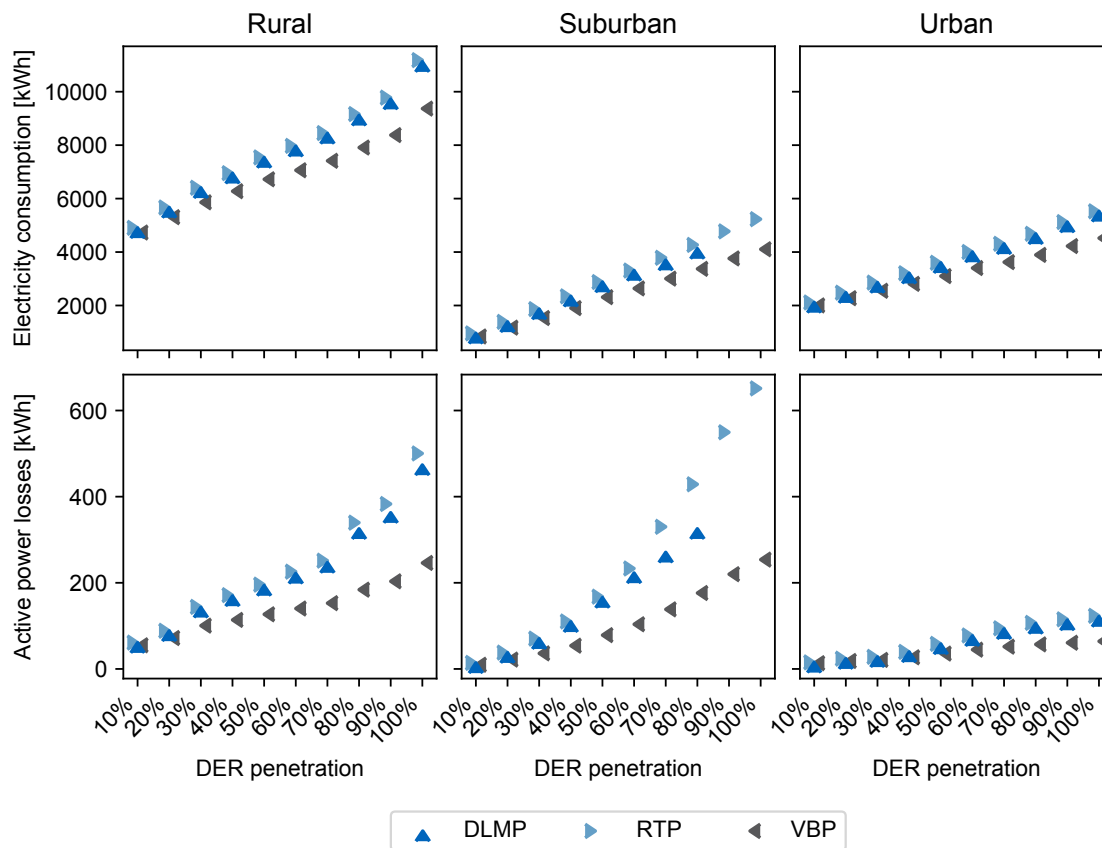
Figure 7.4: System active power consumption excluding losses (top) and corresponding active power losses (bottom)

the time-varying price signals. However, as power losses are part of the DSO's problem with DLMPs, they are also minimized and therefore lower than in the case of RTP. Notably, the overall losses and the respective delta between the price signals in the urban case are much lower than in the other two cases. This is because the overall line length of each sub-grid (feeder) is much smaller than in the other two cases, which decreases the overall resistance. The reason for the general increase of losses under time-varying price signals compared to constant VBP lies in the fact that system losses increase with current quadratically. The increase in current is two-fold: Firstly, as explained above, the overall power demand rises, consequently leading to an increase in current. Secondly, the load peaks increase due to the load coincidence of the price-following HPs, which leads to even higher currents for some time steps. These effects become more evident when looking at asset utilization, which will be the focus of the following subsection.

7.2.3 Asset utilization and violations

In this subsection, the utilization of three different asset types is presented along their adequate respective dimension: (i) line loading, (ii) node voltages, and (iii) transformer loading. The individual distributions of the respective values for all lines and nodes will be presented

separately for each scenario and price signal. In addition, three tables summarize the violations that occur to compare the scenarios and price signals to each other.

Table 7.2: Line flow violations on LV lines for different DER penetration levels under the three price signals

DERs	Rural			Suburban			Urban		
	VBP	RTP	DLMP	VBP	RTP	DLMP	VBP	RTP	DLMP
10%	0%	0%	0%	0%	0%	0%	0%	0%	0%
20%	0%	0%	0%	0%	0%	0%	0%	0%	0%
30%	0%	0%	0%	0%	0%	0%	0%	0%	0%
40%	0%	0%	0%	0%	0%	0%	0%	0%	0%
50%	0%	0%	0%	0%	0%	0%	0%	0%	0%
60%	0%	0%	0%	0%	2%	1%	0%	0%	0%
70%	0%	0%	0%	1%	7%	3%	0%	0%	0%
80%	0%	0%	0%	3%	7%	1%	0%	0%	0%
90%	0%	1%	0%	6%	8%	N/A	0%	0%	0%
100%	0%	1%	0%	6%	12%	N/A	0%	0%	0%

Figures 7.5 to 7.7 present the results for the maximum line utilization during the day under investigation. The utilization level is calculated as the ratio of peak line loading to the rated maximum allowable branch flow of the respective line. The upper portion of the individual plot describes the distribution of line utilization, while the bottom represents the cumulative proportion. From the box plots, we can see that the overall line loading increases proportionally with increasing DER penetration levels. For all scenarios, the VBP price signal yields the lowest maximum line loading, especially when comparing the higher DER penetration scenarios above 40%. The maximum line loading values in the lowest DER penetration levels range from 20% to 40% of the allowable limits for all scenarios (rural, suburban, urban), which means that the grid is being operated far below its limits, which is typical for European power grids in residential areas, as they are usually oversized to achieve high reliability. However, recall that we look at hourly time intervals, which further flatten peak effects. It can be assumed that there exist moments in time where line loading is, in reality, higher than what we see in these graphs.

Most notably, the suburban grid experiences the highest number of lines operating closer to their respective branch flow limits. The reason for this effect is two-fold: First, the buildings in the area under investigation are larger SFHs, which require adequately sized HPs. However, the main reason is that the grid is served through one transformer only, which means that with increasing DER penetration, the lines upstream (closer to the substation) are under very high strain. They represent the outliers in the box plot sections in Figure 7.6. The graphs for the suburban scenario furthermore reveal that for high DER penetration levels under RTP, more than 10% of lines are violating their individual branch flow limits. In contrast to this, the

Table 7.3: Voltage violations on LV nodes for different DER penetration levels under the three price signals

	Rural			Suburban			Urban		
DERs	**VBP**	**RTP**	**DLMP**	**VBP**	**RTP**	**DLMP**	**VBP**	**RTP**	**DLMP**
10%	0%	0%	0%	0%	0%	0%	0%	0%	0%
20%	0%	0%	0%	0%	0%	0%	0%	0%	0%
30%	0%	0%	0%	0%	0%	0%	0%	0%	0%
40%	0%	3%	0%	0%	0%	0%	0%	0%	0%
50%	0%	5%	0%	0%	0%	0%	0%	0%	0%
60%	0%	12%	0%	0%	19%	0%	0%	0%	0%
70%	0%	12%	0%	12%	63%	0%	0%	0%	0%
80%	0%	22%	0%	27%	89%	0%	0%	0%	0%
90%	0%	23%	0%	70%	97%	N/A	0%	0%	0%
100%	0%	28%	0%	79%	98%	N/A	0%	0%	0%

urban scenario shows much lower line utilization values, even at 100% DER penetration and under RTP, 100% of lines are operated below 60% of the allowable limits.

Turning now to Figures 7.8 to 7.10, we can investigate the maximum voltage drops per unit as a direct consequence of the loads. They are calculated as the ratio of maximum voltage drop and nominal voltage at each node. The vertical line at 0.1 indicates the maximum allowable voltage drop of 10% of the nominal voltage level. Again, the mean voltage drop values proportionally increase with rising DER penetration levels in all scenarios and for all price types. For low DER penetration levels, the rural case (see Figure 7.8) indicates maximum voltage drops up to 5% due to the long line lengths, which is typical for rural distribution grids. With rising DER penetration levels, this effect emerges even more dramatically in the suburban case, where voltages drop much more due to higher overall line loading. In contrast, the grid in the urban scenario operates almost all the nodes far away (roughly 5%) from the allowable voltage limit for all DER penetration levels and price types. To show the mechanisms of the DLMPs with regard to its voltage control capabilities, we look at the rural and suburban scenarios, where all nodes stay within the allowable limits under this price signal. This becomes especially obvious in the extreme suburban scenario, where voltage levels under RTP drop significantly under the allowable limit in contrast to the DLMP price signal.

To allow a comparison of the individual asset violations under the three price signals under investigation, we now turn to Tables 7.2 to 7.4, which show the share of assets (lines, nodes, and transformers) that violate their individual operating limits at least once during the time frame under investigation, which is one full day. As we had already seen in the previous Figures 7.5 to 7.7, both the distribution grids in the rural and the suburban scenario experience line flow violations, as seen in Table 7.2. In the rural scenario, under RTP, 1% of lines are

Table 7.4: Transformer violations for different DER penetration levels under the three price signals

	Rural			Suburban			Urban		
DERs	**VBP**	**RTP**	**DLMP**	**VBP**	**RTP**	**DLMP**	**VBP**	**RTP**	**DLMP**
10%	0%	0%	0%	0%	0%	0%	0%	0%	0%
20%	0%	0%	0%	0%	0%	0%	0%	0%	0%
30%	0%	0%	0%	0%	0%	0%	0%	0%	0%
40%	0%	0%	0%	0%	0%	0%	0%	0%	0%
50%	0%	0%	0%	0%	0%	0%	0%	0%	0%
60%	0%	0%	0%	0%	0%	0%	0%	0%	0%
70%	0%	0%	0%	0%	100%	0%	0%	0%	0%
80%	0%	20%	0%	0%	100%	0%	0%	0%	0%
90%	0%	20%	0%	100%	100%	N/A	0%	0%	0%
100%	0%	20%	20%	100%	100%	N/A	0%	0%	0%

operated above their respective limits. We can see how this problem is resolved under nodal pricing (DLMP). The more extreme suburban case experiences much more violated line limits under all pricing signals. Curiously, even under DLMP some line limit violations remain at 60% to 80% DER penetration. This effect can be traced back to an improper linearization in the power flow approximation steps of the trust-region algorithm, which could not be resolved for the suburban case. However, the rather low values suggest that this deviation is small. Curiously, for the same rural case, under VBP, no voltage violations occur due to a generally lower load coincidence and, therefore, lower peak loads.

Concerning the voltage violations, Table 7.3 presents the significant effect that the higher load coincidence, resulting from RTP, has on potential voltage violations. In the rural scenario, starting at 40% DER penetration level, several nodes in the grid already experience voltage levels below their allowable limits. This trend increases until at 100% DER penetration, more than a quarter of nodes in the rural scenario under RTP are violating their respective limits. Under nodal prices (DLMP), these issues are fully resolved.

The suburban example shows a much more dramatic behavior, as already under VBP almost 80% of nodes are experiencing violations of their allowable voltage limits, which increases to almost 100% under RTP. The nodal pricing signal can resolve this up to a DER penetration level of 80%. However, as mentioned above, the optimization problem becomes infeasible for higher values. As could already be derived from the previous graphs in Figure 7.10, the urban case does not experience any voltage violations.

Finally, Table 7.4 presents the share of transformers that are being operated beyond their allowable limits. For the rural scenario, this is true for one out of the five transformers under RTP at a high DER penetration level of 80%. There is also a value greater than 0% in the DLMP

column, as this constraint was relaxed to be able to solve the optimization problem. Once again, this shows the limitations of the power flow linearization, as in theory, there must exist a solution for this case that equals the operating set points of the VBP, which obeys all transformers' limits. The single transformer in the suburban case is also being operated above its limits, as can be seen in the three center columns of the same Table 7.4. In contrast, in the urban example, the transformers are operated below their limits under all defined circumstances.
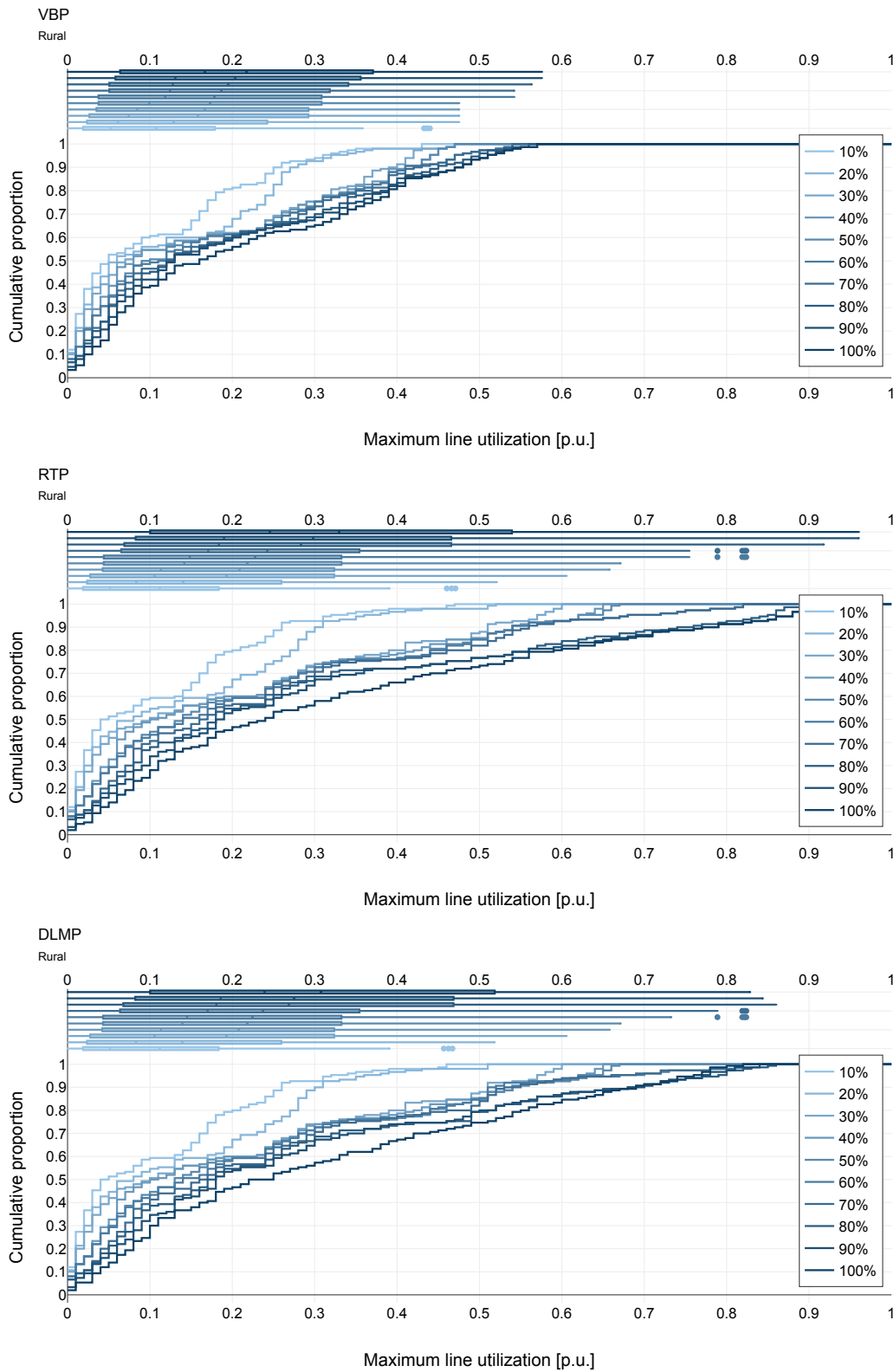
Figure 7.5: Line utilization for different DER penetration levels under three distinct price signals for the rural case
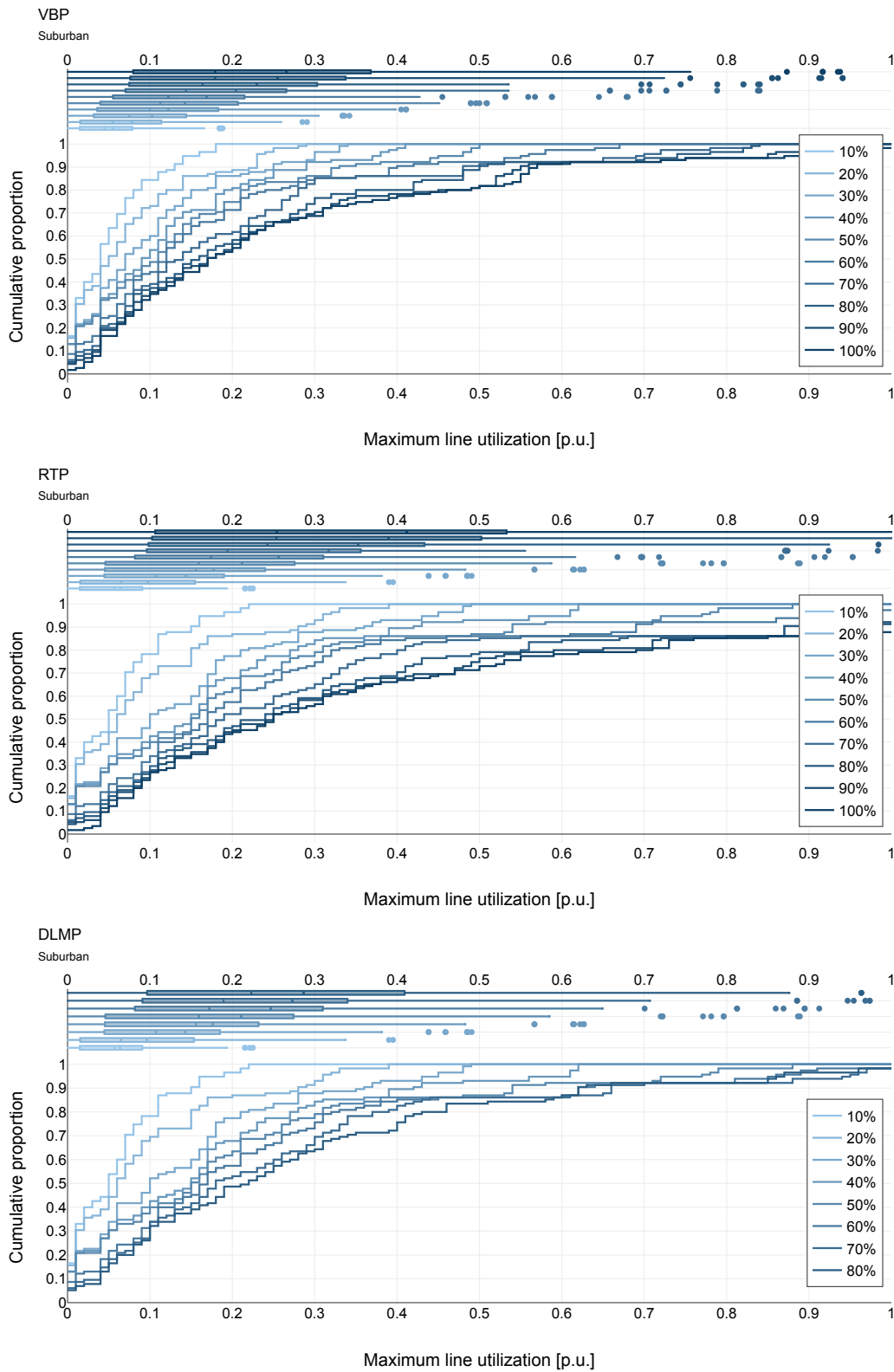
Figure 7.6: Line utilization for different DER penetration levels under three distinct price signals for the suburban case
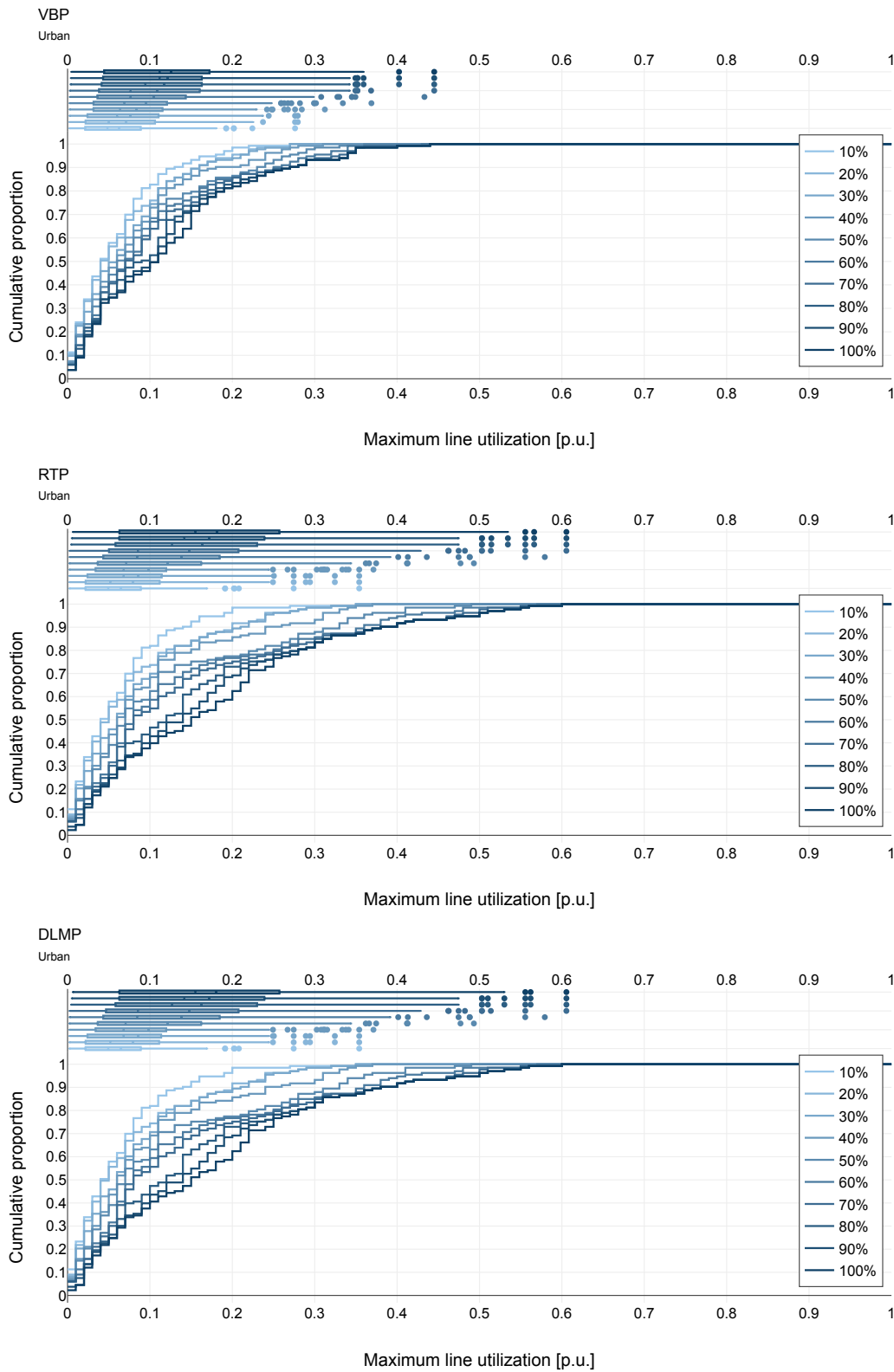
Figure 7.7: Line utilization for different DER penetration levels under three distinct price signals for the urban case
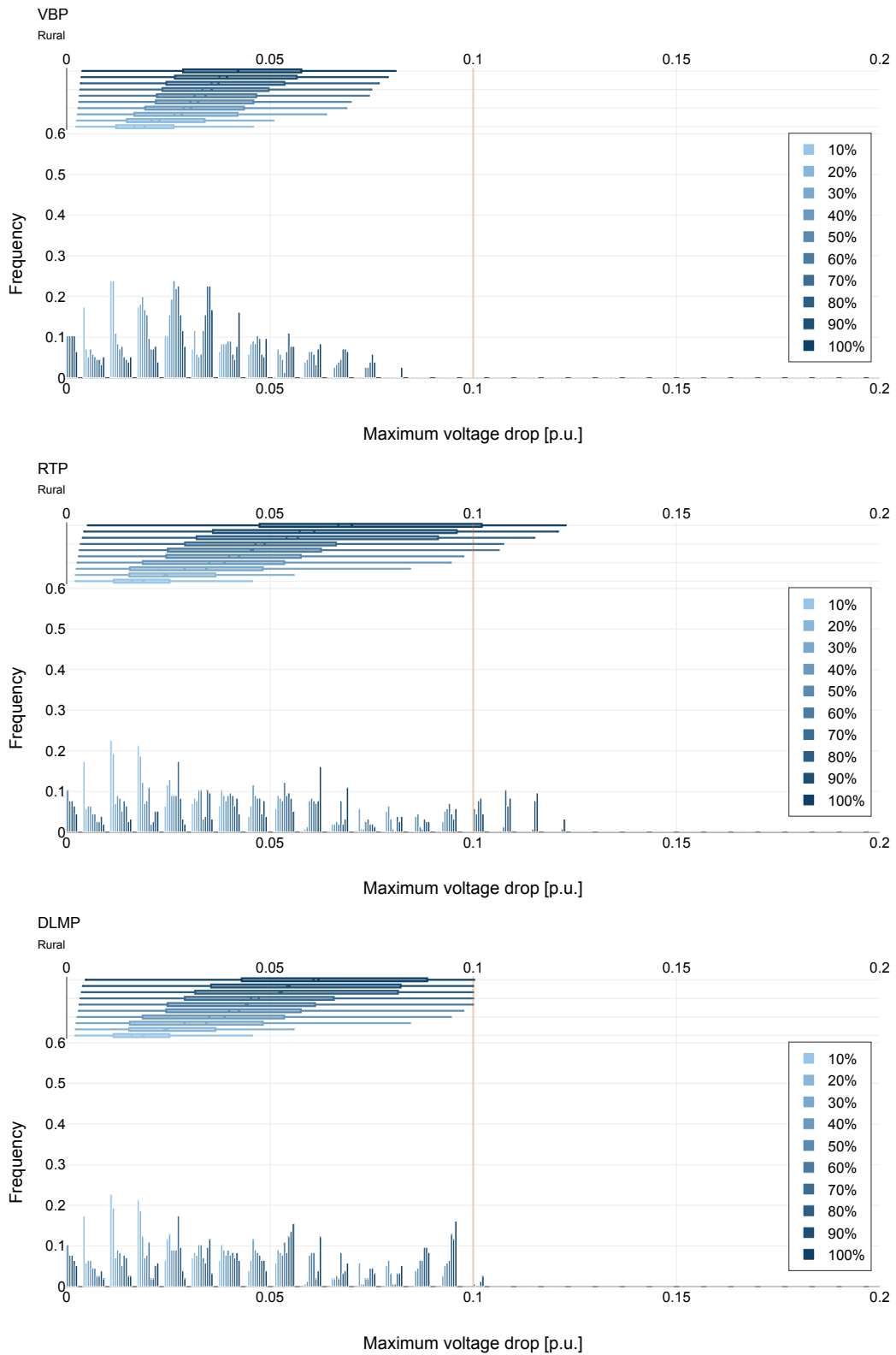
Figure 7.8: Voltage drop for different DER penetration levels under three distinct price signals for the rural case
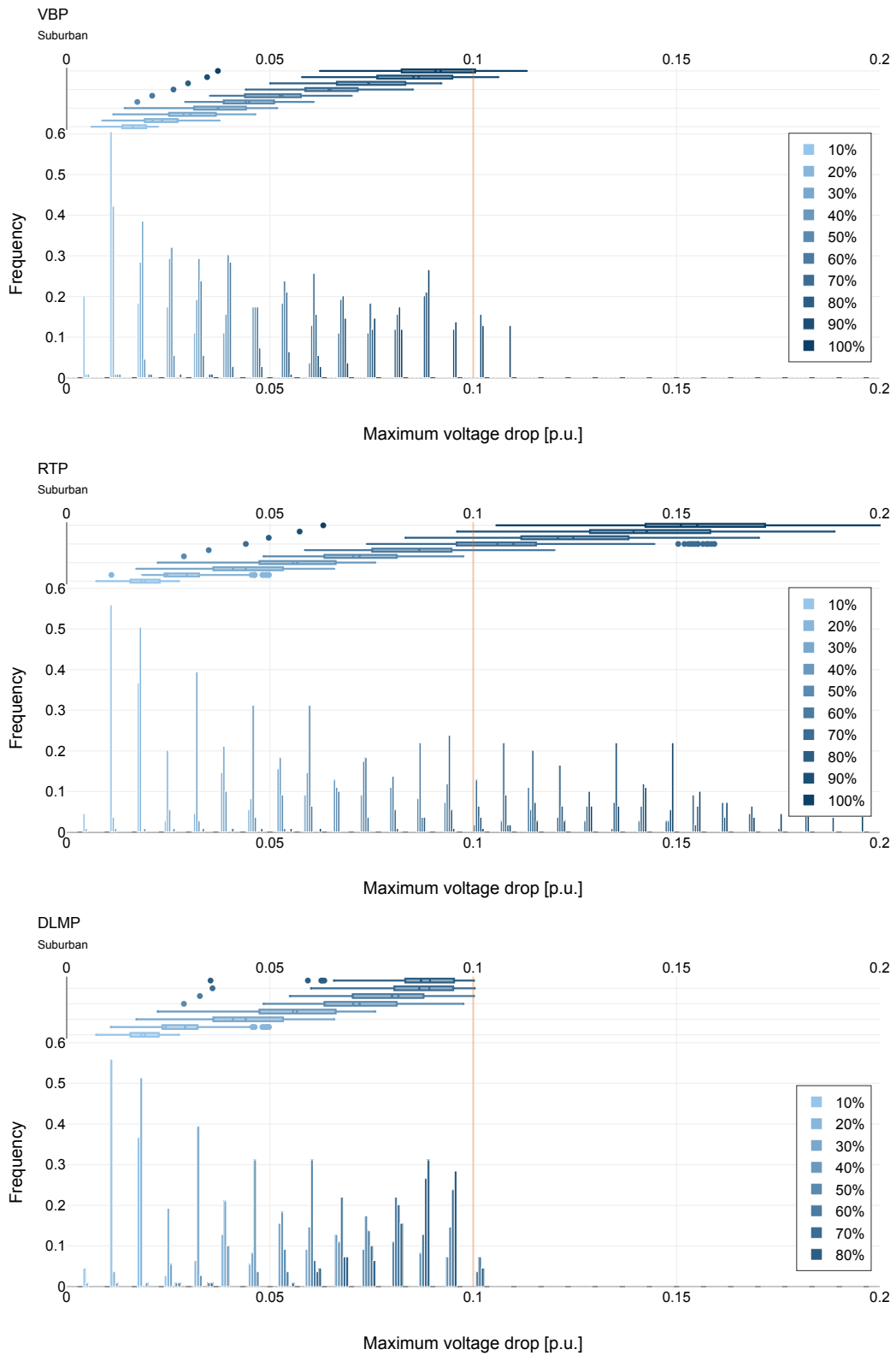
Figure 7.9: Voltage drop for different DER penetration levels under three distinct price signals for the suburban case
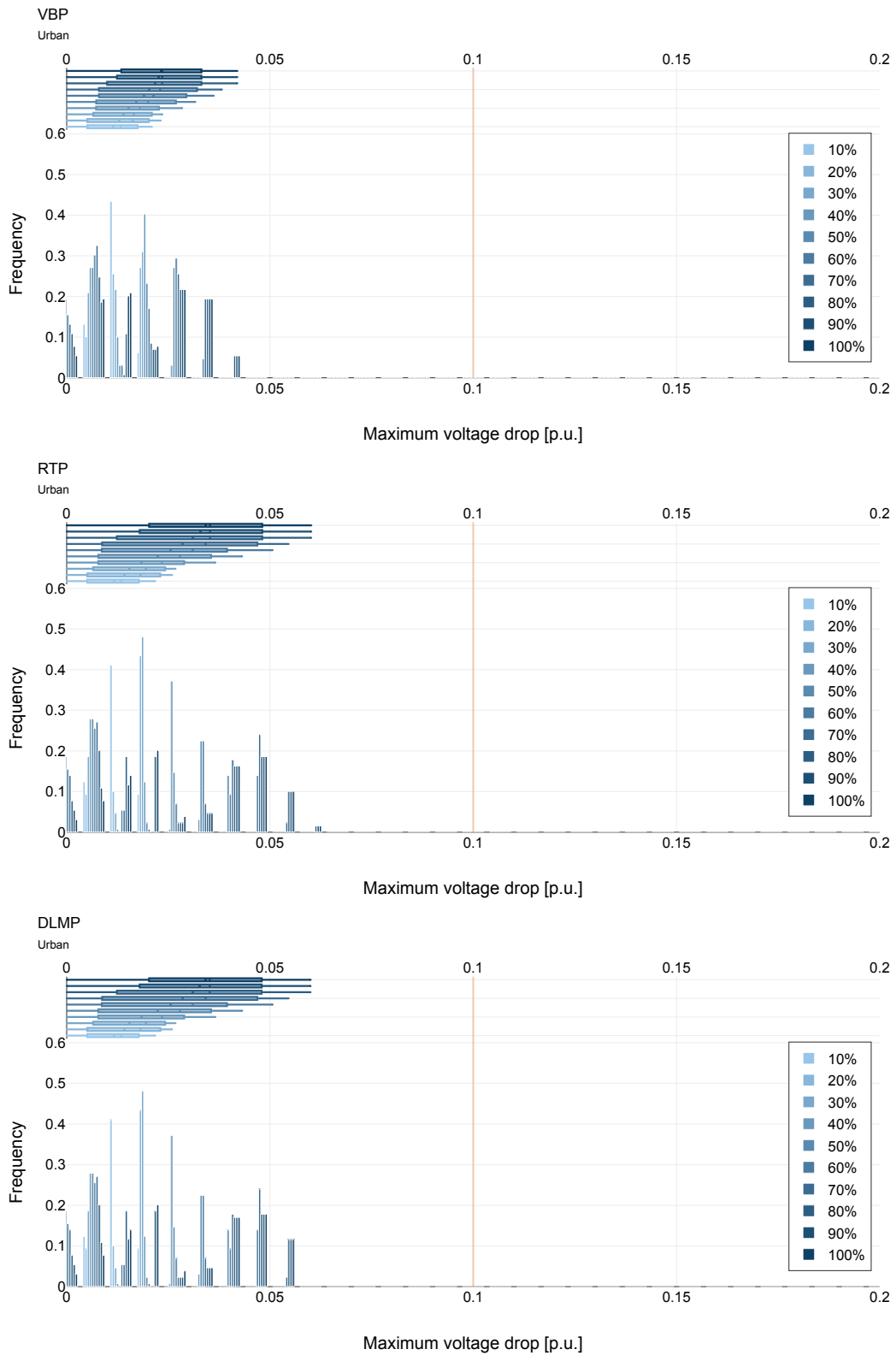
Figure 7.10: Voltage drop for different DER penetration levels under three distinct price signals for the urban case

7.3 Economic efficiency

After having investigated the scenarios from a purely technical point of view, this section now opens up the economic assessment of the price signals by first focusing on how the nodal prices (DLMPs) compare to the underlying RTP signal and how they are distributed over the grid from an equity and fairness perspective. As mentioned earlier, the economic assessment now neglects the VBP price signal and its results, as it is constant and can therefore be set to any arbitrary level. This does not impact operational behavior, however has significant effects on the economic considerations performed in the remainder of this chapter. This investigation again starts by looking at the DLMPs of an individual building to develop an intuition of the price signal and its composition. Then, the perspective is broadened to the distribution of DLMPs over the entire system to subsequently turn to the welfare considerations that were introduced in the previous chapter.

7.3.1 Individual DLMPs

Figure 7.11 presents the DLMPs of an arbitrary building from the suburban scenario at 80% DER penetration. As explained in section 6.1.5, the chosen approach allows us to decompose the nodal prices into its components energy, losses, voltage, and congestion, which are colored individually in the plot. As can be observed in the upper graph of the figure, for the scenario and time frame under investigation, the congestion component is zero at all time steps, while the price is mainly influenced by the voltage component, which helps alleviate the voltage violations, as discussed in the previous section.

At this point, it is essential to highlight that, although we do not assume a reactive power price at the source node along the lines of the active power price from the wholesale market, nodes across the grid experience a reactive power price greater than zero for some time steps. This can be observed in the bottom graph of the same Figure 7.11. Just like the active power DLMPs, they are a result of binding (inter-temporal) constraints and related opportunity costs for, e.g. shifting consumption. However, in this particular case, the maximum reactive power price never amounts to more than 6% of the active power price and is almost neglectable, but it must still be considered later in the welfare investigations.

The grey line in both graphs, which is related to the right y-axis, shows the absolute power output in per unit of the DER, which is in the case of a HP, the active and reactive power demand, respectively. As we consider a fixed power factor of 0.9, the profiles of the individual active and reactive power line graphs are identical. Mainly influenced by the active power DLMP in the top graph, we can see how the demand curves drop at active power price peaks to minimize energy procurement costs.

7.3.2 System DLMPs

Now, we shift to the system perspective again. Figure 7.12 presents the DLMPs compared to the RTP for a full day for all three scenarios under investigation, by representing the delta between the wholesale price (RTP) and the maximum DLMP price as the blue shaded area in the bottom graph, while the top graph presents the distribution of the delta for individual consumers. Recall from the previous technical analysis that at 80% DER penetration, the
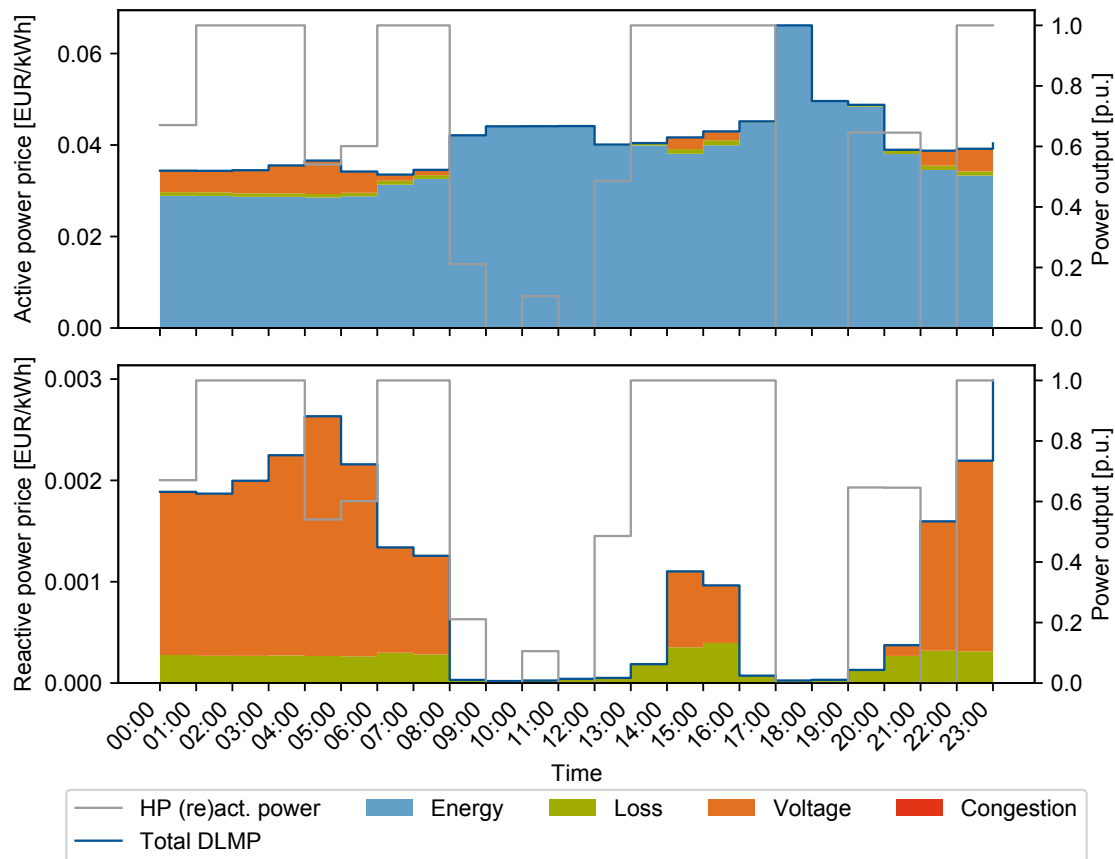
Figure 7.11: Arbitrary building DLMPs for a full day at 80% DER penetration for the suburban scenario in Eindhoven with the HP's power consumption in grey on the second y-axis

suburban case was severely affected under the RTP signal, while DLMPs were able to resolve these issues. This comes at the cost of higher prices, especially in time periods of low wholesale prices. From the box plot in the top row of the suburban scenario, we can see that a few consumers experience much higher price deltas than others. However, this spread only becomes significant in this extreme scenario. In the urban scenario, where the grid is operated well below its voltage and line flow limits even at 80% DER penetration, we can see that DLMPs only slightly differ from the underlying wholesale market price. In this case, they merely contain a loss component greater than zero, which must always be the case, as distribution systems are never lossless.

Most notably, downstream nodes are affected much more by a change in prices compared to RTP as upstream nodes. This can be seen in Figure 7.13 for an arbitrary time step at 19:00h. There clearly exists a general trend for nodes further away from their respective transformer station to experience higher prices, as voltage drops and losses increase downstream of a radial grid. Interestingly, the suburban scenario experiences much higher price deltas at similar distances as the urban scenario. Furthermore, we can see in the rural case that the MV-nodes experience a similar effect which, however, is almost neglectable. This can be explained by the smaller voltage drops and losses on higher voltage levels.
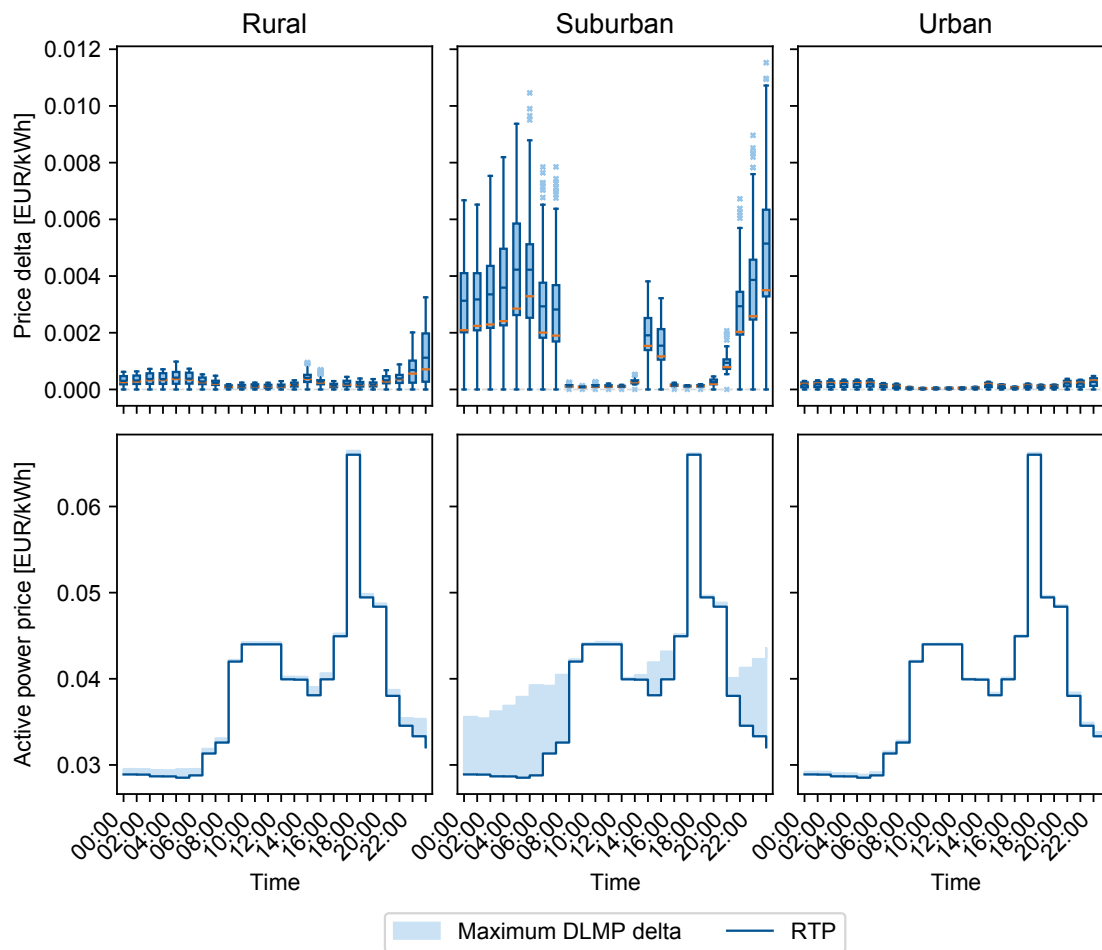
Figure 7.12: DLMPs for a full day at 80% DER penetration with price delta distributions in the top row for all three scenarios

7.3.3 Welfare investigation

This section now builds on the intuition we developed in section 2.2 and welfare definitions from section 6.1.1. Recall that social welfare is defined as the sum of the individual surplus of market participants. Based on our welfare definitions from the previous chapter, we analyze the consumer and merchandising surplus and the resulting overall social welfare and the respective changes. Note that all three simulated days are considered for this part of the analysis instead of just one. This is necessary, as shifting demand outside of the time frame under investigation can distort the welfare examinations, as individual surplus could wrongly increase when overall power demand in the respective time frame is shifted. For convenience, the results are summarized in Figures 7.14, 7.15, and 7.16, as all three components are directly connected. The following subsections present the results for consumer and merchandising surplus and social welfare individually.
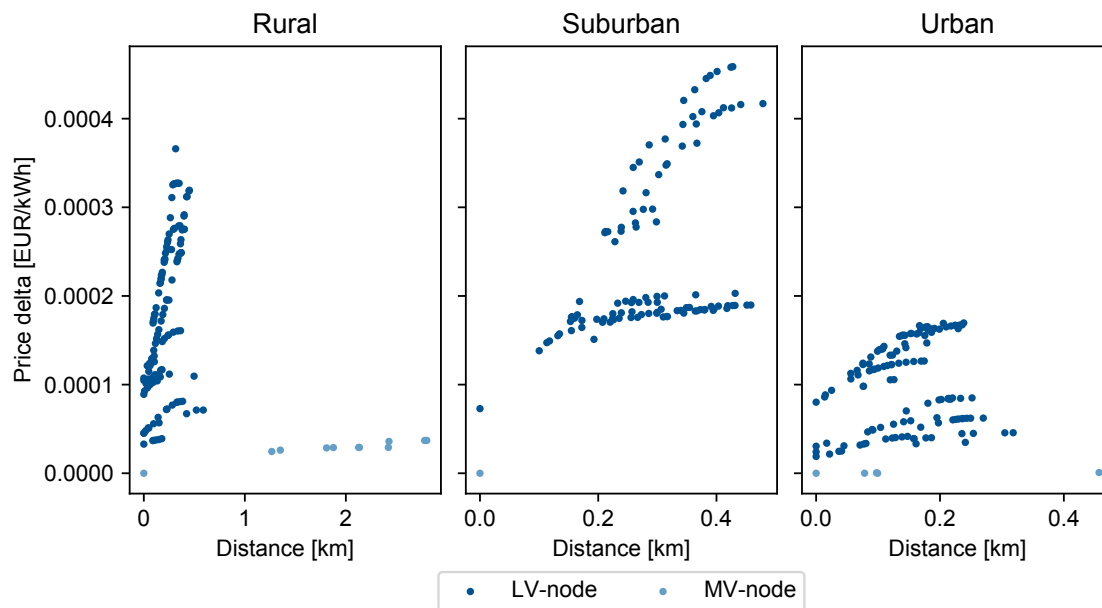
Figure 7.13: Delta between nodal prices (DLMPs) and RTP over the distance from the respective transformer station at 80% DER penetration at 19:00h

Consumer surplus

We first investigate the consumer surplus as defined in (6.2). The sum over all consumers is presented in the top row in Figure 7.14. Based on our definition as the negative cost for consuming active and reactive power, the utility (or surplus) must consequently be negative. Logically, the overall consumer surplus decreases with increasing DER penetration as overall energy demand rises. As in our scenarios DLMPs are generally higher than the RTP prices, we can furthermore observe a decrease in surplus for all scenarios when comparing the two price signals. However, only for high DER penetration scenarios, this delta becomes much more apparent when considering the delta in the top row graphs in Figure 7.15. The colored areas help understand the drivers for change. While the consumer surplus is driven mainly by an increasing loss component of the DLMPs, which proportionally increases with overall system losses, with higher DER penetration, we can furthermore observe congestion and larger voltage components in the nodal pricing signals for the rural and suburban scenarios. Interestingly, we can also observe a decrease in consumer surplus due to higher energy costs (blue area), which can be related to shifting demand to times of higher wholesale market prices.

However, looking at the aggregate consumer surplus only reflects little on the impact on individual aggregators. The top row in Figure 7.16 considers the change in individual consumer surplus (utility) under DLMPs compared to RTP. It becomes clear that in scenarios with high strains on the grid, such as the rural and suburban case, where grid constraints become binding and DLMPs significantly differ from RTP prices, the surplus, and therefore the costs of power procurement for individual consumers vary significantly. This shows that, although absolute price deltas between DLMPs and RTP prices are not very high even for higher DER penetration levels, for a few aggregators, it results in a surplus decrease of up to 25%, such as observed
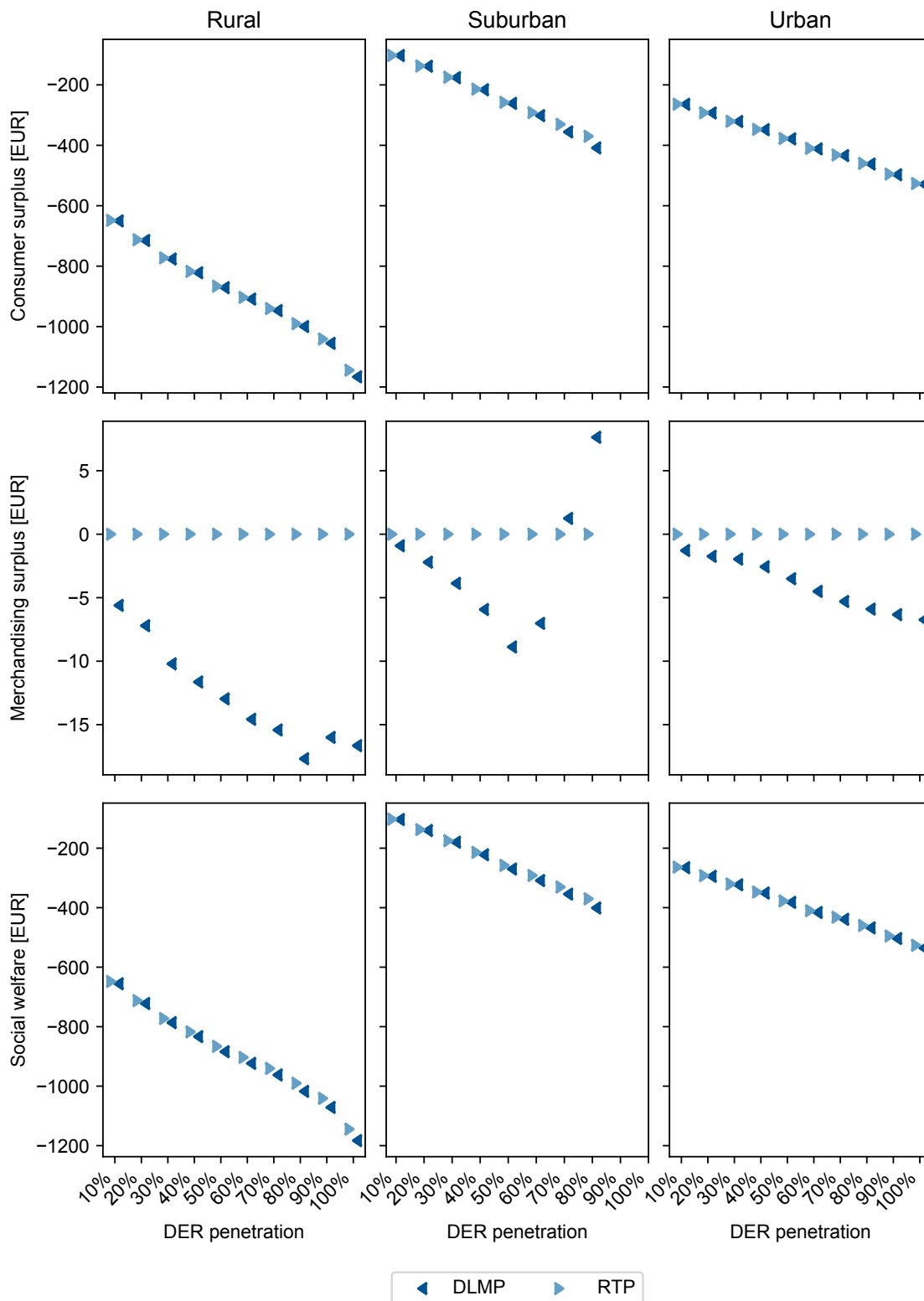
Figure 7.14: Comparison of total consumer surplus, DSO's merchandising surplus and social welfare for all scenarios
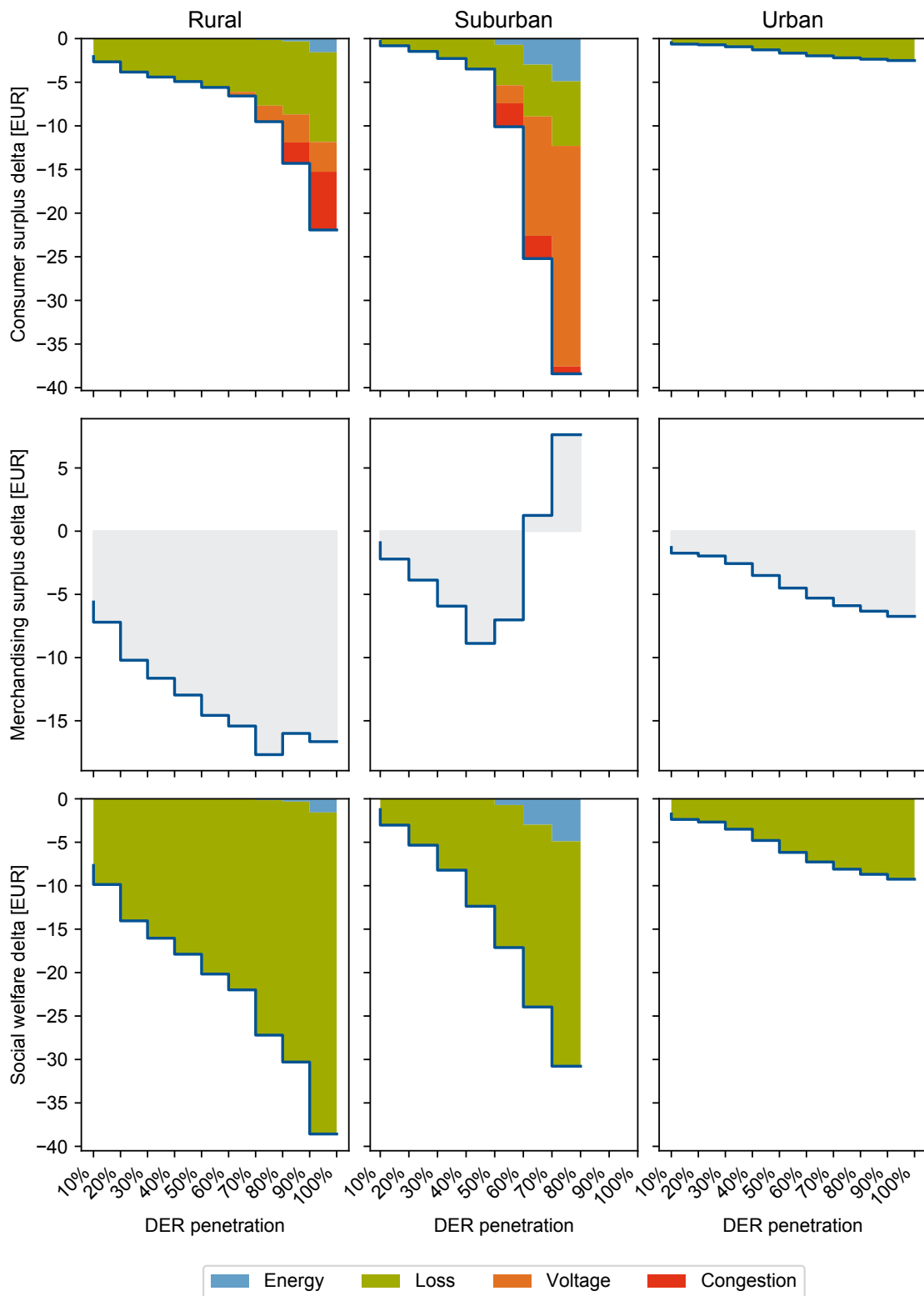
Figure 7.15: Delta of consumer surplus, DSO's merchandising surplus and social welfare for all scenarios between RTP and DLMPs
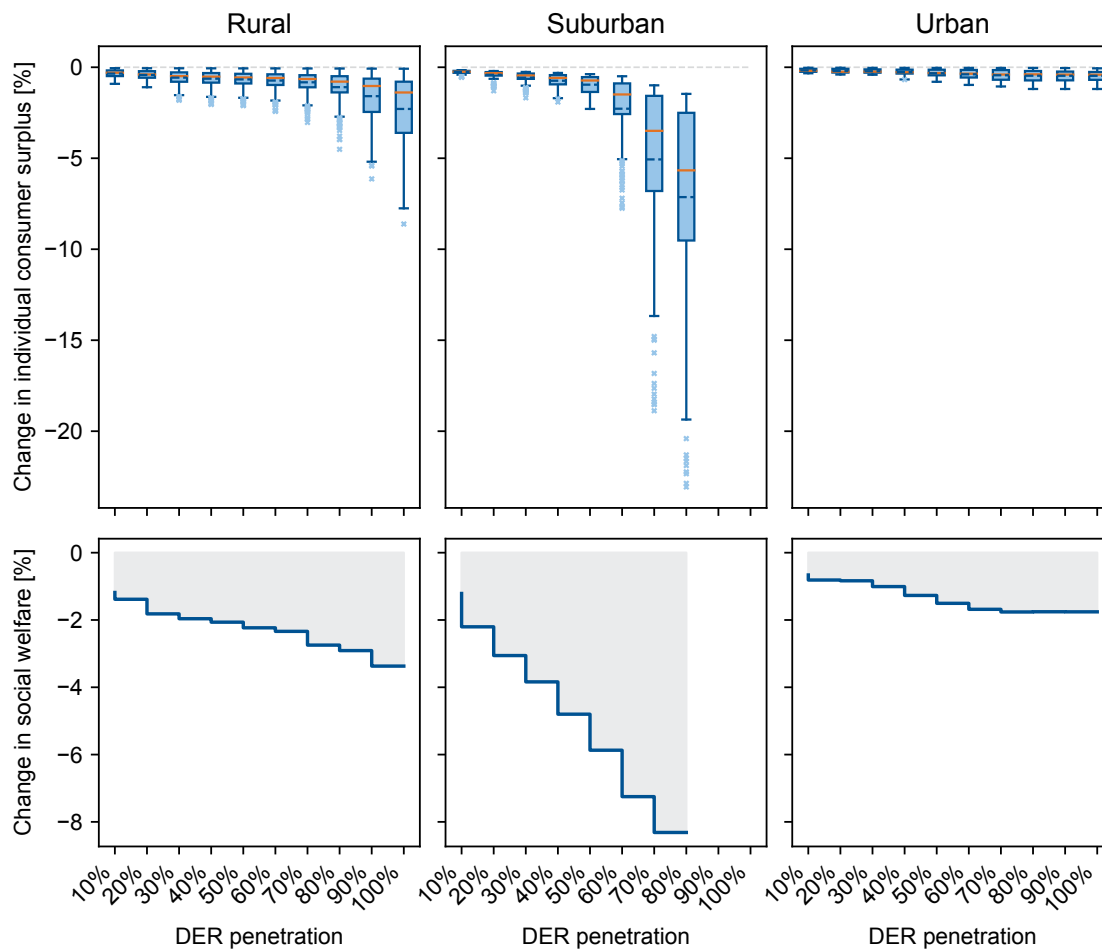
Figure 7.16: Change in consumer surplus and social welfare for all scenarios between RTP and DLMPs

in the suburban scenario, which according to our definitions translates to a 25% increase in electricity procurement costs during this time period. The urban scenario shows that individual utilities change quite uniformly in the grid and only to a small amount of maximum 2% at the highest DER penetration level.

Merchandising surplus

As the market operator, the DSO's role is to clear the market by purchasing electricity at the source node at wholesale market price and selling it to the aggregators (consumers) either at RTP (which is equal to the wholesale market price in the context of this analysis) or at the individual active/reactive power DLMPs. In the latter case, the DSO consequently earns a surplus as the outcome of its economic activity on the local electricity market. Additionally, the DSO also must compensate system losses by buying additional energy on the wholesale market. In the RTP case, with only one node, there is no possibility for spatial arbitrage, nor are system losses considered in the market. Hence, the DSO's surplus is equal to zero at all times and for all scenarios, which is why the change in merchandising surplus is always infinite. Hence the representation is omitted in Figure 7.16.
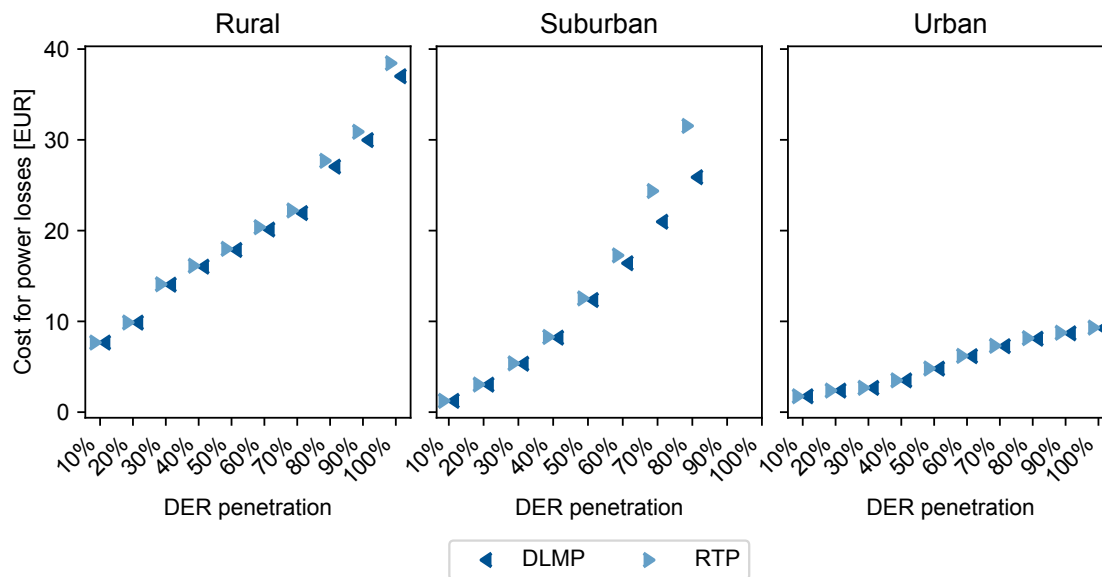
Figure 7.17: Total costs for power losses over the entire time horizon of three days

As can be observed in the middle row in Figure 7.14, the DSO's surplus steadily decreases with increasing DER penetration levels for scenarios with lower strains. However, the rural and suburban scenarios show an upwards trend for very high DER penetration scenarios, with even a positive surplus in the suburban case at 70% and 80% DER penetration. It is important to note at this point that the loss component in the DLMPs which is collected as a surplus by the DSO does not necessarily cover the respective costs for losses. The DLMP price signal merely invokes optimal behavior to reduce losses. This also holds true for the congestion and voltage management capabilities of DLMPs. However, in some situations, they can yield a positive surplus for the DSO. This is in line with the role of independent system operators in nodal pricing-based transmission grid markets, who are intended to invest their surplus into grid reinforcement. From a practical perspective, this means that the DSO would never sell electricity at wholesale market price without adding either a fixed or variable price component that covers system losses. However, in this welfare investigation, it is crucial to abide by the welfare definitions for the sake of comparability.

Social welfare

Social welfare is defined as the sum of consumer and producer surplus. In the context of this thesis, this results in the social welfare equalling the sum of merchandising and consumer surplus, as defined in equation (6.8). Recall that no producer surplus can be generated, as the transmission grid is the only generating source in our scenarios, and the wholesale market price is inelastic. Along the lines of the consumer surplus, the absolute social welfare is negative for both RTP and DLMP price types. As seen in Figure 7.14, it decreases steadily with increasing DER penetration levels in all three scenarios.

For full transparency, the delta in social welfare, as presented in the bottom row of Figure 7.15, is further decomposed into its energy and loss component. Note that these are not directly related

to the respective DLMP components. This delta is a cornerstone of our overall investigations, as it represents what any measure to obtain the same optimal dispatch result would at least cost. Recall that other mechanisms for dealing with congestion, voltage violations, or losses must be consistent with the optimal nodal dispatch quantities to provide the same optimal solution. These quantities, therefore, can serve as a benchmark. The mechanisms or measures come at a cost that is not reflected in the RTP case. That is why it scores a higher social welfare in general (refer to our discussions from section 2.2.1). The largest part of these costs is accounted for by compensating power losses in the distribution grid. However, these measures (i.e., loss compensation, voltage, and congestion management) are inevitable to reach a feasible dispatch for the operation of the distribution grid. Their costs are at least as high as the total social welfare delta. We can therefore deduce that for the time frame of the three days under investigation, the optimal dispatch quantities can be reached for a social cost of between 10 € to roughly 40 € for the individual highest reachable DER penetration level. When investigating respective welfare change in the bottom graphs of Figure 7.16, this equals a change in welfare of 2% to 8%.

Fundamentally, the welfare change can be explained by the overall consumer surplus decrease and the costs incurred by the DSO at the source node for loss compensation, which is not reflected in the RTP case, as no representation of the grid is included in the market. In the less extreme cases (rural and urban), the overall social welfare decrease under DLMPs is quite moderate, even for high DER penetration scenarios, and is mainly defined by the loss compensation portion. Turning now to Figure 7.17, we can see that the loss reduction capabilities of the DLMPs are indeed present. However, the effect is negligible. This, in turn, means that the relatively small energy portion of the social welfare delta, which is responsible for voltage and congestion management, achieves to operate the grid within its boundaries for a very small increase in social cost, which is driven by opportunity costs. However, this comes at the cost of a few individual consumers being much more affected, as explained above.

7.4 Discussion

This chapter presented the results of the techno-economic analysis performed based on the analysis framework developed in Chapter 6. The findings show that under RTP the strains on the underlying distribution grid increase for all scenarios under investigation when compared to the constant VBP price signal, due to the higher load coincidence that was introduced in Chapter 4. With increasing DER penetration, these strains become significant, as operating limits, most notably voltage limits, are commonly violated, especially in grids with few transformers and long line lengths. In all scenarios, DLMPs prove their voltage and congestion management capabilities and furthermore decreased system losses compared to the RTP price type. However, at very high DER penetration levels, in two scenarios, transformers were overloaded, and for one scenario no feasible solution could be found as voltage drops could not be resolved by the nodal pricing signal.

Recall that only the heat demand of residential buildings has been electrified in the scenarios, while all other heat demand was neglected. With all types of buildings being supplied with heat from HPs and in light of the advent of EVs, we can expect an even higher system load.

However, for the sake of the comparison performed in this thesis, the HPs served as a proxy for the impact of flexible (price-following) loads with high load coincidence on the grid and how different price signals steer their dispatch schedules.

The three chosen scenarios (study areas) provide a suitable set of different grid characteristics, as they perform quite differently and therefore serve well in assessing the sensitivity towards different grid configurations. However, for the suburban grid, the coincidence factor applied for the grid dimensioning, which is based on the number of buildings supplied by only one transformer station, causes the nominal load of each building to be relatively small. Consequently, the suburban grid might be under-dimensioned, especially in light of the high thermal demand of rather large buildings in the area. However, in this analysis, this scenario serves as an insightful example of a radial grid with only one transformer and, therefore, rather long line lengths.

Concerning the voltage drops experienced in all scenarios, it must be noted that all transformers are considered to have a static turns ratio and, consequently, cannot adapt their voltage level. However, if voltage issues remain the most significant problem in distribution grids with high DER penetration, modern transformers with adjustable turns ratio could be a satisfactory solution. Furthermore, the chosen scenarios did not consider any distributed generation capacities, which could counteract the voltage drops experienced in all scenarios. However, to investigate the techno-economic impact of different price signals, the focus on HP technology suffices to draw general conclusions.

The economic investigation is based on the economic theory on electricity markets from Chapter 2. As the technical analysis shows, there exist scenarios which could not safely be operated under VBP and RTP without violating operational limits, whereas DLMPs achieve a feasible solution. To this end, we use welfare economics to gain an insight into their economic performance. The social welfare in the optimal dispatch found under DLMPs is naturally lower than for RTP. However, the nodal pricing-based solution is feasible and represents an optimal dispatch schedule that obeys the grid's operational limits. As authors in [58] suggest, the welfare loss (social welfare delta) incurred under DLMPs when compared to RTP, can be interpreted as the minimum cost of any type of measure to yield a close-to-optimal solution. Arguably, the optimal dispatch under DLMPs represents the most efficient option for the operation of the distribution grid for high penetration rates, as it makes use of all resources to their limits, while other investigated price types can result in grid violations. Even though the observed reduction of overall social welfare of between 2% to 8% constitutes merely a minor decrease, the relative change is unevenly distributed across consumers. For some, the cost of electricity may potentially increase significantly (up to 25%), resulting in a drastic loss of individual surplus. Hence, it can be argued that DLMPs might result in a highly unequal distribution of prices, which is not in the spirit of conventional utility pricing rules [154].

Social welfare is a theoretical construct designed to analyze the effects of resource allocation (here: DER dispatch) on well-being on an aggregate level. In the context of this thesis, it is mainly defined by the consumer utility function. Since the adopted utility function effectively reflects consumer preferences for cost minimization, the deduced insights into social welfare are qualitatively valid and present valuable insights into the impact of price signals on a local distribution grid market. However, if the actual change in participants' utility expressed in

monetary units is to be described, the utility function must be based on the consumers' actual monetary valuation of consuming electric energy. Such a utility function could, for example, be derived from demand-side bidding analysis. However, under the assumption of economically rational behavior of the aggregators, the utility function as defined in this thesis appears to be a practical solution. Furthermore, our formulations imply perfect foresight for both the electricity price and the thermal demand and behavior of the buildings. This has an inevitable impact on the inter-temporal constraints that describe the thermal buildings' storage capabilities. In a real-world example, the overall operation of individual HPs would therefore be more conservative, as these influencing factors are not known with such certainty.

Furthermore, the study does not consider the potential abuse of market power, which is a common issue of nodal pricing-based markets, where weaknesses in the grid can be strategically played in the market. Especially in a radial grid, where line capacity is scarce and limited to a single line, only a limited number of flexibility suppliers might exist at relevant neighboring nodes. Thus, the question remains unanswered, how much flexibility and how many market participants are needed in a local distribution grid market to make DLMP-based markets possible in radial grids.

Concerning the efficiency of DLMPs, we can see from the results that under the nodal pricing signal, a high load coincidence persists, and therefore overall line loading remains high in comparison to RTP and VBP. This is no surprise, as this yields maximum social welfare when resources are exploited efficiently. From a DSO perspective, the operational limits would probably be chosen more conservatively. However, this would, in turn, come at a significant welfare decrease.

Finally, the chosen time interval of one hour, which is in the spirit of current wholesale electricity day-ahead markets, must be considered when evaluating the results, especially from a technical perspective. Recall that energy quantities are traded, which flattens short-term peak demand effects, as they are spread over the entire time interval. Consequently, operating the grid close to its limits could come at the cost of overloading for shorter periods of time, which must be evaluated in further studies.

Chapter 8

Policy implications and discussion

This chapter aims to put the results of the previous chapter into the broader context of the current discussions for the European power system and its markets, to finally draw a number of policy implications from them. In section 2.3, we learned that the European Commission strongly advertises demand-side flexibility, which must be exploited through cost-reflexive price signals in real time [65]. They further demand that these prices not be distorted through public intervention. These claims are rooted in the current developments in the power system, such as technological challenges from DERs that are putting new strains on the distribution system. Thus, they call for a change in the underlying electricity market design.

At the same time, technological advances in both the availability of computational power and communication technology facilitate the implementation of more complex market designs that enhance the governance of decentralized systems [15]. While these discussions are led primarily on a transmission grid level, the analysis in this thesis has shown and discussed the technological challenges in the distribution grid and proven the need for adequate instruments. Locationally and temporally highly granular price signals can be an opportunity to relieve potential voltage and congestion problems in the distribution grid while minimizing system losses. Our results show that with increasing DER penetration, DLMPs can efficiently alleviate congestion and voltage problems in the distribution grid to a high degree. At the same time, it has also been shown that exposing flexible DERs to a uniform temporally varying price signal (RTP) can, in turn, put even higher strains on the distribution grid driven by a higher load coincidence. Constant, uniform price signals (VBP) have proven least problematic, as they do not provoke high load coincidence. Adequate instruments to achieve an efficient dispatch must therefore be carefully designed. The following dimensions provide an overview of the policy implications we can derive from our analysis.

Cost of optimal operation

Our results show that for high DER penetration levels, DLMPs can achieve an efficient dispatch schedule at a moderate social cost increase of roughly 2% to 8% when compared to RTP. This delta is rooted in opportunity costs from shifting demand to alleviate voltage violations and congestion in the system and the fact that system loss compensation is not reflected in the RTP case. Interestingly, these opportunity costs only made up a small portion of the

overall social welfare change. This means that the costs induced by the inherent corrective measures for voltage and congestion management of DLMPs are moderate, as most of the social welfare delta of a local market is driven by the reflection of losses in the market-clearing. Even considering that we assumed an ideal market, we can still expect social costs to be relatively small to alleviate these violations.

Alternative corrective measures or compensation schemes, such as redispatch or feed-in management known from the transmission grid level, could also prove effective. However, they have already proven less efficient than nodal pricing on a transmission grid level [15] and are likely to do so as well on a distribution grid level. Furthermore, while a cost-based redispatch compensation is feasible for current actors in the power market, which compose of a small number of large well-known actors, this is likely to become very complex in the future with a high number of different types of DERs or other market participants, and opportunity costs may not be transparent for the system operator. As authors in [15] point out, in the traditional power system, the compensation for corrective measures, such as redispatch, can easily be determined by regulators on a cost basis, as the cost structure of producers can be estimated from their activity on the market. However, new players in the market, such as aggregators of flexible loads, base their bidding on opportunity costs and economic preferences. Sector-coupling will furthermore decrease the transparency and increase dependencies with conditions unrelated to the power sector. In combination, they argue that fair compensation mechanisms based on true costs will be impossible for regulators to design.

Consequently, a nodal pricing-based local energy market would not only provide the most efficient solution. It would also represent a viable solution, which can be implemented with available communication technologies. However, given the complexity of setting up, organizing, and operating such a local market, it remains questionable whether its efficiency gains justify the efforts. Other corrective measures performed by the DSO, even though less efficient from an economic perspective, do represent simple alternatives and should be evaluated first. After all, only very high load coincidence driven by a uniform varying price signal causes significant problems in the grid.

Role of the DSO

In the spirit of the role of the TSO in nodal-pricing based wholesale energy markets, we appointed the DSO to be the independent system operator that also clears the market. The European Commission also promotes a more active role of DSOs [65], allowing them to alleviate some of the challenges associated with a variable generation more locally, which would also favor the role of the DSO as defined in this thesis. However, DSOs are still part of vertically integrated companies. This circumstance must be removed before going ahead with such a solution, as the DSOs' neutrality must be guaranteed when giving them the power to locally manage flexible DERs either directly or through a local market setting. In the context of DLMPs, adequate and fair mechanisms for the distribution of merchandising surplus accumulated by the DSO among market participants must additionally be developed. Considering the arguments from above, which call for a relatively simple solution, a uniform, constant price signal (VBP) might be the preferred way forward in a European setting. This postulates a combination with a set of robust and rigorous rules for a regulated DSO. This way,

it could intervene in the DER dispatch schedules when needed and where needed in exchange for monetary compensation.

Equity and fairness

In their proposal for new energy markets in Europe [65], the European Commission highlights the importance of protecting the most vulnerable in society when looking at the direct participation of consumers (or prosumers) in the electricity market. As we have seen in our analysis, nodal prices can vary significantly from one location to another and consequently decrease individual consumers' surplus, even within a distribution grid. This can be perceived as unfair by some consumers, in particular at the distribution grid level [155], and is not in the spirit of traditional utility tariff design principles [154]. Arguably, RTP, which is uniform for all, but varies over time, can also be perceived as unfair. This problem is particularly relevant for small consumers, as they are (i) unprepared for forecasting volatile prices, or (ii) even predicting their own future consumption [156]. Therefore, volatile prices can expose them to an unacceptable degree of uncertainty [6]. Recent events in the Texas power system [157] have shown this actual risk, as end consumers on RTP tariff were exposed to the entire market risk during extraordinarily high scarcity pricing events throughout an unusually cold weather period. While high scarcity price peaks merely represent the market behaving as designed, they are a direct consequence of an efficiently designed power system that leaves little room for unusual events, like in the case of Texas.

In practice, aggregators that control flexible DERs for their contracted consumers (or prosumers) could, however, provide these forecasting capabilities and carry the market risk in the future. In this case, end consumers would be shielded from these effects, while aggregators make sure to exploit flexibility while safeguarding individual comfort constraints. Authors in [6] furthermore propose an alternative in the form of a practical framework for the coexistence of both fixed tariffs and dynamic nodal prices in the distribution grid. While flexible users pay nodal prices, non-flexible consumers are charged a fixed price derived from the underlying nodal prices. However, the problem of unattractive locations in the distribution grid remains, as prices are inevitably higher at line ends due to losses and voltage drops. In a liberal market setting, aggregators might discriminate against potential customers due to increased market risk and either not contract them or naturally impose higher tariffs at these nodes. Consequently, for the implementation of DLMPs suitable regulatory instruments must be in place to (i) protect end consumers from high market risks, and (ii) ensure fair treatment of consumers independent of their location in the grid.

It should be furthermore considered that our constant and equal-for-all VBP price signal achieved the lowest strains on the power system rooted in a lower load coincidence. This type of pricing scheme remains the most equal in terms of equity and fairness. In combination with an independent DSO that optimally controls DERs obeying all comfort constraints at the cost of a well-designed compensation scheme would still represent the fairest yet an inefficient solution for the future distribution system.

Flexibility markets

The European Commission favors the implementation of a flexibility market. However, it remains undefined what the flexibility market would look like and in what form the flexibility services would be traded [158]. With efficient market signals (nodal prices), this type of extra market might not be necessary as undistorted prices would unlock the full flexibility potential in the right places at the right time, as our results show. A high granularity of price signals makes the true value of electricity visible at every place and for every moment. This furthermore implies that, with decreasing ramp-up and ramp-down times of fast DERs, such as storage systems or HPs, a granular price signal decreases the need for planning horizons and allows to move towards true real-time markets, which is in the spirit of the claims by the European Commission. However, as pointed out above, it remains a challenge how to best price flexibility. Large flexibility aggregators could play an essential role in this regard.

Market power

Although market power has not been the focus of this analysis, it must be addressed in the envisioned DLMP-based market, as high liquidity can only be assured with sufficient flexible DER penetration which are controlled by an adequate number of different aggregators. As distribution grids are not meshed, such as transmission grids, the problem of abuse of market power becomes even more relevant because alternative flexibility sources are usually only available at two neighboring nodes. This provides opportunities for the abuse of market power through strategic bidding. While the European Commission demands a new market design that aims at ensuring that prices are free of any public intervention, and only with duly justified exceptions [65]. In light of the infamous scarcity pricing events in combination with rolling blackouts in California [59], it becomes clear that there is a need for enough competition at single nodes and adequate regulatory instruments. However, in a future scenario, sector coupling with gaseous energy carriers and district heating could significantly increase the competition in one node and safeguard the availability of sufficient flexibility.

Integration with higher-level markets

Authors in [15] promote a nodal-pricing based market design for European transmission grids, while the ENTSO-E positions itself against such a market design in a first discussion paper [16]. They believe a switch involves significant changes for all relevant stakeholders and that a shift of one market to nodal pricing, while surrounding markets maintain their zonal pricing settings, disturbs the underlying power flows so much that it cannot be reliably operated. Similar arguments can be found for the integration of a local market with the higher-level markets, such as the wholesale market. As it is computationally highly expensive to simultaneously clear the market for both transmission and distribution grid level, it has been proposed to clear them sequentially in an iterative manner, so that TSO and DSOs, which would be operating the markets as independent market operators, exchange data strictly based on price information. From a practical position, California's TSO and independent market operator CAISO already considers this exact type of interconnection and coordination between DSOs and TSO, where one DSO provides a single aggregated bid to the wholesale market at the connection point between transmission grid and the respective distribution system, which represents, in their
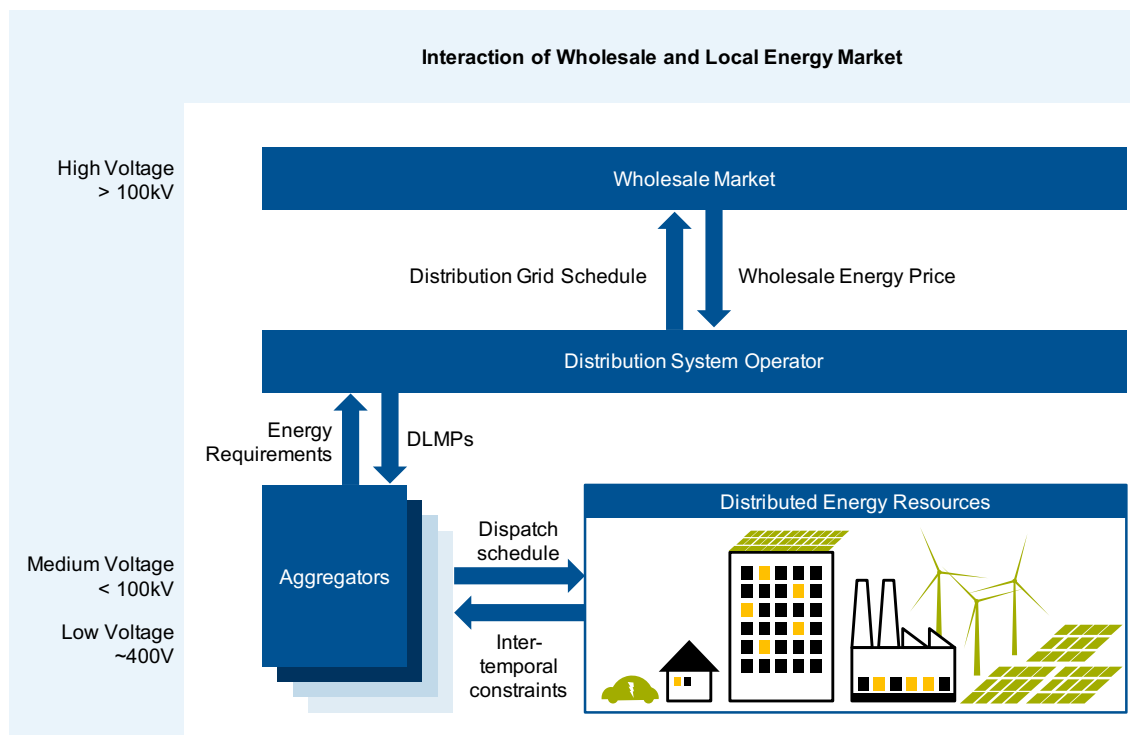
Figure 8.1: Interaction of the proposed local market with the wholesale market, based on [29]

view, the most robust and scalable model [159]. Similar efforts can be found in [160] for the case of ERCOT in Texas. As proposed by the authors in [29] and in the spirit of the suggestions in [159], on a day-ahead basis our local market could be organized as follows (see Figure 8.1):

1. The aggregators obtain the respective energy requirements from their contracted DERs based on individual price forecasts and submit them to the DSO.
2. The DSO collects this information together with prices cleared at the wholesale market and grid states and accordingly turns them into the overall social welfare of the distribution system as reflected in (6.8).
3. The DSO then solves the social welfare maximization problem, considering the system constraints.
4. The prices (DLMPs) are then obtained for each time interval of the entire planning horizon and communicated back to the aggregators.

Summary

Taking all of the above into account, it remains questionable if the efforts required for the implementation of a local DLMP-based market can be justified by the efficiency increase that furthermore comes at the cost of grid robustness against unusual events and an obvious hindrance in equity and fairness. However, the analysis shows that a central optimizer in the form of an independent third party, such as the DSO can ensure an optimal operation of the grid by exploiting the flexibility potential of DERs. At the cost of social welfare loss,

an alternative compensation scheme could be imagined that lets the DSO control DERs according to the DERs' and the grid's operational and comfort limits, in exchange for monetary compensation. As the underlying theory presented in this thesis emphasizes, this will never be as efficient and therefore less favorable from a social cost perspective as the purely market-based mechanisms of DLMPs. However, the costs will not be carried by a few market participants but by the system as a whole, which is in the spirit of the rather social philosophy behind European market setups.

Chapter 9

Conclusion and outlook

9.1 Summary

This thesis developed and applied a framework to systematically analyze the application of DLMPs from a technical and an economic perspective. To this end, this thesis covered the following subjects:

- Rooted in the fact that the design of energy markets is highly dependent on the context in which it is applied, a large dataset of power system-related data was collected and aggregated from publicly available sources. DSOs in the Netherlands provide unique and detailed data on their distribution systems. Other Dutch public institutions are equally progressive in making data available to the public. To this end, the focus of the thesis was laid on the Netherlands, which represents a common central European country.
- To develop a better understanding of the impact of electricity price signals on price-following DERs and consequently the system load, a case study was performed for a portion of the city of Eindhoven. Publicly available data was leveraged to parameterize realistic thermal building models applying the existing flexible building model CoBMo. The results of the case study showed how price-following HPs optimize their consumption based on the underlying prices, which leads to a much higher load coincidence in the case of RTP and consequently higher system peak loads.
- Based on spatial distribution grid data, a synthetization method was developed, which allows the automatic generation of a calculable electric grid model for use in the simulation software MESMO. The resulting grid models were validated for two representative regions based on a statistical analysis using CNA. Independent of the analysis of this thesis, this work can serve as a basis for the generation of representative distribution grid models, which remain a scarce resource in power system research.
- Based on the intuition we gained from the case study on the residential heating demand, a general analysis framework was developed for assessing the impact of DLMPs in comparison with different price signals both from a technical and economic perspective. We apply this framework for three different cases, namely a rural, suburban, and urban case, which were all parameterized based on the dataset from the Netherlands to ensure realistic behavior. The results were presented in full detail and analyzed from a technical

as well as an economic perspective, with a particular focus on social welfare effects. Ultimately, based on the results, potential policy implications of DLMPs in the context of current discussions were derived and discussed.

9.2 Conclusion

Despite reasonable uncertainty about the grid synthetization and thermal building parameterization procedures, which have a significant impact on all results discussed in this thesis, the analysis shows that price signals must be carefully designed and may induce considerable additional cost and/or strains on the underlying grid. From a technical perspective, DLMPs inherently lead to efficient grid usage, which comes at the cost of smaller security margins, as any dynamic pricing signal increases load coincidence of price-following DERs and therefore, the grid is operated closer to its limits. From an economic perspective, we can conclude that the overall impact on social welfare is small, which means that the DLMP-based local energy market represents a cost-efficient solution to minimize losses, voltage violations, and congestion in the distribution grid. However, as long as these cases remain rare, the advantages do not seem to justify the efforts for the implementation of such a market design. In addition, the unfair distribution of prices over the grid and, therefore, the cost burden of individual consumers (i.e., their individual surplus) is not in the spirit of traditional tariff design principles and can be perceived as unfair.

9.3 Future work

From a technical perspective, the linearization issues rooted in the chosen power flow approximation that led to potential infeasibilities should be investigated further. Furthermore, the influence of shorter time intervals for the local electricity market should be analyzed. As mentioned above, the results of this thesis are subject to uncertainties concerning the underlying data and models. Therefore, the analysis should be repeated based on actual grid models and consumption data provided by a DSO for a case-specific assessment. This should furthermore include other types of DERs, such as EVs and distributed generation capacities. Another critical aspect for the applicability of DLMPs is the investigation of strategic bidding and market power in the context of different grid configurations, as future distribution grids are expected to be able to change from radial to ring structures dynamically. Furthermore, the influence of the chosen consumer utility function, which was assumed to be inelastic for single time steps in this thesis, should be further analyzed in the context of DLMPs. The true valuation of electric power by consumers is difficult to measure. However, it can have a significant influence on the social welfare investigation. Finally, appropriate alternative measures that achieve an almost equal optimal solution should be designed, and their impact on social welfare should be evaluated and compared to the benchmark solution that DLMPs provide.

Bibliography

[1] *Proposal for a Regulation of the European Parliament and of the Council Establishing the Framework for Achieving Climate Neutrality and Amending Regulation (EU) 2018/1999 (European Climate Law)*, Mar. 4, 2020. [Online]. Available: `https://eur-lex.europa.eu/legal-content/EN/TXT/?qid=1588581905912&uri=CELEX:52020PC0080` (visited on Mar. 22, 2021).

[2] W. H. Kersting, *Distribution System Modeling and Analysis*, 3rd ed. Boca Raton, FLA: CRC Press, 2012, ISBN: 978-1-4398-5622-2.

[3] K. Lummi, A. Rautiainen, P. Järventausta, P. Heine, J. Lehtinen, and M. Hyvärinen, "Electricity Distribution Network Tariffs - Present Practices, Future Challenges and Development Possibilities", presented at the CIRED Workshop 2016, Helsinki, Finland: Institution of Engineering and Technology, Jun. 14–15, 2016. DOI: `10.1049/cp.2016.0773`.

[4] I. Perez-Arriaga and A. Bharatkumar, "A Framework for Redesigning Distribution Network Use-of-System Charges Under High Penetration of Distributed Energy Resources", *MIT CEEPR Working Paper*, Oct. 2014. [Online]. Available: `http://hdl.handle.net/1814/39570` (visited on Aug. 30, 2021).

[5] J. P. Lopes, N. Hatziargyriou, J. Mutale, P. Djapic, and N. Jenkins, "Integrating Distributed Generation into Electric Power Systems: A Review of Drivers, Challenges and Opportunities", *Electric Power Systems Research*, vol. 77, no. 9, Jul. 2007. DOI: `10.1016/j.epsr.2006.08.016`.

[6] I. Savelli and T. Morstyn, "Electricity Prices and Tariffs to Keep Everyone Happy: A Framework for Fixed and Nodal Prices Coexistence in Distribution Grids with Optimal Tariffs for Investment Cost Recovery", *Omega*, Mar. 2021. DOI: `10.1016/j.omega.2021.102450`.

[7] G. T. Heydt, B. H. Chowdhury, M. L. Crow, *et al.*, "Pricing and Control in the Next Generation Power Distribution System", *IEEE Transactions on Smart Grid*, vol. 3, no. 2, Jun. 2012. DOI: `10.1109/TSG.2012.2192298`.

[8] R. A. Verzijlbergh, L. J. D. Vries, and Z. Lukszo, "Renewable Energy Sources and Responsive Demand. Do We Need Congestion Management in the Distribution Grid?", *IEEE Transactions on Power Systems*, vol. 29, no. 5, Sep. 2014. DOI: `10.1109/TPWRS.2014.2300941`.

[9] K. Zhang, S. Troitzsch, S. Hanif, and T. Hamacher, "Coordinated Market Design for Peer-to-Peer Energy Trade and Ancillary Services in Distribution Grids", *IEEE Transactions on Smart Grid*, 2020. DOI: `10.1109/TSG.2020.2966216`.

[10] C. Utama, S. Troitzsch, and J. Thakur, "Demand-Side Flexibility and Demand-Side Bidding for Flexible Loads in Air-Conditioned Buildings", *Applied Energy*, vol. 285, Mar. 2021. DOI: `10.1016/j.apenergy.2020.116418`.

[11] J. A. Pecas Lopes, F. J. Soares, and P. M. Rocha Almeida, "Integration of Electric Vehicles in the Electric Power System", *Proceedings of the IEEE*, vol. 99, no. 1, Jan. 2011. DOI: `10.1109/JPROC.2010.2066250`.

[12] A. A. K. Abeygunawardana, A. Arefi, and G. Ledwich, "Estimating and Modeling of Distribution Network Costs for Designing Cost-Reflective Network Pricing Schemes", presented at the 2015 IEEE Power & Energy Society General Meeting, Denver, CO, USA: IEEE, Jul. 2015. DOI: `10.1109/PESGM.2015.7286418`.

[13] I. J. Pérez-Arriaga and C. Knittel, "Utility of the Future: An MIT Energy Initiative Response to an Industry in Transition", Dec. 2016. [Online]. Available: `https://energy.mit.edu/wp-content/uploads/2016/12/Utility-of-the-Future-Full-Report.pdf` (visited on Apr. 17, 2020).

[14] U. Liyanapathirane, M. Khorasany, and R. Razzaghi, "Optimization of Economic Efficiency in Distribution Grids Using Distribution Locational Marginal Pricing", *IEEE Access*, vol. 9, 2021. DOI: `10.1109/ACCESS.2021.3073641`.

[15] M. Bichler, H. U. Buhl, and L. Hanny, "Electricity Spot Market Design 2030-2050", 2021. DOI: `10.24406/FIT-N-621457`.

[16] "Options for the Design of European Electricity Markets in 2030 - Discussion Paper for Stakeholder Consultation", ENTSO-E AISBL, Mar. 31, 2021. [Online]. Available: `https://bit.ly/2QsKl0C` (visited on Apr. 6, 2021).

[17] R. Tabors, R. Masiello, M. Caramanis, and P. Andrianesis, "The Value of Distributed Energy Resources to the Grid: Introduction to the Concepts of Marginal Capital Cost and Locational Marginal Value", presented at the Hawaii International Conference on System Sciences, Jan. 8–11, 2019. DOI: `10.24251/HICSS.2019.419`.

[18] P. M. Sotkiewicz and J. M. Vignolo, "Towards a Cost Causation-Based Tariff for Distribution Networks With DG", *IEEE Transactions on Power Systems*, vol. 22, no. 3, Aug. 2007. DOI: `10.1109/TPWRS.2007.901284`.

[19] K. Lummi, A. Rautiainen, P. Jarventausta, P. Heine, J. Lehtinen, and M. Hyvarinen, "Cost-Causation Based Approach in Forming Power-Based Distribution Network Tariff for Small Customers", presented at the 2016 13th International Conference on the European Energy Market (EEM), Porto, Portugal: IEEE, Jun. 2016. DOI: `10.1109/EEM.2016.7521251`.

[20] W. W. Hogan, *Revenue Sufficiency Guarantees, Cost Causation, and Cost Allocation*, Oct. 9, 2008. [Online]. Available: `https://scholar.harvard.edu/whogan/files/hogan_rsg_100908.pdf` (visited on Aug. 30, 2021).

[21] F. C. Schweppe, M. C. Caramanis, R. D. Tabors, and R. E. Bohn, *Spot Pricing of Electricity* (Power Electronics and Power Systems). Springer US, 1988, ISBN: 978-0-89838-260-0.

[22] W. W. Hogan, "Contract Networks for Electric Power Transmission", *Journal of Regulatory Economics*, vol. 4, no. 3, Sep. 1992. DOI: 10.1007/BF00133621.

[23] A. Radovanovic, T. Nesti, and B. Chen, "A Holistic Approach to Forecasting Wholesale Energy Market Prices", *IEEE Transactions on Power Systems*, vol. 34, no. 6, Nov. 2019. DOI: 10.1109/TPWRS.2019.2921611.

[24] P. Cramton, "Electricity Market Design", *Oxford Review of Economic Policy*, vol. 33, no. 4, Nov. 2, 2017. DOI: 10.1093/oxrep/grx041.

[25] C. Sabillon, A. A. Mohamed, B. Venkatesh, and A. Golriz, "Locational Marginal Pricing for Distribution Networks: Review and Applications", presented at the 2019 IEEE Electrical Power and Energy Conference (EPEC), Montreal, QC, Canada: IEEE, Oct. 2019. DOI: 10.1109/EPEC47565.2019.9074794.

[26] L. Kristov, P. De Martini, and J. D. Taft, "A Tale of Two Visions: Designing a Decentralized Transactive Electric System", *IEEE Power and Energy Magazine*, vol. 14, no. 3, May 2016. DOI: 10.1109/MPE.2016.2524964.

[27] M. Caramanis, E. Ntakou, W. W. Hogan, A. Chakrabortty, and J. Schoene, "Co-Optimization of Power and Reserves in Dynamic T&D Power Markets With Nondispatchable Renewable Generation and Distributed Energy Resources", *Proceedings of the IEEE*, vol. 104, no. 4, Apr. 2016. DOI: 10.1109/JPROC.2016.2520758.

[28] A. Papavasiliou, "Analysis of Distribution Locational Marginal Prices", *IEEE Transactions on Smart Grid*, 2017. DOI: 10.1109/TSG.2017.2673860.

[29] S. Hanif, K. Zhang, C. Hackl, M. Barati, H. B. Gooi, and T. Hamacher, "Decomposition and Equilibrium Achieving Distribution Locational Marginal Prices using Trust-Region Method", *IEEE Transactions on Smart Grid*, 2018. DOI: 10.1109/TSG.2018.2822766.

[30] S. Huang, Q. Wu, S. S. Oren, R. Li, and Z. Liu, "Distribution Locational Marginal Pricing Through Quadratic Programming for Congestion Management in Distribution Networks", *IEEE Transactions on Power Systems*, vol. 30, no. 4, Jul. 2015. DOI: 10.1109/TPWRS.2014.2359977.

[31] S. Hanif, T. Massier, H. B. Gooi, T. Hamacher, and T. Reindl, "Cost Optimal Integration of Flexible Buildings in Congested Distribution Grids", *IEEE Transactions on Power Systems*, vol. 32, no. 3, May 2017. DOI: 10.1109/TPWRS.2016.2605921.

[32] S. Hanif, H. B. Gooi, T. Massier, T. Hamacher, and T. Reindl, "Distributed Congestion Management of Distribution Grids Under Robust Flexible Buildings Operations", *IEEE Transactions on Power Systems*, vol. 32, no. 6, Nov. 2017. DOI: 10.1109/TPWRS.2017.2660065.

[33] R. Li, Q. Wu, and S. S. Oren, "Distribution Locational Marginal Pricing for Optimal Electric Vehicle Charging Management", *IEEE Transactions on Power Systems*, vol. 29, no. 1, Jan. 2014. DOI: 10.1109/TPWRS.2013.2278952.

[34] Z. Yuan, M. R. Hesamzadeh, and D. R. Biggar, "Distribution Locational Marginal Pricing by Convexified ACOPF and Hierarchical Dispatch", *IEEE Transactions on Smart Grid*, vol. 9, no. 4, Jul. 2018. DOI: 10.1109/TSG.2016.2627139.

[35] M. N. Faqiry, L. Wang, and H. Wu, "HEMS-Enabled Transactive Flexibility in Real-Time Operation of Three-Phase Unbalanced Distribution Systems", *Journal of Modern Power Systems and Clean Energy*, vol. 7, no. 6, Nov. 2019. DOI: 10.1007/s40565-019-0553-2.

[36] S. Hanif, M. Barati, A. Kargarian, H. B. Gooi, and T. Hamacher, "Multiphase Distribution Locational Marginal Prices: Approximation and Decomposition", presented at the 2018 IEEE Power & Energy Society General Meeting (PESGM), Portland, OR: IEEE, Aug. 2018. DOI: 10.1109/PESGM.2018.8585925.

[37] L. Edmonds, M. N. Faqiry, H. Wu, and A. Palani, "Three-Phase Distribution Locational Marginal Pricing to Manage Unbalanced Variable Renewable Energy", presented at the 2020 IEEE Power & Energy Society General Meeting (PESGM), Montreal, QC, Canada: IEEE, Aug. 2020. DOI: 10.1109/PESGM41954.2020.9281895.

[38] Yikui Liu, Jie Li, Lei Wu, and Qingzhen Liu, "Ex-Post Real-Time Distribution LMP Based on State Estimation", presented at the 2016 IEEE Power and Energy Society General Meeting (PESGM), Boston, MA, USA: IEEE, Jul. 17–21, 2016. DOI: 10.1109/PESGM.2016.7741682.

[39] T. Schelo, A. Bidel, and T. Hamacher, "Biogas Plant Operation under Distribution Locational Marginal Prices", presented at the 2021 IEEE Madrid PowerTech, Madrid, Spain: IEEE, Jun. 28, 2021. DOI: 10.1109/PowerTech46648.2021.9494774.

[40] S. Hanif, T. Massier, T. Hamacher, and T. Reindl, "Evaluating Demand Response in the Presence of Solar PV: Distribution Grid Perspective", presented at the 2016 4th International IEEE Conference on Smart Energy Grid Engineering (SEGE), Oshawa, ON: IEEE, Aug. 2016. DOI: 10.1109/SEGE.2016.7589558.

[41] S. Parhizi and A. Khodaei, "Active/Reactive Locational Pricing in Distribution Networks", presented at the 2019 North American Power Symposium (NAPS), Wichita, KS, USA: IEEE, Oct. 2019. DOI: 10.1109/NAPS46351.2019.8999973.

[42] K. Shaloudegi, N. Madinehi, S. H. Hosseinian, and H. A. Abyaneh, "A Novel Policy for Locational Marginal Price Calculation in Distribution Systems Based on Loss Reduction Allocation Using Game Theory", *IEEE Transactions on Power Systems*, vol. 27, no. 2, May 2012. DOI: 10.1109/TPWRS.2011.2175254.

[43] E. A. Farsani, H. A. Abyaneh, M. Abedi, and S. H. Hosseinian, "A Novel Policy for LMP Calculation in Distribution Networks Based on Loss and Emission Reduction Allocation Using Nucleolus Theory", *IEEE Transactions on Power Systems*, vol. 31, no. 1, Jan. 2016. DOI: 10.1109/TPWRS.2015.2398821.

[44] J.-F. Toubeau, T. Morstyn, J. Bottieau, *et al.*, "Capturing Spatio-Temporal Dependencies in the Probabilistic Forecasting of Distribution Locational Marginal Prices", *IEEE Transactions on Smart Grid*, 2020. DOI: 10.1109/TSG.2020.3047863.

[45] P. Sotkiewicz and J. Vignolo, "Nodal Pricing for Distribution Networks: Efficient Pricing for Efficiency Enhancing DG", *IEEE Transactions on Power Systems*, vol. 21, no. 2, May 2006. DOI: 10.1109/TPWRS.2006.873006.

[46] H. Yuan, F. Li, Y. Wei, and J. Zhu, "Novel Linearized Power Flow and Linearized OPF Models for Active Distribution Networks With Application in Distribution LMP", *IEEE Transactions on Smart Grid*, vol. 9, no. 1, Jan. 2018. DOI: 10.1109/TSG.2016.2594814.

[47] S. Hanif, P. Creutzberg, H. B. Gooi, and T. Hamacher, "Pricing Mechanism for Flexible Loads using Distribution Grid Hedging Rights", *IEEE Transactions on Power Systems*, 2018. DOI: 10.1109/TPWRS.2018.2862149.

[48] K. Zhang, S. Hanif, C. M. Hackl, and T. Hamacher, "A Framework for Multi-Regional Real-Time Pricing in Distribution Grids", *IEEE Transactions on Smart Grid*, vol. 10, no. 6, Nov. 2019. DOI: 10.1109/TSG.2019.2911996.

[49] Z. Liu, Q. Wu, S. S. Oren, S. Huang, R. Li, and L. Cheng, "Distribution Locational Marginal Pricing for Optimal Electric Vehicle Charging Through Chance Constrained Mixed-Integer Programming", *IEEE Transactions on Smart Grid*, vol. 9, no. 2, Mar. 2018. DOI: 10.1109/TSG.2016.2559579.

[50] N. O'Connell, Q. Wu, J. Østergaard, A. H. Nielsen, S. T. Cha, and Y. Ding, "Day-Ahead Tariffs for the Alleviation of Distribution Grid Congestion from Electric Vehicles", *Electric Power Systems Research*, vol. 92, Nov. 1, 2012. DOI: 10.1016/j.epsr.2012.05.018.

[51] P. Siano and D. Sarno, "Assessing the Benefits of Residential Demand Response in a Real Time Distribution Energy Market", *Applied Energy*, vol. 161, Jan. 2016. DOI: 10.1016/j.apenergy.2015.10.017.

[52] P. Andrianesis and M. C. Caramanis, "Optimal Grid – Distributed Energy Resource Coordination: Distribution Locational Marginal Costs and Hierarchical Decomposition", presented at the 2019 57th Annual Allerton Conference on Communication, Control, and Computing, Monticello, IL, USA: IEEE, Sep. 2019. DOI: 10.1109/ALLERTON.2019.8919689.

[53] E. Ntakou and M. Caramanis, "Price Discovery in Dynamic Power Markets with Low-Voltage Distribution-Network Participants", presented at the 2014 IEEE/PES Transmission & Distribution Conference & Exposition (T&D), Chicago, IL, USA: IEEE, Apr. 2014. DOI: 10.1109/TDC.2014.6863212.

[54] S. Troitzsch, M. Grussmann, K. Zhang, and T. Hamacher, "Distribution Locational Marginal Pricing for Combined Thermal and Electric Grid Operation", presented at the 2020 IEEE PES Innovative Smart Grid Technologies Europe (ISGT-Europe), The Hague, Netherlands: IEEE, Oct. 2020. DOI: 10.1109/ISGT-Europe47291.2020.9248832.

[55] S. Stoft, *Power System Economics: Designing Markets for Electricity*. Piscataway, NJ : New York: IEEE Press ; Wiley-Interscience, 2002, ISBN: 978-0-471-15040-4.

[56] L. Meeus, *The Evolution of Electricity Markets in Europe* (Loyola de palacio series on european energy policy). Northampton: Edward Elgar Publishing, 2020, ISBN: 978-1-78990-546-5.

[57] M. Weibelzahl, "Nodal, Zonal, or Uniform Electricity Pricing: How to Deal with Network Congestion", *Frontiers in Energy*, vol. 11, no. 2, 2017. DOI: `10.1007/s11708-017-0460-z`.

[58] M. Bjørndal and K. Jörnsten, "Benefits from Coordinating Congestion Management—the Nordic Power Market", *Energy Policy*, vol. 35, no. 3, Mar. 2007. DOI: `10.1016/j.enpol.2006.06.014`.

[59] S. Borenstein, J. B. Bushnell, and F. A. Wolak, "Measuring Market Inefficiencies in California's Restructured Wholesale Electricity Market", *American Economic Review*, vol. 92, no. 5, Nov. 1, 2002. DOI: `10.1257/000282802762024557`.

[60] D. S. Kirschen and G. Strbac, *Fundamentals of Power System Economics*. Chichester, West Sussex, England ; Hoboken, NJ: John Wiley & Sons, 2004, ISBN: 978-0-470-84572-1.

[61] P. Engelkamp, F. L. Sell, and B. Sauer, *Einführung in die Volkswirtschaftslehre*. Berlin, Heidelberg: Springer Berlin Heidelberg, 2020. DOI: `10.1007/978-3-662-62248-3`.

[62] H. Weigt, "A Time-Variant Welfare Economic Analysis of a Nodal Pricing Mechanism in Germany", *SSRN Electronic Journal*, 2006. DOI: `10.2139/ssrn.1137403`.

[63] R. Green, "Nodal Pricing of Electricity: How Much Does It Cost to Get It Wrong?", *Journal of Regulatory Economics*, vol. 31, no. 2, Mar. 8, 2007. DOI: `10.1007/s11149-006-9019-3`.

[64] P. Olivella-Rosell, P. Lloret-Gallego, Í. Munné-Collado, *et al.*, "Local Flexibility Market Design for Aggregators Providing Multiple Flexibility Services at Distribution Network Level", *Energies*, vol. 11, no. 4, Apr. 2, 2018. DOI: `10.3390/en11040822`.

[65] *Proposal for a Regulation of the European Parliament and of the Council on the Internal Market for Electricity*, Nov. 30, 2016. [Online]. Available: `https://eur-lex.europa.eu/resource.html?uri=cellar:d7108c4c-b7b8-11e6-9e3c-01aa75ed71a1.0001.02/DOC_1&format=PDF` (visited on Mar. 23, 2021).

[66] G. Antonopoulos, S. Vitiello, G. Fulli, and M. Masera, "Nodal Pricing in the European Internal Electricity Market", European Commission, LU, 2020. [Online]. Available: `https://data.europa.eu/doi/10.2760/41018` (visited on Mar. 29, 2021).

[67] B. Thormann and T. Kienberger, "Evaluation of Grid Capacities for Integrating Future E-Mobility and Heat Pumps into Low-Voltage Grids", *Energies*, vol. 13, no. 19, Sep. 29, 2020. DOI: `10.3390/en13195083`.

[68] K. Schneider, P. Phanivong, and J.-S. Lacroix, "IEEE 342-Node Low Voltage Networked Test System", presented at the 2014 IEEE Power & Energy Society General Meeting, National Harbor, MD, USA: IEEE, Jul. 2014. DOI: `10.1109/PESGM.2014.6939794`.

[69] R. F. Arritt and R. C. Dugan, "The IEEE 8500-Node Test Feeder", presented at the IEEE PES T&D 2010, New Orleans, LA, USA: IEEE, 2010. DOI: `10.1109/TDC.2010.5484381`.

[70] R. C. Dugan, W. H. Kersting, S. Carneiro, R. F. Arritt, and T. E. McDermott, "Roadmap for the IEEE PES Test Feeders", presented at the 2009 IEEE/PES Power Systems Conference and Exposition (PSCE), Seattle, WA, USA: IEEE, Mar. 2009. DOI: 10.1109/PSCE.2009.4840231.

[71] K. Strunz, R. H. Fletcher, R. Campbell, and F. Gao, "Developing Benchmark Models for Low-Voltage Distribution Feeders", presented at the Energy Society General Meeting (PES), Calgary, Canada: IEEE, Jul. 2009. DOI: 10.1109/PES.2009.5260227.

[72] K. Rudion, A. Orths, Z. Styczynski, and K. Strunz, "Design of Benchmark of Medium Voltage Distribution Network for Investigation of DG Integration", presented at the 2006 IEEE Power Engineering Society General Meeting, Montreal, QC, Canada: IEEE, 2006. DOI: 10.1109/PES.2006.1709447.

[73] Conseil International des Grands Réseaux Électriques and Comité d'études C6, *Benchmark Systems for Network Integration of Renewable and Distributed Energy Resources*. Paris: CIGRÉ, 2014, ISBN: 978-2-85873-270-8.

[74] F. Postigo Marcos, C. Mateo Domingo, T. Gómez San Román, *et al.*, "A Review of Power Distribution Test Feeders in the United States and the Need for Synthetic Representative Networks", *Energies*, vol. 10, no. 11, Nov. 18, 2017. DOI: 10.3390/en10111896.

[75] Stedin Groep. "Enduris Distribution Grid Data". (Dec. 18, 2020), [Online]. Available: https://www.enduris.nl/over-enduris/energietransitie/open-data.htm (visited on May 18, 2020).

[76] Enexis Groep. "Enexis Distribution Grid Data". (2020), [Online]. Available: https://www.enexis.nl/over-ons/wat-bieden-we/andere-diensten/open-data (visited on May 18, 2020).

[77] Liander N.V. "Liander Distribution Grid Data". (2020), [Online]. Available: https://www.pdok.nl/introductie/-/article/liander-elektriciteitsnetten-1.

[78] Stedin Groep. "Stedin Distribution Grid Data". (2020), [Online]. Available: https://www.stedin.net/zakelijk/open-data/liggingsdata-kabels-en-leidingen (visited on May 18, 2020).

[79] "Map Tiles", Stamen Design Studios. (2021), [Online]. Available: http://maps.stamen.com/#terrain/12/37.7706/-122.3782 (visited on Jun. 30, 2021).

[80] "BAG – Basisregistratie Adressen en Gebouwen", Kadaster - Cadastre, Land Registry and Mapping Agency. (2021), [Online]. Available: https://www.kadaster.nl/zakelijk/registraties/basisregistraties/bag (visited on Mar. 15, 2021).

[81] B. Dukai, "3D Registration of Buildings and Addresses (BAG) / 3D Basisregistratie Adressen en Gebouwen (BAG)", version 1, in collab. with L. Hugo and S. Jantien, Nov. 26, 2018. DOI: 10.4121/UUID:F1F9759D-024A-492A-B821-07014DD6131C.

[82] T. Loga, B. Stein, and N. Diefenbach, "TABULA Building Typologies in 20 European Countries—Making Energy-Related Features of Residential Building Stocks Comparable", *Energy and Buildings*, vol. 132, Nov. 2016. DOI: 10.1016/j.enbuild.2016.06.094.

[83] H. Meier, C. Fünfgeld, T. Adam, and B. Schieferdecker, *Repräsentative VDEW- Lastprofile*, 1999. [Online]. Available: `https://www.bdew.de/energie/standardlastprofile-strom/` (visited on Feb. 22, 2021).

[84] M. Sterner and I. Stadler, Eds., *Energiespeicher - Bedarf, Technologien, Integration*, 2nd ed. Springer Vieweg, 2017, ISBN: 978-3-662-48892-8.

[85] "World Bank National Accounts Data, and OECD National Accounts Data Files", World Bank. (2021), [Online]. Available: `https://data.worldbank.org/indicator` (visited on May 21, 2021).

[86] M. Müller, F. Biedenbach, and J. Reinhard, "Development of an Integrated Simulation Model for Load and Mobility Profiles of Private Households", *Energies*, vol. 13, no. 15, Jul. 27, 2020. DOI: `10.3390/en13153843`.

[87] "Data Center", Koninklijk Nederlands Meteorologisch Instituut. (2020), [Online]. Available: `https://data.knmi.nl/datasets` (visited on May 25, 2020).

[88] ENTSO-E. "Transparency Platform", ENTSO-E. (2020), [Online]. Available: `https://transparency.entsoe.eu` (visited on Jun. 27, 2020).

[89] *Energy Consumption in Households*, 2018. [Online]. Available: `https://ec.europa.eu/eurostat/statistics-explained/index.php?title=Energy_consumption_in_households` (visited on Jun. 16, 2021).

[90] A. Kieft, R. Harmsen, and M. P. Hekkert, "Heat Pumps in the Existing Dutch Housing Stock: An Assessment of Its Technological Innovation System", *Sustainable Energy Technologies and Assessments*, vol. 44, Apr. 2021. DOI: `10.1016/j.seta.2021.101064`.

[91] R. de Best, *Number of Heat Pumps in Operation in the Netherlands 2013-2019*, Jan. 29, 2021. [Online]. Available: `https://www.statista.com/statistics/740480/heat-pumps-in-operation-netherlands/` (visited on Feb. 15, 2021).

[92] W. Grassi, *Heat Pumps: Fundamentals and Applications* (Green Energy and Technology), 1st ed. 2018. Cham: Springer International Publishing, 2018. DOI: `10.1007/978-3-319-62199-9`.

[93] D. Papadaskalopoulos, G. Strbac, P. Mancarella, M. Aunedi, and V. Stanojevic, "Decentralized Participation of Flexible Demand in Electricity Markets—Part II: Application With Electric Vehicles and Heat Pump Systems", *IEEE Transactions on Power Systems*, vol. 28, no. 4, Nov. 2013. DOI: `10.1109/TPWRS.2013.2245687`.

[94] F. Samweber, "Systematischer Vergleich Netzoptimierender Maßnahmen zur Integration elektrischer Wärmeerzeuger und Fahrzeuge in Niederspannungsnetze", Dissertation, Technical University of Munich, Munich, Feb. 12, 2018. [Online]. Available: `https://bit.ly/3gFC9on` (visited on Dec. 7, 2020).

[95] S. Troitzsch and T. Hamacher, "Control-oriented Thermal Building Modelling", presented at the 2020 IEEE Power & Energy Society General Meeting (PESGM), Montreal, QC, Canada: IEEE, Aug. 2, 2020. DOI: `10.1109/PESGM41954.2020.9281503`.

[96] S. Troitzsch, T. Miori, and A. Vautrin, *CoBMo - Control-oriented Building Model*, version 0.3.0, Zenodo, Nov. 13, 2019. DOI: `10.5281/ZENODO.3523539`.

[97] C. Utama, "Demand Side Flexibility and Bidding Strategies for Flexible Loads in Air-Conditioned Buildings", Master's Thesis, KTH School of Industrial Engineering and Management, Stockholm, Sweden, Oct. 21, 2020.

[98] M. Burggraf, "Impact of Different Price Signals on Social Welfare in Distribution Grids", Master's Thesis, Technical University of Munich, Munich, Apr. 28, 2021.

[99] "Energetische verbeteringsmaatregelen in de sociale-huursector – enkele uitkomsten van de SHAERE-monitor 2010-2013", TU Delft, 2016. [Online]. Available: `https://bit.ly/3qCGD26` (visited on Jun. 27, 2021).

[100] F. Filippidou, N. Nieboer, and H. Visscher, "Energy Efficiency Measures Implemented in the Dutch Non-Profit Housing Sector", *Energy and Buildings*, vol. 132, Nov. 2016. DOI: `10.1016/j.enbuild.2016.05.095`.

[101] Optotherm. "Emissivity Values". (2018), [Online]. Available: `https://www.optotherm.com/emiss-table.htm` (visited on Jun. 27, 2021).

[102] *Table of Emissivity of Various Surfaces*. [Online]. Available: `https://www.transmetra.ch/images/transmetra_pdf/publikationen_literatur/pyrometrie-thermografie/emissivity_table.pdf` (visited on Jun. 27, 2021).

[103] *Solar Absorption/Emmittance*, 1999. [Online]. Available: `http://web.archive.org/web/20020118010715/http://fridge.arch.uwa.edu.au/materials/` (visited on Jun. 27, 2021).

[104] "Absorbed Solar Radiation", Engineering ToolBox. (2009), [Online]. Available: `https://www.engineeringtoolbox.com/solar-radiation-absorbed-materials-d_1568.html` (visited on Jun. 27, 2021).

[105] *Energy Efficiency and Use of Renewable Energy for Residential Buildings - Code of Practice*, 2017. [Online]. Available: `https://bit.ly/3A32SCw` (visited on Jun. 27, 2021).

[106] "Solar Absorptivity", Integrated Environmental Solutions. (2018), [Online]. Available: `https://help.iesve.com/ve2018/table_14_solar_absorptivity.htm` (visited on Jun. 27, 2021).

[107] S. Wonorahardjo, I. M. Sutjahja, Y. Mardiyati, *et al.*, "Characterising Thermal Behaviour of Buildings and Its Effect on Urban Heat Island in Tropical Areas", *International Journal of Energy and Environmental Engineering*, vol. 11, no. 1, Mar. 2020. DOI: `10.1007/s40095-019-00317-0`.

[108] "Einschalige Außenwände", Baunetz Wissen. (2021), [Online]. Available: `https://www.baunetzwissen.de/mauerwerk/fachwissen/wand/einschalige-aussenwaende-162708` (visited on Jun. 27, 2021).

[109] *ISO 52016-1:2017 - Energy Performance of Buildings*, 2017.

[110] I. H. Bell, J. Wronski, S. Quoilin, and V. Lemort, "Pure and Pseudo-pure Fluid Thermophysical Property Evaluation and the Open-Source Thermophysical Property Library CoolProp", *Industrial & Engineering Chemistry Research*, vol. 53, no. 6, Feb. 12, 2014. DOI: `10.1021/ie4033999`.

[111] "Calculation of Global Radiation (SumSW) from DIF and DIR", World Radiation Monitoring Center. (2021), [Online]. Available: `https://bsrn.awi.de/en/data/calculation-of-global-radiation/` (visited on Jun. 27, 2021).

[112] W. F. Holmgren, C. W. Hansen, and M. A. Mikofski, "Pvlib Python: A Python Package for Modeling Solar Energy Systems", *Journal of Open Source Software*, vol. 3, no. 29, Sep. 7, 2018. DOI: `10.21105/joss.00884`.

[113] "Indoor Environment: Health Aspects of Air Quality, Thermal Environment, Light and Noise", *World Health Organization. Environmental Health in Rural and Urban Development and Housing Unit*, 1990. [Online]. Available: `https://apps.who.int/iris/handle/10665/62723` (visited on Jun. 27, 2021).

[114] S. Troitzsch, "Multi-Energy System Modelling & Optimization (MESMO) - Development of a Software Tool for District-Scale Electric and Thermal Energy System Operation", Dissertation, Technical University of Munich, Munich, 2021.

[115] A. Molar-Cruz, "A GIS-Based Gray-Box Approach for the Estimation of Heat Demand at the Urban Scale", Workshop, presented at the 38th International Energy Workshop (Paris), Jun. 3–5, 2019. [Online]. Available: `http://mediatum.ub.tum.de/doc/1525656/686237.pdf` (visited on Jun. 27, 2021).

[116] V.-F. Facility-Management, *VDI 3807-3 – Characteristic Consumption Values for Buildings - Characteristic Water Consumption Values*, Nov. 2015. [Online]. Available: `https://www.vdi.de/richtlinien/details/vdi-3807-blatt-3-verbrauchskennwerte-fuer-gebaeude-teilkennwerte-wasser` (visited on Jun. 27, 2021).

[117] I. Sarbu and C. Sebarchievici, "A Comprehensive Review of Thermal Energy Storage", *Sustainability*, vol. 10, no. 2, Jan. 14, 2018. DOI: `10.3390/su10010191`.

[118] "Pufferspeicher-Technik, Auslegung und Kosten: Auslegung und Dimensionierung", Greenhouse Media GmbH. (Jun. 27, 2021), [Online]. Available: `https://www.energie-experten.org/heizung/heizungstechnik/pufferspeicher` (visited on Jun. 27, 2021).

[119] *VDI 2067-2: Economy Calculation of Heat Consuming Installations; Heating Installations*, Dec. 1993. [Online]. Available: `https://www.vdi.de/richtlinien/details/vdi-2067-blatt-2-berechnung-der-kosten-von-waermeversorgungsanlagen-raumheizung` (visited on Jun. 27, 2021).

[120] M. Kramer, "Hierarchical Distributed Control to Integrate Prosumer Flexibility in Smart Grids", Dissertation, Technical University of Munich, Munich, Jul. 2020.

[121] W. Rogatty, "Wärme nach Maß – Wie groß muss der neue Wärmeerzeuger in einem Altbau sein?", *IKZ-Haustechnik*, vol. 14/2006, 2006. [Online]. Available: `https://www.ikz.de/uploads/media/050.pdf` (visited on Jun. 27, 2021).

[122] Umwelt Bundesamt. "Energieverbrauch privater Haushalte", Umwelt Bundesamt. (Jan. 7, 2020), [Online]. Available: `https://www.umweltbundesamt.de/daten/private-haushalte-konsum/wohnen/energieverbrauch-privater-haushalte#endenergieverbrauch-der-privaten-haushalte` (visited on Jun. 27, 2021).

[123]   J. Brugmann, "Planung von Luft/ Wasser-Wärmepumpen für Altbauten", *KI Luft- und Kältetechnik*, May 2006.

[124]   T. Stetz, "Autonomous Voltage Control Strategies in Distribution Grids with Photovoltaic Systems - Technical and Economic Assessment", Dissertation, University of Kassel, Dec. 18, 2013.

[125]   A. Franco and F. Fantozzi, "Optimal Sizing of Solar-Assisted Heat Pump Systems for Residential Buildings", *Buildings*, vol. 10, no. 10, Oct. 4, 2020. DOI: `10.3390/buildings10100175`.

[126]   B. Parrish, R. Gross, and P. Heptonstall, "On Demand: Can Demand Response Live up to Expectations in Managing Electricity Systems?", *Energy Research & Social Science*, vol. 51, May 2019. DOI: `10.1016/j.erss.2018.11.018`.

[127]   A. Bidel, T. Schelo, and T. Hamacher, "Synthetic Distribution Grid Generation Based on High Resolution Spatial Data", presented at the IEEE International Conference on Environment and Electrical Engineering (EEEIC), Bari, Italy: IEEE, Sep. 9, 2021.

[128]   T. Gómez, C. Mateo, Á. Sánchez, P. Frías, and R. Cossent, "Reference Network Models: A Computational Tool for Planning and Designing Large-Scale Smart Electricity Distribution Grids", in *High Performance Computing in Power and Energy Systems*, ser. Power Systems, S. K. Khaitan and A. Gupta, Eds., Berlin, Heidelberg: Springer Berlin Heidelberg, 2013. DOI: `10.1007/978-3-642-32683-7_9`.

[129]   C. Mateo, F. Postigo, F. de Cuadra, *et al.*, "Building Large-Scale U.S. Synthetic Electric Distribution System Models", *IEEE Transactions on Smart Grid*, vol. 11, no. 6, Nov. 2020. DOI: `10.1109/TSG.2020.3001495`.

[130]   J. Amme, G. Pleßmann, J. Bühler, L. Hülk, E. Kötter, and P. Schwaegerl, "The Ego Grid Model: An Open-Source and Open-Data Based Synthetic Medium-Voltage Grid Model for Distribution Power Supply Systems", *Journal of Physics: Conference Series*, vol. 977, Feb. 2018. DOI: `10.1088/1742-6596/977/1/012007`.

[131]   S. S. Saha, E. Schweitzer, A. Scaglione, and N. G. Johnson, "A Framework for Generating Synthetic Distribution Feeders using OpenStreetMap", presented at the 2019 North American Power Symposium (NAPS), Wichita, KS, USA: IEEE, Oct. 2019. DOI: `10.1109/NAPS46351.2019.9000187`.

[132]   A. Seack, J. Kays, and C. Rehtanz, "Generating Low Voltage Grids on the Basis of Public Available Map Data", *CIRED Workshop*, no. 311, 2014. [Online]. Available: `http://www.cired.net/publications/workshop2014/papers/CIRED2014WS_0338_final.pdf` (visited on Mar. 2, 2021).

[133]   G. Pisano, N. Chowdhury, M. Coppo, *et al.*, "Synthetic Models of Distribution Networks Based on Open Data and Georeferenced Information", *Energies*, vol. 12, no. 23, Nov. 26, 2019. DOI: `10.3390/en12234500`.

[134]   A. Trpovski, D. Recalde, and T. Hamacher, "Synthetic Distribution Grid Generation Using Power System Planning: Case Study of Singapore", presented at the 2018 53rd International Universities Power Engineering Conference (UPEC), Glasgow: IEEE, Sep. 2018. DOI: `10.1109/UPEC.2018.8542054`.

[135] L. Verheggen, "Kombinierte Grundsatzplanung von Mittel- und Niederspannungsnetzen unter Berücksichtigung betrieblicher Maßnahmen und Unsicherheiten", Dissertation, Rheinisch-Westfälische Technische Hochschule Aachen, Aachen, Dec. 20, 2016.

[136] B. Wille-Haussmann, D. Fischer, B. Köpfer, S. Bercher, P. Engelmann, and F. Ohr, *Synthetische Lastprofile für eine effiziente Versorgungsplanung für nicht-Wohngebäude*, 2020.

[137] *Dwelling Sizes of Dutch Households*, 2015. [Online]. Available: `https://www.cbs.nl/en-gb/custom/2016/14/dwelling-sizes-of-dutch-households` (visited on May 17, 2021).

[138] G. Kerber, "Aufnahmefähigkeit von Niederspannungsverteilnetzen für die Einspeisung aus Photovoltaikkleinanlagen", Dissertation, Technical University of Munich, Mar. 21, 2011. [Online]. Available: `https://mediatum.ub.tum.de/doc/998003/998003.pdf` (visited on Apr. 22, 2020).

[139] M. Arnold, *Planungsgrundsätze für Niederspannungsnetze unter Berücksichtigung regelbarer Ortsnetztransformatoren*. Technische Universität Kaiserslautern: Prof. Dr.-Ing. Wolfram H. Wellßo, 2019, ISBN: 978-3-8440-6495-7.

[140] F. Stern and J. Spencer, "Chapter 10: Peak Demand and Time-Differentiated Energy Savings Cross-Cutting Protocol. The Uniform Methods Project: Methods for Determining Energy Efficiency Savings for Specific Measures", *National Renewable Energy Laboratory (NREL)*, NREL/SR-7A40-68566 Oct. 3, 2017. DOI: `10.2172/1406991`.

[141] L. Thurner, A. Scheidler, F. Schafer, *et al.*, "Pandapower: An Open-Source Python Tool for Convenient Modeling, Analysis, and Optimization of Electric Power Systems", *IEEE Transactions on Power Systems*, vol. 33, no. 6, Nov. 2018. DOI: `10.1109/TPWRS.2018.2829021`.

[142] *Nexans Outdoor Energy Cables Product Specifications Catalogue*, Jun. 23, 2020. [Online]. Available: `https://www.nexans.de/eservice/Germany-en/navigate_243/Outdoor_Energy_cables.html` (visited on Jun. 23, 2020).

[143] G. A. Pagani and M. Aiello, "Towards Decentralization: A Topological Investigation of the Medium and Low Voltage Grids", *IEEE Transactions on Smart Grid*, vol. 2, no. 3, Sep. 2011. DOI: `10.1109/TSG.2011.2147810`.

[144] S. Troitzsch, S. Hanif, K. Zhang, A. Trpovski, and T. Hamacher, "Flexible Distribution Grid Demonstrator (FLEDGE): Requirements and Software Architecture", presented at the 2019 IEEE Power & Energy Society General Meeting (PESGM), Atlanta, GA, USA: IEEE, Aug. 2019. DOI: `10.1109/PESGM40551.2019.8973567`.

[145] W. van Bijsterveld. "AlleCijfers.nl". (2020), [Online]. Available: `https://allecijfers.nl/wijk/zuidermeer-koggenland/` (visited on Jun. 24, 2021).

[146] "CBS – Toelichting Wijk- en Buurtkaart 2017,18,19". (2019), [Online]. Available: `https://www.cbs.nl/nl-nl/dossier/nederland-regionaal/geografische-data/wijk-en-buurtkaart-2019` (visited on May 18, 2020).

[147] E. Schweitzer, A. Scaglione, A. Monti, and G. A. Pagani, "Automated Generation Algorithm for Synthetic Medium Voltage Radial Distribution Systems", *IEEE Journal on Emerging and Selected Topics in Circuits and Systems*, vol. 7, no. 2, Jun. 2017. DOI: `10.1109/JETCAS.2017.2682934`.

[148] J. A. Taylor, *Convex Optimization of Power Systems*. Cambridge, United Kingdom ; New York: Cambridge University Press, 2015, ISBN: 978-1-107-07687-7.

[149] E. Litvinov, T. Zheng, G. Rosenwald, and P. Shamsollahi, "Marginal Loss Modeling in LMP Calculation", *IEEE Transactions on Power Systems*, vol. 19, no. 2, May 2004. DOI: `10.1109/TPWRS.2004.825894`.

[150] F. Li and R. Bo, "DCOPF-Based LMP Simulation: Algorithm, Comparison With ACOPF, and Sensitivity", *IEEE Transactions on Power Systems*, vol. 22, no. 4, Nov. 2007. DOI: `10.1109/TPWRS.2007.907924`.

[151] S. Troitzsch, T. Schelo, V. Kleinschmidt, and K. Zhang, *FLEDGE - Flexible Distribution Grid Demonstrator*, version Version 0.4.1, Zenodo, 2021. [Online]. Available: `https://doi.org/10.5281/zenodo.4896047` (visited on Mar. 19, 2020).

[152] A. M. Giacomoni and B. F. Wollenberg, "Linear Programming Optimal Power Flow Utilizing a Trust Region Method", presented at the 2010 North American Power Symposium (NAPS 2010), Arlington, TX, USA: IEEE, Sep. 2010. DOI: `10.1109/NAPS.2010.5619970`.

[153] J. Nocedal and S. J. Wright, *Numerical Optimization* (Springer Series in Operations Research and Financial Engineering). Springer New York, 2006. DOI: `10.1007/978-0-387-40065-5`.

[154] J. C. Bonbright, A. L. Danielsen, and D. R. Kamerschen, *Principles of Public Utility Rates*, 2nd ed. Arlington, VA: Public Utilities Reports, 1988, ISBN: 978-0-910325-23-3.

[155] D. Biggar and A. Reeves, "Network Pricing for the Prosumer Future: Demand-Based Tariffs or Locational Marginal Pricing?", in *Future of Utilities Utilities of the Future*, Elsevier, 2016. DOI: `10.1016/B978-0-12-804249-6.00013-0`.

[156] M. Fotouhi Ghazvini, J. Soares, H. Morais, R. Castro, and Z. Vale, "Dynamic Pricing for Demand Response Considering Market Price Uncertainty", *Energies*, vol. 10, no. 9, Aug. 23, 2017. DOI: `10.3390/en10091245`.

[157] C. W. King, J. D. Rhodes, J. Zarnikau, and N. Lin, "The Timeline and Events of the February 2021 Texas Electric Grid Blackouts", University of Texas at Austin Energy Institute, Jul. 2021.

[158] *Workshop on Flexibility Markets and TSO-DSO Cooperation*, Feb. 13, 2020. [Online]. Available: `https://ec.europa.eu/energy/sites/default/files/20200213_conclusions_-_workshop_on_flexibility_markets_and_tso-dso_cooperation_final.pdf` (visited on Apr. 15, 2021).

[159] L. Kristov, "Modernizing Transmission-Distribution Interface Coordination for a high-DER Future", presented at the CAISO Energy Advisory Committee Meeting, Mar. 29, 2017. [Online]. Available: `https://bit.ly/3xlFyh2` (visited on Mar. 29, 2021).

[160] "Integrated Transmission and Distribution (ITD) Project", Iowa State University. (Feb. 24, 2021), [Online]. Available: `http://www2.econ.iastate.edu/tesfatsi/ITDProjectHome.htm` (visited on Apr. 1, 2021).